INFORMATION TO USERS

This manuscript has been reproduced from the microfilm master. UMI films the text directly from the original or copy submitted. Thus, some thesis and dissertation copies are in typewriter face, while others may be from any type of computer printer.

The quality of this reproduction is dependent upon the quality of the copy submitted. Broken or indistinct print, colored or poor quality illustrations and photographs, print bleedthrough, substandard margins, and improper alignment can adversely affect reproduction.

In the unlikely event that the author did not send UMI a complete manuscript and there are missing pages, these will be noted. Also, if unauthorized copyright material had to be removed, a note will indicate the deletion.

Oversize materials (e.g., maps, drawings, charts) are reproduced by sectioning the original, beginning at the upper left-hand corner and continuing from left to right in equal sections with small overlaps. Each original is also photographed in one exposure and is included in reduced form at the back of the book.

Photographs included in the original manuscript have been reproduced xerographically in this copy. Higher quality 6" x 9" black and white photographic prints are available for any photographs or illustrations appearing in this copy for an additional charge. Contact UMI directly to order.

UMI

A Bell & Howell Information Company
300 North Zeeb Road, Ann Arbor MI 48106-1346 USA
313/761-4700 800/521-0600

BEHAVIOR OF COMPOSITE CASTELLATED BEAMS

by

Jihad Dokali Megharief

May 1997

Department of Civil Engineering
and Applied Mechanics

McGILL UNIVERSITY
Montreal, CANADA

A thesis submitted to the Faculty of Graduate Studies and Research
in partial fulfillment of the requirements for the Degree of
Master of Engineering

I dedicate this thesis to my beloved parents Rose and Dokali

for all their love and support throughout the years

ABSTRACT

While the study of non-composite castellated beams have received much attention, very little work has been done on composite castellated beams. The effect of the composite concrete slab is to significantly increase the flexural resistance of a steel section; it is however uncertain what effect this will have on the shear resistance.

In this research project tests to destruction of five composite castellated beams were performed, and relate to previous tests on non-composite castellated beams. Ultimate failure loads of the three shear critical test beams were associated with web-post buckling, comprising double curvature bending. The remaining two flexural test beams failed when most of the studs in one-half of the span failed, resulting in lateral torsional buckling of the suddenly unconstrained flange; but before this occurred, high strains had already developed following tensile yield of the lower part of the steel section.

A numerical study using the finite element method was then employed in investigating the nonlinear buckling behavior of the web-posts in shear critical composite and non-composite castellated beams. Buckling of the web-posts was observed to be the dominant mode of failure in all finite element models; the composite beams were found to have significantly higher ultimate shear carrying capacities than their non-composite counterparts. It was found that the effect of the composite slab is to reduce the shear force in the web-posts, thus increasing the beam ultimate shear carrying capacity. The predicted loads causing buckling for the shear critical beams, using the FEM, were found to be in good agreement with those obtained from the tests. The effect of other parameters on the buckling behavior of web-posts in castellated beams was also addressed; these included the effect of opening eccentricity, hole geometry, partial shear connection, and variable slab sizes.

Finally, yield analyses were performed on castellated beams using moment-to-shear interaction diagrams originally developed for isolated web openings; these were successfully applied to castellated beams. Results based on yield failures were found to be in good agreement with the test failure loads for the flexure critical beams; on the other hand, the yield analysis tended to slightly overestimate the failure loads for the shear critical composite test beams, due largely to the buckling failures of the web-posts in the tests, which are not accounted for in the yield analysis.

RÉSUMÉ

Alors que beaucoup d'attention a été porté sur l'étude des poutres ajourées non-composites, très peu de travaux ont été réalisés concernant les poutres composites ajourées. Pour ce dernier type, le rôle de la dalle de béton est d'augmenter de manière importante la résistance à la flexion de la poutre en acier; l'effet sur la résistance au cisaillement est par contre incertain.

Pour ce projet de recherche, cinq tests destructifs de poutres ajourées composites ont été effectués. Lors de trois tests de cisaillement critique, les charges maximales produisant la rupture sont apparues avec le flambage de l'âme, allant même jusqu'au flambage de deuxième ordre. Les deux autres tests de flexion ont échoué alors que la plupart des crampons de liaison se sont brisés sur une demi-longueur de la poutre, entraînant la déformation en torsion latérale de la semelle soudainement libérée. Néanmoins, avant l'apparition de cet incident, de fortes contraintes s'étaient déjà développées entraînant l'affaissement de la partie inférieure en acier.

Une étude numérique utilisant la méthode des éléments finis a été employée pour définir la déformation non-linéaire du flambage en cisaillement critique dans les poutres ajourées composites ou non. Le flambage a été le mode de défaillance dominant pour tous les modèles en éléments finis; les poutres composites ont montré une bien meilleure résistance au cisaillement en charge supportable que les poutres non-composites. Nous avons trouvé que la dalle de béton permettait de réduire le cisaillement lors du flambage, permettant d'augmenter la charge maximale admise en cisaillement sur la poutre. Les charges estimées par MEF provoquant le flambage sur les poutres travaillant en cisaillement donnent une bonne corrélation avec les tests réalisés. L'effet d'autres paramètres sur le comportement en flambage de l'âme sur les poutres ajourées, comme l'eccentricité ou la géométrie des ouvertures, le transfert partiel du cisaillement de l'acier au béton et les dimensions de la dalle de béton, ont été traités.

Enfin, les analyses concernant la fracture ont été réalisées sur des poutres ajourées en utilisant des diagrammes moment/cisaillement initiallement developpés pour les ouvertures locales de l'âme. L'application aux poutres ajournées de ce procedé c'est révélée satisfaisante. Les résultats basés sur les défaillances en fracture ont montré une bonne concordance avec les charges appliquées lors des test déstructifs sur les poutres travaillant en flexion; par contre, l'analyse des fractures a eu tendance à surestimer légèrement la charge nécessaire à la fracture pour les poutres composites travaillant en cisaillement, en grande partie à cause du flambage apparaissant lors des tests, ce dernier n'ayant pas été pris en compte lors de l'analyse des fractures.

ACKNOWLEDGMENTS

The author wishes to express his sincere gratitude and gratefulness to his supervisor, Professor R.G. Redwood, for his constant guidance and encouragement and for his invaluable input throughout the course of this research project.

The supply and fabrication of the castellated beams by Castelite Steel Products of Midlothian Texas and the gift of the shear studs by the TRW Nelson Stud Welding Division are gratefully acknowledged.

The partial support of the National Science and Engineering Research Council of Canada is gratefully appreciated.

Particular thanks are due to the staff of the Structural Engineering Laboratory at McGill University: Mr. R. Sheppard, M. Przykorski, J. Bartczak, and D. Kiperchuk for their assistance in the fabrication and testing of the composite specimens.

A special thanks is owed to Sevak Demirdjian for assisting me in processing the data from the experimental program, and to Frédéric Chave and Michael Caron for their assistance in translating the abstract from English to French. The author would also like to thank all his friends from the bottom of his heart for making his years at McGill and in Canada that much more memorable.

Finally, the author would like to thank his brother and sister, Ramsey and Randa, for their constant support. The author would also like to take advantage of this opportunity to say thank you to his parents to whom he owes a debt of gratitude and appreciation that could never be repaid. Thank you for all the sacrifices you have made, and for the love and support you have constantly given. You are simply the best; God bless you.

TABLE OF CONTENTS

page

page

page

page

LIST OF FIGURES

page

CHAPTER ONE

CHAPTER TWO

page

CHAPTER THREE

page

page

CHAPTER FOUR

CHAPTER FIVE

APPENDIX A

page

LIST OF TABLES

page

CHAPTER TWO

CHAPTER THREE

page

CHAPTER FOUR

CHAPTER FIVE

NOTATIONS

CHAPTER ONE

d	Depth of the original rolled section before the castellation process
h	Depth of the cut (i.e. half of the opening height)
$\mathbf{d_g}$	Gross depth of the castellated beam
$\mathbf{h_o}$	Opening height
ϕ	Cut angle
e	Throat distance (i.e. length of welded joint)
ecc.	Opening eccentricity
$\mathbf{t_w}$	Web thickness
$\mathbf{t_f}$	Flange thickness
$\mathbf{d_t}$	Depth of top tee
$\mathbf{d_b}$	Depth of bottom tee
S	Opening pitch (i.e.distance from centreline-to-centreline of adjacent holes)
$\mathbf{b_f}$	Flange width
b	Width of one sloping edge of the hole
Z	The plastic sectional modulus
$\mathbf{V_T}$	Shear in the top tee section

CHAPTER TWO

LVDT	Linear Variable Displacement Transducer
$\mathbf{f_c'}$	Concrete compressive strength
ε_y	Yield strain
$\mathbf{F_u}$	Ultimate load in coupon tests

t	Thickness of coupon specimen
F_y(Stat.)	Static yield strength of coupon specimen
F_y(Dyn.)	Dynamic yield strength of coupon specimen
LM	Low Moment
HM	High Moment

CHAPTER THREE

FEM	Finite Element Method
I_i	Moment of Inertia about Plane i
J	Torsional constant
k	Stiffness
E	Modulus of Elasticity
l	Length
RHS	Right Hand Side
LHS	Left Hand Side
D.O.F	Degree(s) of Freedom
V_{hcr}	Web-post shear when buckling occurs
V_{cr}	Beam shear at failure (i.e. when buckling occurs)
V_{ph}	Web-post shearing force which would cause yield at the mid-depth of the web-post
M_1	Internal moment at the top of the web-post
M_2	Internal moment at the bottom of the web-post
V_v	An applied beam shear
P-Δ	Load-deflection
FEA	Finite Element Analysis

P_{cr}	Load causing buckling
H_{its}	Horizontal force in the top tee at section i
H_{ibs}	Horizontal force in the bottom tee at section i
y_{its}	Distance between horizontal force in the top tee and top of the opening at section i
y_{ibs}	Distance between horizontal force in the bottom tee and top of the opening at section i
V_{its}	Shear force in top tee at section i
V_{ibs}	Shear force in bottom tee at section i
V_h	Web-post shear
V_p	Cross section plastic shear strength
y_{tc}	Distance between the centreline of concrete slab and top of the opening
H_{itc}	Horizontal force in the concrete slab at section i
V_{itc}	Shear force in concrete slab at section i

CHAPTER FOUR

M_p	Plastic moment value of unperforated steel section
V_p	Plastic shear value of unperforated steel section
M_o	Moment at point "0" on the moment-to-shear interaction diagram
M_1	Moment at point "1" on the moment-to-shear interaction diagram
V_1	Shear at point "1" on the moment-to-shear interaction diagram
T_i	Horizontal force in bottom tee at section i
y_i	Distance between extreme tension fiber and location of horizontal force in bottom tee at section i
n_c	Modular ratio ($=E_s/E_c$)
E_s	Modulus of Elasticity of Steel
E_c	Modulus of Elasticity of Concrete

F_y	Nominal yield strength of the steel section
V_3	Vertical beam shear which would produce horizontal shear yield of the web-post
M/V	Moment-to-Shear ratio
n	Number of shear connectors

CHAPTER FIVE

$V_{h,comp}$	Horizontal shear in the web-post of a composite beam
$V_{h,noncomp}$	Horizontal shear in the web-post of a non-composite beam
V_u	Beam shear at failure (i.e. causing buckling)
n	Number of shear connectors

CHAPTER ONE

INTRODUCTION

1.1 Introduction

The process of producing castellated beams from rolled sections has been used in steel construction since the late 1930s. Even though the advantages of castellated beams have long been established, they have not been used in North America on a widespread basis in the past. In Europe, on the other hand, the castellation process gained wide popularity because of the high cost of materials and the lower labor cost of fabricating steel. Today, with the development of newly automated cutting and welding equipment, castellated beams are produced in the United States at greatly reduced cost which allows their use in floor systems as an alternative choice to open-web steel joists.

A castellated beam is a flexural member whose performance is analogous to that of a Vierendeel truss. Castellated beams, Figure 1.1, are produced by expanding rolled structural beams into deeper sections which results in greater load-carrying capacity without increasing the weight of the beam. They are made economically by flame cutting a rolled structural beam in a zig-zag pattern, Figure 1.2(a); one of the two halves is then displaced and butt welded to the other half, Figure 1.2(b). This increases the depth *(d)* of the original beam by the depth of the cut *(h)*, and results in a deeper beam (d_g), stronger and stiffer than the original one. Various geometries of castellation openings can be produced, based on the angle of the sloping sides (i.e. angle of cut, ϕ) and the length of the horizontal portion (i.e. welded joint length, e).

The principal advantage of castellation is the significant increase in bending stiffness and in the overall bending capacity: the increase in the depth of a beam increases its sectional modulus and moment of inertia, which results in greater strength and rigidity. It offers savings due to the increase in strength without increasing the weight of the beam. The use of castellated beams, therefore, materially reduces the weight of a structure and eliminates the need for heavy built-up sections. Hence, when designing

with lighter rolled beam sections, immediate savings in material and handling costs can be realized.

Castellated beams have proven to be efficient elements for moderately loaded longer spans where the design is controlled by moment capacity or deflection. The web openings of castellated beams provide a convenient passage for the installation of ducts and services, which ultimately leads to useful savings in the overall heights of multistory structures. When exposed, castellated beams present an attractive structural design for stores, schools, service buildings, etc.

Applications of expanded (castellated) beams are claimed for ships, aircraft and vehicles as well as for buildings: they have been employed in building construction as floor joists, purlins, bracing, tapered open-web expanded beams, hybrid beams, and as arched roof girders. Their use has also been extended to many industrial and commercial structures.

Even though castellated beams are produced in a variety of depths and spans, suitable for light to medium loading conditions, there are examples of more ambitious applications (Dougherty 1993): they were used as arched roof girders spanning 28 m; and they were used as the composite floors for a 21-storey Washington Building in Seattle and featured as exposed longitudinal roof girders in the Tulsa Exposition Center. There are also early examples of their use in bridge construction: two simply supported bridges with spans of 20 m and 30 m were constructed for the Texas State Highway Department in 1952, while a three-span continuous bridge in New-Zealand incorporated castellated beams in its composite deck.

While the study of non-composite castellated beams have received much attention, very little work has been done on composite castellated beams. Castellated beams can be used compositely in long span floors, whereby floor heights are kept to a minimum by passing the services through the web-openings. The use of composite beams in multistory buildings enabled structural engineers to offer larger uninterrupted floor spans. The benefits of long span floors include flexibility of internal planning, and

reducing the number of columns, resulting in savings in the number of foundations required and in the cost of erection, Dougherty (1993).

The increased stiffness and strength of a composite beam over its simple beam counterpart results from the force developed in the concrete slab, which increases the effective depth of the beam and raises the neutral axis position closer to the top flange of the beam. Nevertheless, the load carrying capacity of a composite beam may be limited by the local bending and shear strength of the web posts and upper and lower tees, as is the case with non-composite castellated beams.

Despite the long-term use of castellated beams in steel construction, their exists little in terms of firm design recommendations owing to their complex geometry and high degree of internal indeterminacy (Dougherty 1993). Experimental work on castellated beams has shown that the mode of failure is dependent of the beam slenderness, castellation parameters, and loading type. The resistance of the web to shear is often the limiting factor in the design of castellated beams. Composite action, on the other hand, provides a considerable increase in bending strength relative to that of the steel section alone; it is however uncertain what effect this will have on the shear resistance. The behaviour of a composite beam with one isolated web-opening showed that the presence of the slab does significantly increase the shear carrying capacity beyond that of the steel beam alone (Redwood and Cho 1993). This is due to the enhanced flexural capacity of the upper part of the beam within the length of the opening; however there is no reason to anticipate that the web-post would be less susceptible to buckling. Ward (1990) states that composite beams are subject to higher shear forces for the same beam size than non-composite beams, which in turn exacerbates the buckling problem.

Comparatively, little research has been done on composite castellated beams comprising hexagonal openings and ribbed concrete slabs. There is evidence that investigations are warranted to determine the criterion for buckling of the slender web-posts between the openings and to determine the shear distribution in the steel and concrete elements at the openings. This prompted the investigation described herein.

1.2 Literature Review

1.2.1 Experimental Work

There exists in the literature a comprehensive resume of experimental and theoretical work related to castellated beams, dating back to the late thirties. An extensive literature review has been presented by Dougherty (1993), in which he reviews the various techniques developed for the analysis of castellated beams, and gives recommendations pertaining to the safest and most economical design methods. An extensive list of bibliographical references relating to castellated beams and beams with web openings are also provided. Despite the long-term usage of castellated beams and the extensive body of literature, designers have long labored under the difficulty of not having a firm design method for castellated beams, Knowles (1991). This stems from the fact that they are highly indeterminate structures, which are not susceptible to simple methods of analysis. This is why so much work has been put into investigating the different modes of failure associated with castellated beams and into finding theoretical means of predicting and modeling such behaviours.

Experimental work on non-composite castellated beams showed that in order for the beams to reach their maximum in-plane capacity, the component tees above and below the openings and the web-posts between them must perform satisfactorily, Dougherty (1993). In the work of Kolosowski (1964), elastic in-plane behavior of castellated beams was investigated in terms of stress and deflection. On the other hand, plastic modes of failure due to pure bending and Vierendeel action was documented in the works of Sherburne (1966), Halleux (1967), Bazile and Texier (1968), and Hosain and Speirs (1973). Shear buckling of web-posts in castellated beams are also featured in the work of these authors and in the work done by Aglan and Redwood (1974). This failure mode generally occurred only after the parent beams reached the maximum in-plane carrying capacity.

The web-posts can also exhibit compression buckling, which results from the lack of appropriate stiffening in the immediate area of a concentrated load. This mode of failure has been reported in the works of Toprac and Cook (1959), Hosain and Spiers (1973), Kerdal and Nethercot (1984), and Okubo and Nethercot (1985).

The most recent publication relating to buckling of web-posts in castellated beams is featured in the work of Zaarour and Redwood (1996), in which the behaviour of twelve castellated bantam beams of different opening geometry is described. The common mode of failure in these specimens was associated with shear buckling of the web-posts. A graphical method, developed by Aglan and Redwood (1974), was considered in their work, where it gave good correlation with the maximum test loads.

There also exists in the literature a valuable body of supplementary information pertaining to the behavior of beams with web openings. The works of Redwood (1983) and Redwood and Cho (1993) are just a few of the many currently in publications.

Composite action between castellated beams and a concrete slab was the subject of experimental studies in the work of Larnach and Park (1964): tests on six different castellated composite T-beams, under heavy shear loading, were carried out. The beams were fabricated from universal sections with the top concrete flange attached to the steel beam via spiral shear connectors. Several point loads were used in loading the beams; these were loaded to destruction and failed by buckling of interior web panels, accompanied by cracking of the underface of the concrete flange. It was also found that the neutral axis position at a section with a solid web was lower than the apparent position of the neutral axis at a section with a web-opening.

Giriyappa and Baldwin (1966) performed tests on two composite hybrid castellated beams. These were loaded with a system of loads representing the action of a uniformly loaded beam. Although web buckling is a potential problem in castellated beams, buckling occurred only after general yielding of the tension flange and after the posts in the region of maximum shear developed full plastic shear yielding.

A recent publication relating to composite castellated beams by Hartono and Chiew (1996) describes experimental and numerical studies on six composite half castellated beams: one half of a castellated beam with a horizontal flange plate welded to the top of the web posts and shear studs attached to the plate. The beams were tested to failure as simply supported beams under the action of two concentrated loads. The first

observed failure pattern was associated with the development of longitudinal cracks along the beam's span followed by transverse cracking of the slab near the supports. The beams ultimately failed when the steel web-post, nearest to the support, buckled. The nonlinear behavior and the corresponding failure load and mode was then compared with those obtained from numerical modeling using finite element analysis. The specimens were modeled using 3D solid elements, and good agreement was observed between the experimental and numerical results.

In general, little work has been done on composite castellated beams, particularly on those with ribbed concrete slabs and thin plated-steel sections. These are investigated in this work.

1.2.2 Failure Modes in Castellated Beams

The presence of web openings in castellated beams means that their structural behaviour will be different in several respects from that of beams with solid webs: the presence of the web holes does not only alter the relative importance of certain modes of failure, but it will also introduce new ones. These new modes stem from the different way in which the shear transfers from web-post to web-post through the perforated sections. The occurrence of these new modes is also dictated by beam stiffness (web slenderness), castellation properties (expansion ratio or height, angle of cut, and weld length), and loading scheme.

Several points are worth mentioning from the work of Dougherty (1993): the cutting angle (ϕ) dictates the number of castellations (N); while tests have shown that increasing the value of (N) has little effect on the elastic stiffness of castellated beams, it considerably enhances their ductility and rotational capacity. In the past, the cutting angle varied between 45° and 70°, but current practice has adopted a 60° cutting angle as the effective industry standard. The expansion ratio (α), on the other hand, should be as large as practicable: theoretically, the beam original depth could almost double, but the depth of the top and bottom tee-sections (d_t and d_b) is a limiting factor. If the tees are too shallow, they would fail prematurely by Vierendeel bending over the span

(e), as defined in Figures 1.2(a) and 1.2(b). In practice the depth of the cut (h) is typically half of the opening depth (h_o). These are summarized in the following:

$$\tan(\phi) = h / b$$

$$d_g = d + h$$

$$d_t = (d - h) / 2 \approx (h_o / 4)$$

$$\alpha = d_g / d$$

$$b = 0.5\, h_o / \sqrt{3} = 0.289\, h_o \quad \textit{(for a } 60^\circ \textit{ cutting angle)}$$

where,

h = *depth of cut,*

b = *width of one sloping edge of the hole, and*

d= *original beam depth*

Furthermore, too short a welded joint (e) may cause the web weld to fail prematurely in horizontal shear when the yield strength is exceeded, while too long a welded joint produces tees of long spans, which are prone to Vierendeel bending, Dougherty (1993). A reasonable balance can be achieved between these two modes of failure if,

$$\textit{throat distance} = \textit{weld length (e)} = h_o / 4, \textit{ and}$$

$$\textit{opening pitch (S)} = 2\,(b + e) = 1.08\, h_o$$

The potential modes of failure associated with castellated beams, as observed in previous studies, are summarized bellow:

- *Formation of a flexural mechanism,*
- *Lateral-torsional buckling of the beam,*
- *Formation of a Vierendeel mechanism,*
- *Rupture of the welded joint in a web post,*
- *Shear buckling of the web posts, and*
- *Compression buckling of web posts.*

1.2.2.1 Flexural Mechanism Mode of Failure

This mode of failure can occur when a section is subject to pure bending (i.e. significant bending moment and negligible shear). This mode of failure was reported in the works of Toprac and Cooke (1959) and Halleux (1967), Figure 1.3. In the earlier work by Toprac and Cooke, it was found that in the span under pure bending, the tee-sections above and below the openings yielded in a manner similar to that of beams with solid webs. Consequently, in composite and non-composite castellated beams, the overall flexural capacity can be assessed by considering the plastic moment capacity, M_p, of the cross section through the centerline of the opening. Hence, the maximum moment in a beam should not exceed the plastic moment capacity of the reduced section of the beam, Ward (1990).

$$M_p = Z * F_y$$

where,

Z = *the plastic sectional modulus at an opening.*

F_y = *the nominal yield stress of the beam.*

It should be noted that when the critical span is subjected to an approximately uniform moment, collapse is likely to occur either by lateral-torsional buckling in the case of unbraced beams or by the formation of a flexural mechanism for laterally restrained beams. In these two modes, the appropriate failure loads can be determined utilizing a slightly modified version of the methods used to treat the equivalent failure modes in solid-webbed beams.

1.2.2.2 Lateral-Torsional Buckling of the beam

Non-composite castellated beams are more susceptible to lateral-torsional buckling than composite beams due to lack of lateral support to the compression flange. These are prone to buckle laterally because of their relatively deeper and more slender section and due to the reduced torsional stiffness of the web. In composite castellated beams, the composite slab provides continuous lateral support to the compression flange.

The lateral-torsional buckling behavior of castellated beams is similar to that of beams with solid webs, Figure 1.4. This mode of failure was investigated by Nethercot and Kerdal (1982), where they concluded that the web openings had negligible influence on the lateral-torsional buckling behaviour of the beams they tested. All the buckled spans exhibited the same continuous smooth lateral buckling configuration without web-post distortions. They therefore proposed that castellated beams can be analyzed in a similar manner to solid web beams, but with the exception of using the properties of the reduced section.

1.2.2.3 Failure by the formation of a Vierendeel Mechanism

This mode of failure was first reported in the works of Alfillisch (1957), and Toprac and Cooke (1959). Vierendeel bending is caused by the need to transfer the shear force across the opening to be consistent with the rate of change of bending moment, Ward (1990). In the absence of local or overall instability, hexagonal castellated beams have two basic modes of plastic collapse, depending on the opening geometry, Knowles (1991). These are:

- Plastic extension and compression of the lower and upper tees respectively in a region of high bending moment, Figure 1.5(a).

- Parallelogram or Vierendeel action due to the formation of plastic hinges at the four corners of the opening in the region of high shear force, Figure 1.5(b). This can be explained as follows: when a castellated beam must sustain a vertical shear *(V)*, the tee sections above and below an opening must then undertake not only the conventional primary bending moment but also a Vierendeel moment (V_T * e). This Vierendeel moment results from the action of the shear force in the tee-section (V_T) over the horizontal length of the opening (e), which is also the length of the welded joint. As can be seen in Figure 1.5(c), the formation of the plastic hinges at the ends of the tees is characterized by the tearing and crushing of the re-entrant corners.

In composite castellated beams, the secondary bending effects of the upper and lower tee sections are similar to those of non-composite beams. The composite action

between the concrete slab and the upper steel web tee provides considerable additional resistance to Vierendeel bending. Redwood and Wong (1982) have reported this mode of failure in their work on composite beams with web openings; their work demonstrated the significance of the moment-to-shear ratio at an opening on the beam behavior. It showed that the modes of failure are primarily flexural under the action of a high moment-to-shear ratio. In addition, it also revealed that the Vierendeel parallelogram mechanism would be the dominant mode of failure in cases of low moment-to-shear ratios.

1.2.2.4 Rupture of the Welded Joints

Rupture of a welded joint in a web-post can result when the width of the web-post, or length of welded joint, is small. This mode of failure can be easily analyzed based on the free body diagram, Figure 1.6(a), implemented by Hosain and Spiers (1971), and Redwood (1968). This mode of failure is caused by the action of the horizontal shearing force in the web-post, which is needed to balance the shear forces applied at the points of contraflexure at the ends of the upper tee section. The tests performed by Hosain and Spiers gave emphasis to the brittle nature of such a failure, which can occur without preemptive warning, Figure 1.6(b). Due consideration must therefore be given to this mode of failure when designing castellated beams.

In the literature review presented by Dougherty (1993), it is pointed out that the weld metal is usually stronger than that of the web-post. It is, hence, more likely that the horizontal shear failure will occur in the web material adjacent to the weld, rather than in the weld itself. Experimental work by Maalek and Burdekin (1991), on British Standard Castellated Universal Beams, investigated the use of different qualities of welded joints. Maalek and Burdekin demonstrated the adequacy of using partial penetration butt welds and the use of the free-body diagram , shown in Figure 1.6(a), in assessing the shear strength of welded joints.

1.2.2.5 Shear Buckling of the Web-posts

A web-post subject to the same force system as that shown in Figure 1.6(a), used earlier in the analysis of welded joints, will be subject to horizontal shear forces that will produce double curvature bending which may ultimately cause it to undergo lateral-torsional buckling (Aglan and Redwood 1974), as illustrated in Figure 1.7(a). Several cases of beams failing by buckling of the web posts caused by shear have been reported in the literature. It is featured in the works of Sherbourne (1966), Halleux (1967), Bazile and Texier (1968), Kolosowski (1982), and Zaarour and Redwood (1996). The shear buckling of web-posts in castellated beams is portrayed in Figure 1.7(b).

Several methods have been proposed for predicting the value of the shear force causing buckling (Kerdal and Nethercot 1984). From the work done by Delesque (1968), it was concluded that elastic buckling was unlikely to occur. Aglan and Redwood (1974) tackled the problem using a finite difference approximation for an ideally elastic-plastic-hardening material. They confirmed that the web-posts would normally be yielding before they would buckle. This method was used successfully in the work of Zaarour and Redwood (1996), where it gave good correlation with the maximum test loads. This graphical method provides a quick means of estimating the shear buckling capacity of web posts in perforated beams. Web-post buckling has also been observed in composite castellated beams and is reported in the works of Larnach and Park (1964) and Hartono and Chiew (1996); these works were described earlier in this chapter.

1.2.2.6 Compression Buckling of Web-posts

This mode of failure is similar to the crippling of the web in a plain webbed beam, Kerdal and Nethercot (1984). It can occur regions near concentrated loads or reaction forces. Contrary to shear buckling, the web-post undergoes only lateral displacement and does not twist. Experimental work by Okubo and Nethercot (1985) on sixteen castellated beams showed the possibility of web-post buckling under the action of a local load with the absence of appropriate stiffeners. They also found that contrary to solid webs, the buckling behavior was insensitive to the size of the loaded area. A

strut approach was proposed where the web-post could be modeled as a column, and as such, one can make use of standard column curves to determine the strength of the post (Dougherty 1993). A stiffener could be used to reinforce the web-post when its compressive strength is exceeded under heavy loading.

1.3 Research Program

1.3.1 Objective and Scope of Work

The project described in this thesis is a continuation of the work previously performed by Zaarour and Redwood (1996) on non-composite castellated bantam beams. Buckling of the web-post was the observed mode of failure in these beams, which employed common opening geometries utilized by the Castelite Steel Products Company in Midlothian, Texas. This company was the supplier of the castellated Bantam steel beams for the earlier work by Zaarour and Redwood, and was also the supplier of the beams used in the research program described herein. The company is interested in exploring new markets for composite and non-composite castellated beams, which are made from their proprietary Bantam Beam shapes. In this research program, experimental and numerical studies were carried-out on full-scale composite castellated bantam beams.

In the first part of the research program, the experimental work, five composite castellated beams, with ribbed concrete slabs, were tested. The effect of composite action was investigated on the overall shear and flexural capacities of non-composite castellated beams. The composite beam specimens were designed and manufactured in conformance with the castellation properties used in specimen 12-1 of the earlier work by Zaarour and Redwood (1996). In addition, particular emphasis was put on studying whether improvements to the buckling capacity of the web-posts could be realized from using composite construction. Two other topics of interest from the experimental work were: to investigate the effect of opening eccentricity on the shear and bending behavior, and to study the effect of shored and unshored construction on composite castellated beams.

The second part of the research program focused on performing a numerical study on composite and non-composite castellated beams utilizing finite element analysis. The objective was to simulate the experimental work using finite element modeling, and to investigate the non-linear behavior of web-post buckling in both composite and non-composite beams of specific opening geometries. The finite element analysis also includes the study of the effects of opening eccentricity and composite action on the shear distribution in the upper and lower tee-sections and concrete slab at an opening, since current composite beam design codes tend to ignore any shear contribution from the composite concrete slab. Moreover, partial shear connection and the use of different slab stiffness were also investigated.

1.3.2 Outline of the thesis

The experimental test program on five composite castellated beams is fully described in Chapter 2. In Chapter 3, a numerical study using the finite element method was employed to simulate the test program and to investigate the shear carrying capacity of non-composite and composite castellated beams under variable conditions, such as: hole geometry, opening eccentricity, degree of connectivity, and slab stiffness. Yield analyses related to castellated beams were then performed in Chapter 4, where different yield methods, based on previous research, and failure modes were investigated. Results from theories implemented in the previous chapters are brought together in Chapter 5, where a reconciliation is made between tests and theories, and conclusions are then drawn and summarized in Chapter 6.

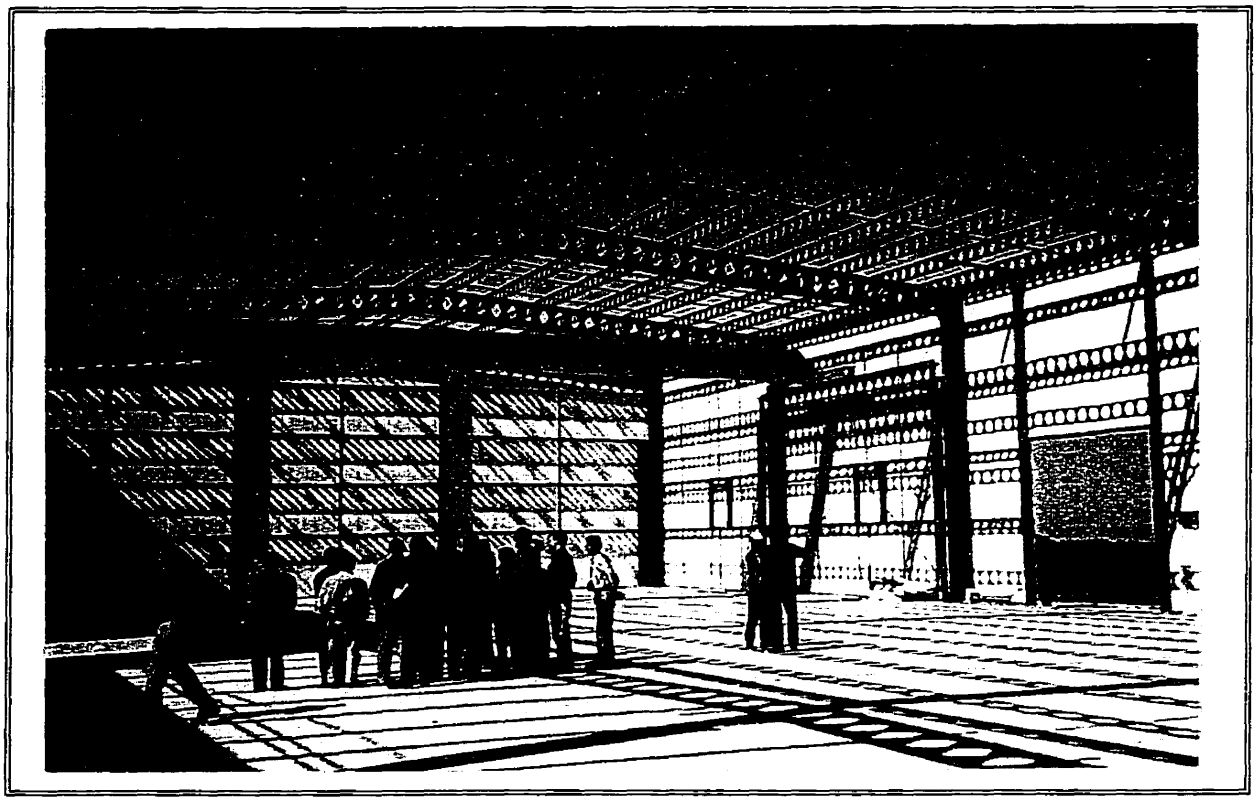

Figure 1.1: Castellated Beams

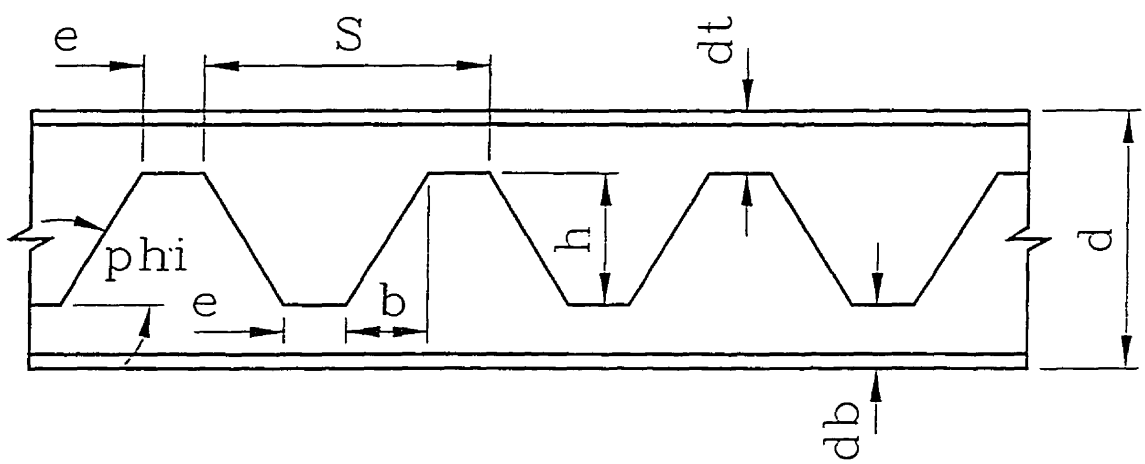

Figure 1.2 (a): Rolled section cut in a Zig-Zag pattern

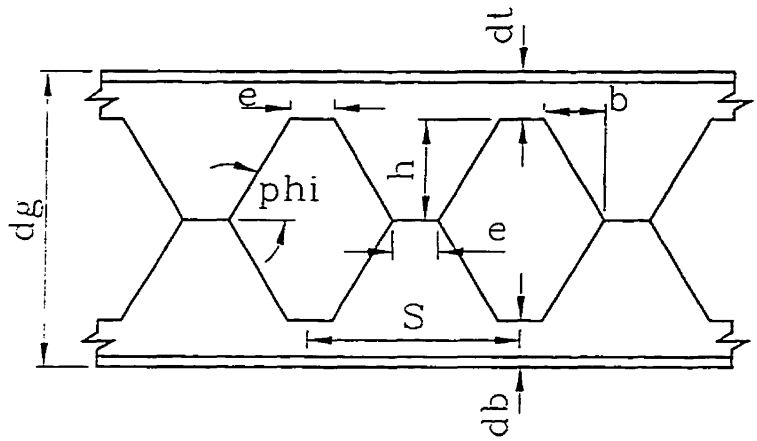

Figure 1.2 (b): Open-web expanded beam

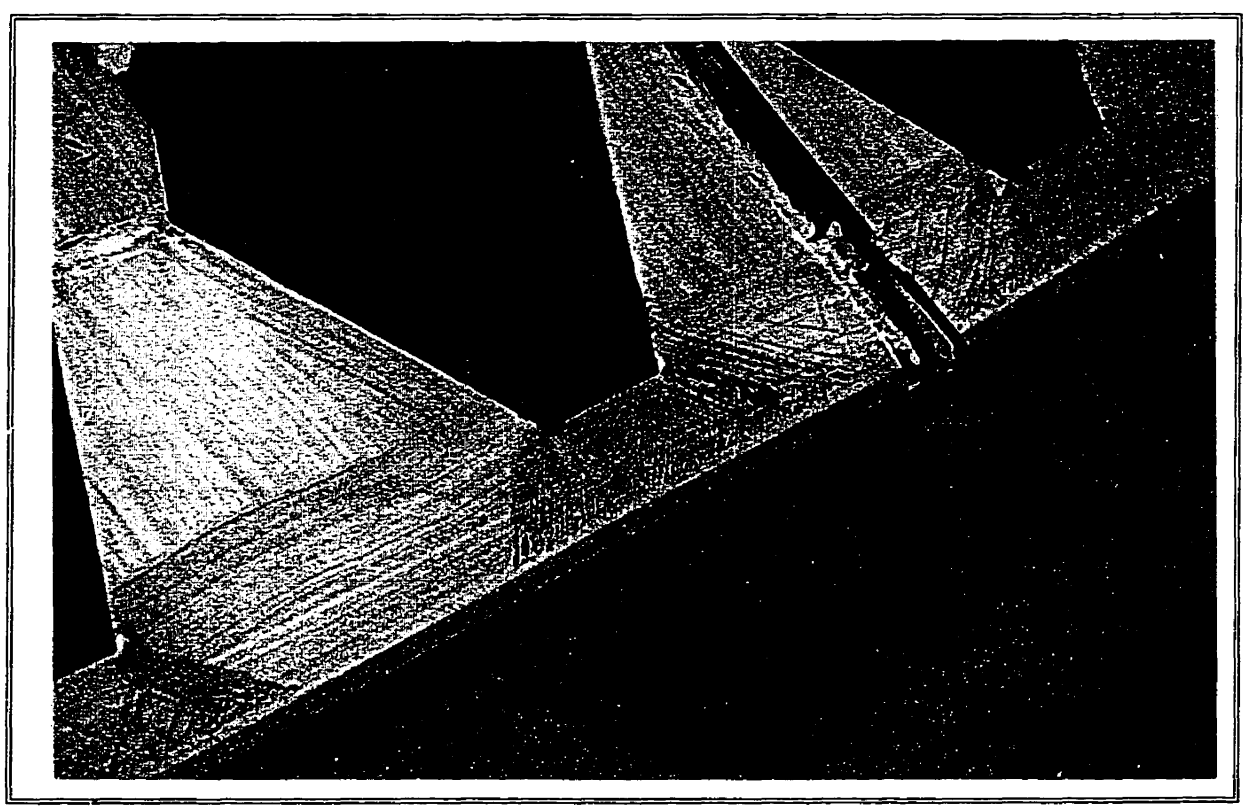

Figure 1.3: Flexural mechanism mode of failure (yield of top and bottom tees)

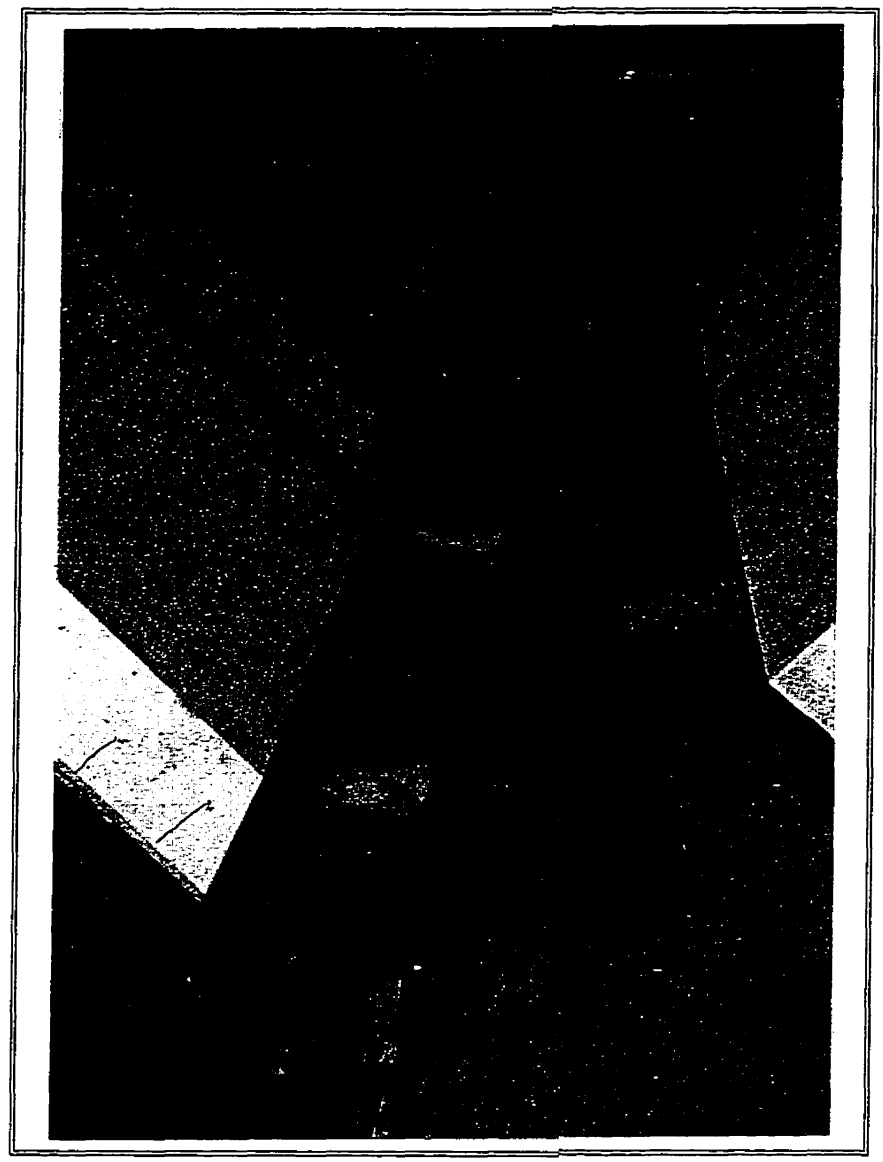

Figure 1.4: Lateral-torsional buckling mode of failure in a castellated beam

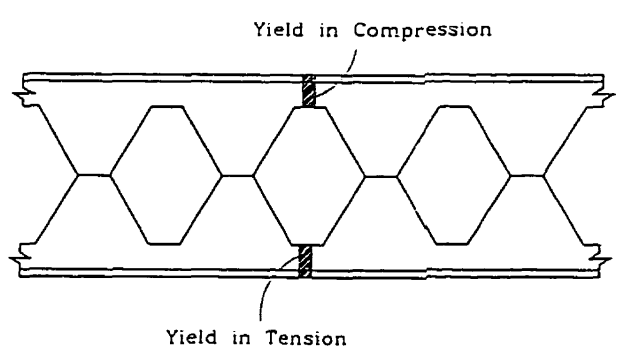

Figure 1.5 (a): Plastic collapse in region of high bending

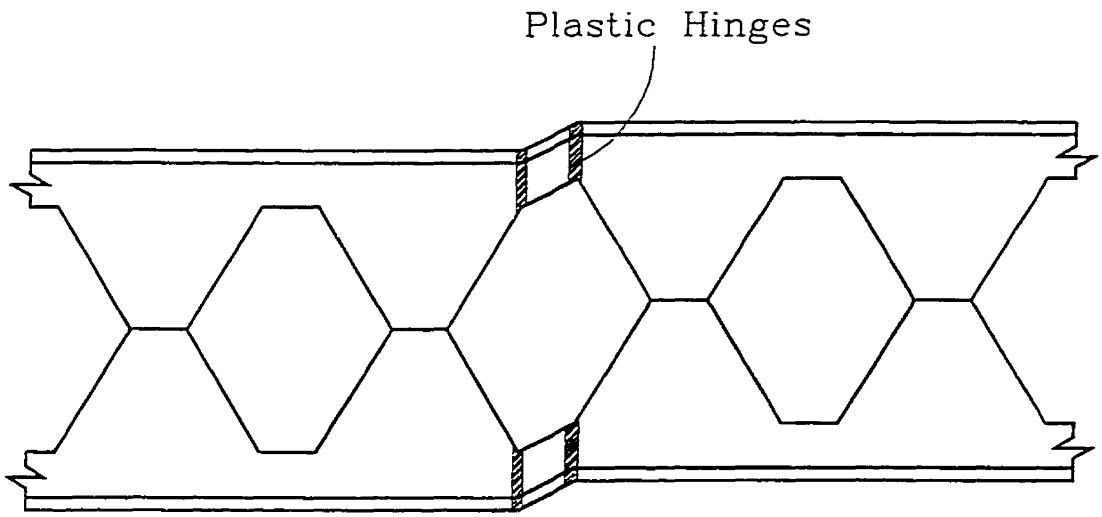

Figure 1.5 (b): Plastic collapse in region of high shear (Parallelogram Mechanism)

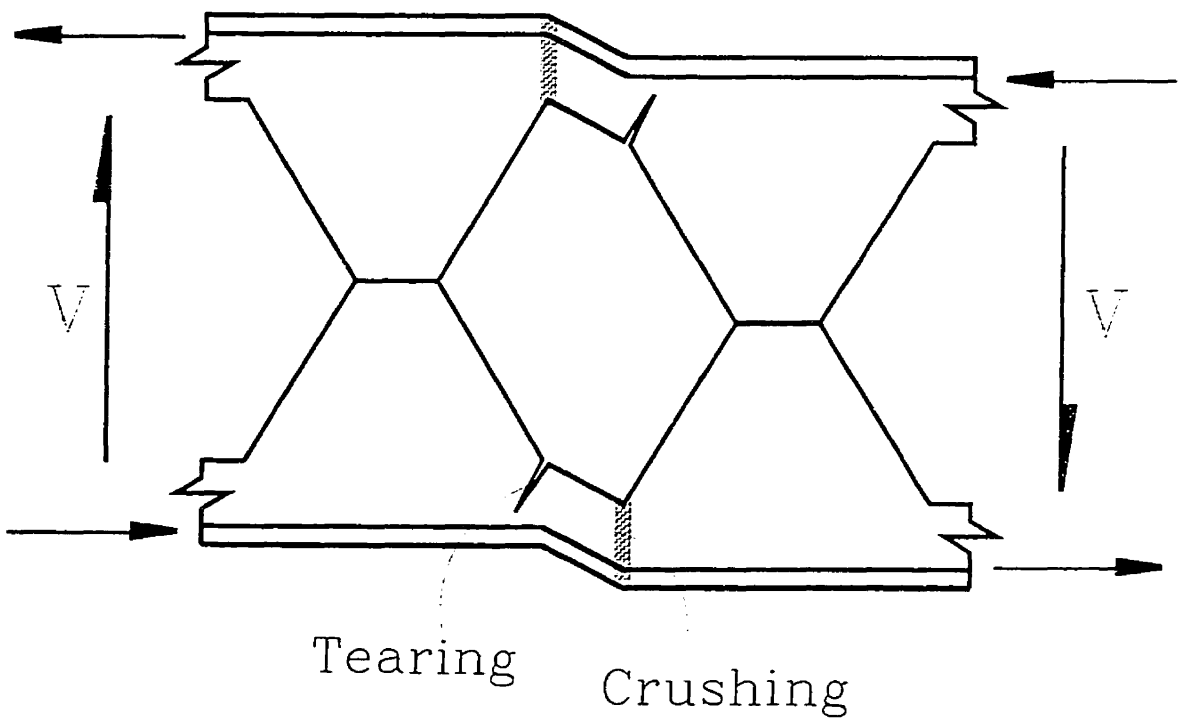

Figure 1.5 (c): Vierendeel action

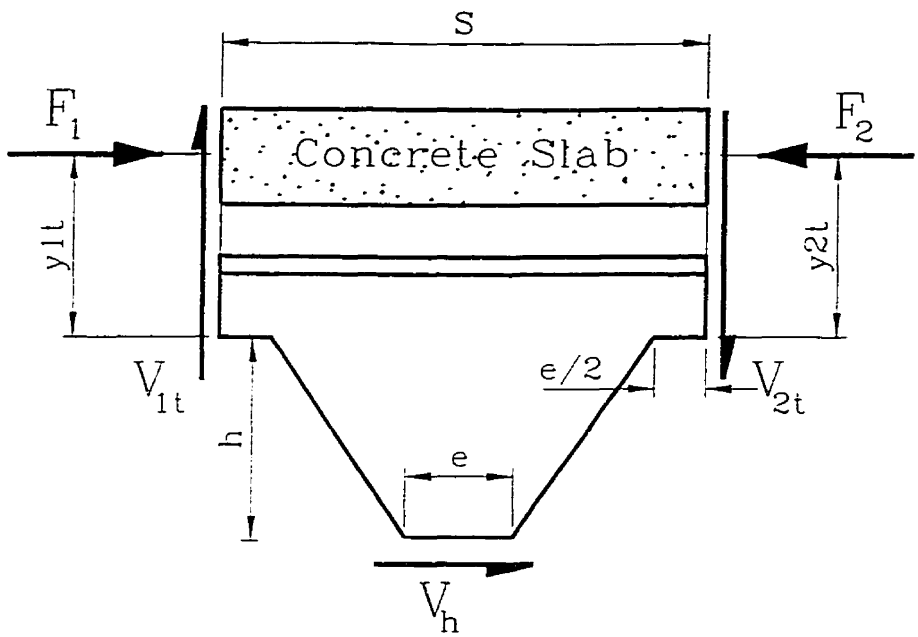

Figure 1.6 (a): Free-body diagram used in the analysis of welded-joints

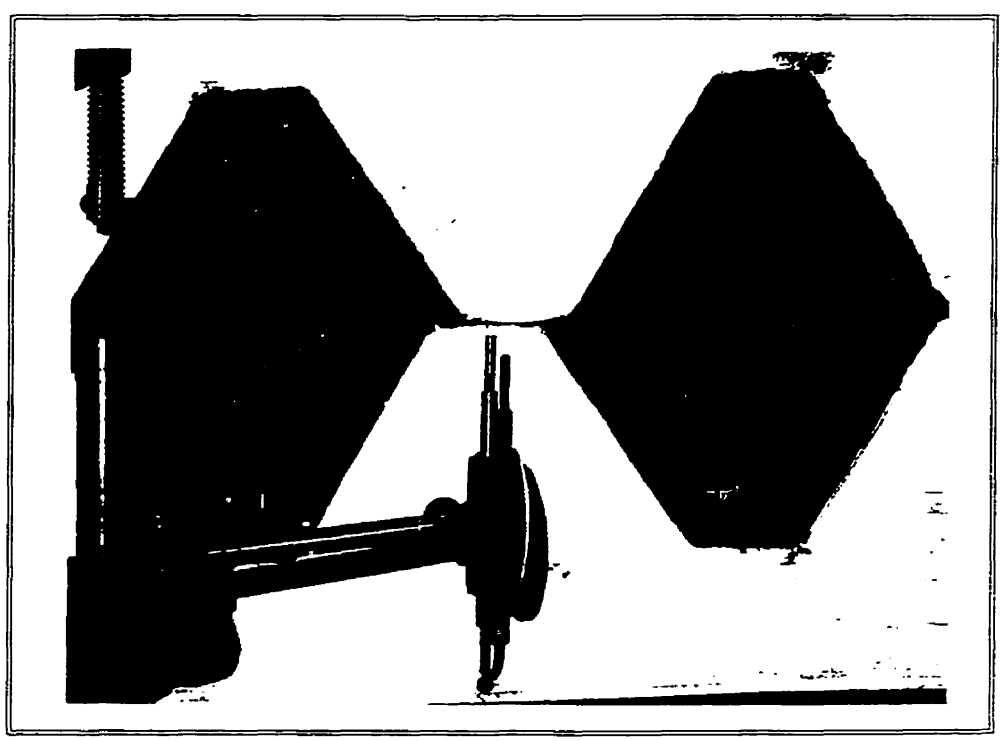

Figure 1.6 (b): A ruptured welded-joint (Hosain and Speirs, 1973)

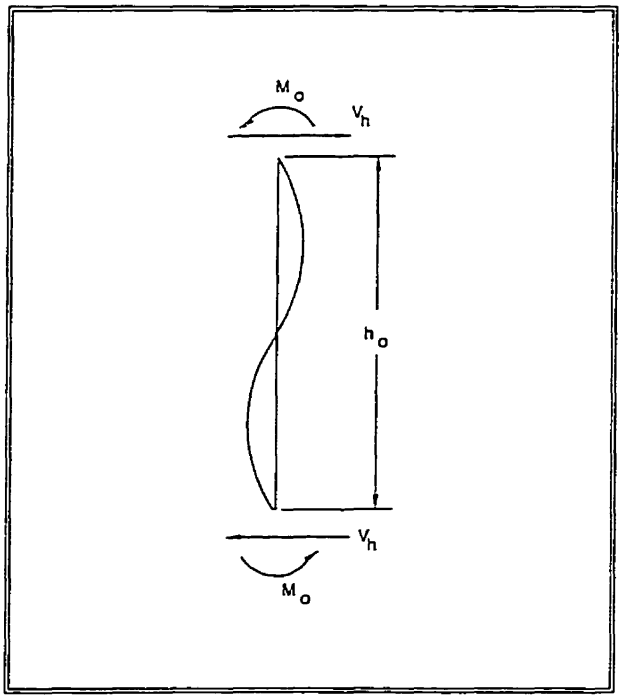

Figure 1.7 (a): Double curvature lateral-torsional buckling of a web-post (Aglan and Redwood, 1974)

Figure 1.7 (b): Shear buckling in the web-posts of a castellated beam

CHAPTER TWO

EXPERIMENTAL TEST PROGRAM

Tests to destruction of five composite castellated beams are described herein. These tests were carried out in the Structural Engineering Laboratory of McGill University. Three beams were tested over a short span, 2180 mm, under high shear-to-moment ratio to investigate buckling of the web-posts; while, two beams of a longer span, 5940 mm, under a much lower shear-to-moment ratio, were also tested to investigate their flexural behaviour. Push-out tests were also performed to establish the shear stud resistance.

2.1 Introduction

All castellated beams were fabricated by Castelite Steel Products Inc. from Bantam sections produced by the Chaparral Steel Company. The castellation parameters used in manufacturing the non-composite steel specimens were based on those used in specimen 12-1 of the earlier work by Zaarour and Redwood (1996). In this earlier work, tests of non-composite castellated beams demonstrated that buckling of the web-post represents a possible mode of failure for some practical sized beams. The web-posts of these non-composite beams with mid-depth openings were analysed using both an approximate beam analysis and the finite element method. In both cases reasonably good agreement with test results were obtained.

Unless the slab carries a significant amount of shear, a composite castellated beam will likely be more shear critical than a corresponding non-composite section. Determination of the shear behaviour was one of the objectives of the tests described herein. Also, little information is available on the flexural behaviour of composite castellated beams, and tests were therefore carried out to determine the limiting behaviour in bending.

Composite action makes feasible a modified castellated section in which the opening is placed eccentrically above the steel section mid-depth. Both mid-depth and eccentric openings were therefore considered in the testing. In addition to flexure, shear and opening

eccentricity, the effect of unshored construction compared with shored construction was investigated.

2.2 Test Specimens

Figures 2.1 and 2.2 give details of the steel beams used in Specimens 3 and 5 respectively, and the main parameters studied in each test are summarized in Table 2.1. All beams were fabricated from a Bantam beam section B12x11.8. For all specimens, the nominal overall depth was 478 mm; the flange had a width of 102 mm and a thickness of 5.72 mm; the web on the other hand had a thickness of 4.5 mm. In the two specimens with eccentric openings, the holes were displaced towards the compression flange and were centered 19 mm above the steel section mid-depth. The concrete cover slabs were all nominally 76 mm thick above a 51 mm, 22ga. (0.76 mm) steel deck. A concrete cylinder strength of 25MPa was incorporated in the design of the composite specimens. The deck profile is shown in Figure 2.3; the top and bottom rib widths were 127 and 178 mm respectively. Beams and deck were provided by Castelite Steel Products Inc.; nominal dimensions are given in Table 2.2. Measurements were made of dimensions of all specimens and are also given in Table 2.2. Since all were fabricated from the same rolled length, the average values are given where appropriate.

Shear connection was provided by 12.7 mm diameter Nelson studs 79 mm long before welding. Welding the studs onto the top steel flange was performed by a qualified welder. Because of the narrow flange width (76 mm), the pair of studs per rib in the shear specimens could not respect both recommended minimum distance to flange edge, Chien and Ritchie (1984), and transverse separation (4 diameters), specified in the Canadian Standard S16.1-94. The recommended minimum flange edge distance of 25.4 mm was maintained, and by offsetting the studs longitudially the diagonal distance between studs was 5.4 diameters. The ratio of stud diameter to flange thickness was 2.2, slightly lower than the code specified upper limit of 2.5 (CSA 1994); also, the studs projected the minimum two diameters into the cover slab. Figure 2.4(b) shows a shear specimen prior to casting.

The slab widths were 584 mm and 1092 mm for the short and long span beams respectively. Slab reinforcement consisted of a 152x152 MW9.1xMW9.1 welded wire mesh (0.1% reinforcement ratio). At support points a grid of 7 mm diameter reinforcing bars were provided to prevent local cracking, Redwood and Wong (1982); this grid extended only into the first rib. A similar grid was provided at the load point in the flexural specimens.

To ensure no flexural failure in the shear specimens, the maximum possible number of studs were used between the support and centre; this led to 45% of full shear connection (two studs in each rib). Conversely, to avoid shear failure in the flexural specimens the flexural resistance had to be limited by using a partial degree of shear connection: 54% was provided (one stud in alternate ribs). Stud positioning within the ribs, Figure 2.4(a), was based on the earlier works of Robinson (1988) and Jayas and Hosain (1989). The single studs in the flexural specimens were placed on the low moment side (LMS), of the rib, this giving a slightly improved strength compared with placement on the high moment side.

Because the web of the steel section was non-compact, the design procedure for the flexural specimens had to ensure that under the ultimate bending moment, compression would be confined to the slab and top flange, which was compact. This was achieved since this requirement is satisfied if shear connection exceeds 46%. For the shear specimens, compression would be confined to the slab if the shear connection exceeded 43%; the provided value was 45%. It should be noted that Specimen 1 was unshored during construction, while for all others the slab was supported from the laboratory floor until cured. The procedure followed for Specimen 1 is described later in this chapter.

2.3 Test Arrangement

All beams were provided with simple supports, with one end placed on a fixed roller and the other on a free one. A pair of lateral supports was provided at each beam end: these consisted of an adjustable plate which could be brought into light contact with top and bottom flanges of the castellated section. One plate was then backed off to permit a gap of paper thickness between surfaces. The top flange contact was made in the region between

concrete ribs. The precense of the continuous concrete slab between supports avoided the need for any other lateral support.

The simply supported composite beams were to be tested under the action of a concentrated monotonic load. The load was provided by two hydraulic jacks reacting on the laboratory floor and aligned equally on each side of the beam. A spreader beam was bedded on top of the slab. Because of the wider slabs of the flexural specimens, the loading rods passed through sleeves cast in the slabs. Separate load cells were used for the two jacks, each being placed above the spreader beam. A diagram of the test arrangement is shown in Figure 2.5, and Specimen 1 is shown in Figure 2.6.

The concentrated load was offset one inch from mid-span in order to provoke failure on one side, which was then more labouriously instrumented. Sufficient instrumentation was however provided on the other side, as a precautionary measure, to record the essential behaviour in case failure unexpectedly occured on that side.

2.4 Instrumentation

Instrumentation consisted of electric resistance strain gauges for measurement of steel strains, mechanical strain gauges (DEMEC) for measurement of concrete strains, linear variable displacement transducers (LVDT), and load cells. All electronic data was recorded on a Doric data acquisition system.

The linear strain gauges used were manufactured by Tokyo Sokki Kenkyujo Co. and the rosettes by Kyowa Co., all with 120 W resistance. The locations of these gauges are shown in Figure 2.7. The linear strain gauges were placed on both sides of the web, in order to capture the buckling of the web-post. They were oriented parallel to the edge of the opening, at a distance of 11 mm from the edge. In the shear specimens (1, 2 & 3), 3 gauge rosettes were placed on the webs of the top and bottom tees of the critical opening, 15 mm from the edge of the hole, to determine the normal and shear stresses. Two 3 gauge rosettes were also placed alongside the weld, at mid length and at the quarter point, to determine the horizontal shearing force acting in the critical web-post. Beams with

eccentric openings had space for two rosettes on the bottom tee web, whereas with mid-depth openings only one was feasible.

In the case of the flexural specimens (4 & 5), the critical web-posts were provided with similar instrumentation to that used on the shear specimens, except for placing one 3 gauge rosette at the middle of the critical web-post just above the weld. More linear strain gauges were utilized on the flexural specimens at the centre of the critical opening to provide a complete picture of the strain variation with depth.

To record lateral displacements of the web on a vertical section at the centreline of the critical web-post, seven LVDT's were mounted on a jig which was supported on the web close to the two flanges, as illustrated in Figure 2.12(b) at the end of the chapter. The jig was utilized in measuring the web profile before and duri ng testing. LVDT's were also used to measure the beam vertical deflections at mid-span and at the centrelines of nearby openings. Critical parts of the steel beams were provided with a brittle coating of whitewash to identify regions of high straining.

2.5 Test Procedure

Careful adjustment of the loading rod positions, each side of the beam, was necessary in order to minimize rotation of the beam under load. This adjustment was carried out by applying several small load increments to the system and observing if the slab remained level in the transverse direction. Several adjustments were usually necessary, and in spite of this, in most cases unloading was necessary one or more times during each test in order to re-align the loading system.

In all cases load was applied to failure. Increments of load were used initially. In the case of the flexural specimens, when the beam stiffness dropped significantly, the load application was subsequently controlled by deflection.

2.6 Material Properties

All beams were fabricated from sections from the same heat, and a short length of the Bantam section was provided for material testing. Four tensile test coupons from both web and flange were tested, and results are given in Table 2.3. The steel material conformed to ASTM A529 Grade 50, and the average yield stress from webs and flanges was 314 MPa and 318 MPa respectively.

Concrete cylinder testing was carried out at 39 days after casting, this being at the end of the 10 day testing period. Results are given in Table 2.4. Average concrete cylinder strengths at the time of testing was 38.4 MPa. It may be noted that this strength is much greater than that used in desigining the composite specimens (25 MPa).

2.7 Push-out Tests

Two push-out tests were carried-out to establish the capacity of the shear connection. In these tests, the width of the steel deck and the stud layout conformed to those used in the shear and flexural specimens. Thus corresponding to the shear test, the push-out specimen had a 584 mm wide slab with one rib containing two studs; for the flexural test a 1092 mm wide slab with one stud in the rib was used. Figures 2.8(a) and 2.8(b) show the test arrangement, and indicates the instrumentation used. The push-out specimens were tested under a high capacity MTS machine, as shown in Figure 2.8(b).

In the push-out test representing the flexural specimens, the ultimate failure load was 68.7 kN per stud, at which the slip between the steel section and the steel deck was 3.23 mm. The variation in slip is shown in Figure 2.8(c). On the other hand, in the push-out test representing the shear specimens, the mode of failure was by cracking through the solid part of the concrete slab at the root of a rib. The ultimate shearing capacity attained was 53.8 kN per stud, at which a slip of 0.94 mm was recorded.

In design of the tests, stud resistances were obtained from code formulae: these values were 52 and 31.5 kN per stud for the one and two studs per rib respectively (based on a concrete

strength of 25 MPa). Corrected for the actual concrete strength, these become 64.5 and 39 kN per stud.

2.8 Test Results and Observations

2.8.1 Shear Tests

The objective in tests of specimens 1, 2 and 3 was to determine the load at which web-post buckling occurred. In earlier tests of non-composite castellated beams under high shear loads in which web post buckling occurred, various means of identifying the buckling load were studied, and it was concluded that the maximum test load was an appropriate one to associate with the buckling. Where such buckling occurs, this is therefore taken here to represent the buckling strength. Another indication of buckling is given by strains measured on opposite faces of the critical web-post, 11 mm from the edge of the hole. The divergence of these as lateral bending occurs is shown in Figure 2.9 for specimen 3.

Fabrication of the beams may lead to initial out-of-plane web deformations. The maximum values recorded in the web posts near the beam mid-spans were 2.5, 0.6, 5.8, 8.9 and 6.35 mm in Specimens 1 to 5 respectively. A common limit for welded wide-flange shapes with solid webs is depth/150, which for all these beams is 3.175 mm (CSA).

The three beams tested under high shear had spans of 2184 mm. Figure 2.10 gives a summary of the loading history ($P-\Delta$) for the three shear specimens. In all three tests the primary mode of failure was associated with web-post buckling, as illustrated in Figure 2.11 for Specimen 1.

2.8.1.1 Specimen 1

This specimen was constructed under unshored conditions, that is, during construction and curing, the non-composite steel section will have to carry the weight of the concrete and formwork (Kulak et al 1990). Because of the small dimensions (2180 mm span and 584 mm width) compared with a practical installation, a preload was applied to supplement the

weight of the poured slab. A mid-span load simulating the slab weight of a 7000 mm span beam was applied. In addition the weight of concrete and formwork was supported directly by the castellated beam. The preload was applied by tightening a nut on a threaded rod, and adjusting the load by means of a load cell. This load of 22.2 kN was applied at the time of pouring the concrete. During the test it should have been reduced to zero within a few load increments; however, as indicated in the table of observations, Table 2.5, transfer took place much later, indicating that a much greater pre-load than planned had been applied. Since this beam behaved in a very similar way to the identical beam without pre-load (Specimen 2), it can be concluded that, even with this very large preload, the ultimate behaviour was not significantly affected.

The test load was applied one inch from mid-span in the east direction. It was initially applied in increments of 4 kN. Table 2.5 summarizes the test observations. The ultimate load of 184 kN corresponds to a shear in the region that failed of 95.2 kN. The mid-span displacements shown in Figure 2.10 illustrate the effect of the preload, since this beam had to be unloaded in order to rectify some unbalance. This also illustrates the very high value that the preload had, compared with that intended. The double curvature buckled shape of the web-post is illustrated by the web transverse displacements at the end of the test, Figures 2.11 and 2.12(a).

2.8.1.2 Specimens 2 and 3

These beams were not preloaded, and their deflection variations therefore differ from Specimen 1 (Figure 2.10). Like specimen 1, specimen 2 had to be unloaded during the test to correct twisting. In other respects these beams behaved in a very similar way to specimen 1, Figures 2.12 (b) and 2.12(c). Details of the behaviour are given in Tables 2.6 and 2.7.

2.8.1.3 Distribution of Vertical Shear

To determine the shearing stresses in the tee-sections above and below the openings in the shear specimens, some strain rosettes were located on an opening centreline. The small depth of the tee-section webs limited the number of gauges to one, except below the eccentric opening of Specimen 3 where two were used. The measurements made in the elastic range were analysed.

The measured shear stresses in the lower tee were used to estimate the shear force carried below the opening. This was done using the "strength of materials" solution relating shear stress to shear force in a prismatic beam. The results indicate that the bottom tees of Specimens 1, 2 and 3 carry 11%, 25% and 19%, respectively, of the total shearing force on the section. These results confirm only that most of the shear is carried above the opening; the reliability of the specific values is uncertain, since it could have been anticipated that Specimen 3 with a deeper web would have carried more than Specimen 2; also there seems to be no reason why Specimens 1 and 2 should differ.

Analysis of the top section is made intractable by the presence of the slab with less than full shear connection. However, ignoring the presence of the slab, and treating the upper tee-sections in the same way as the bottom ones, suggests that they carry 10%, 13% and 8% of the total shearing force. These results will be discussed further in Chapter 5, where they will be compared with the finite element results.

2.8.1.4 Web-Post Shear Force

Rosette strain gauges near the mid-height of the web-post were used to estimate the horizontal shearing force in the web-posts of Specimens 1, 2 and 3 in the elastic range. Two gauges, at the middle and at the quarter point were used to give two estimates. For a unit vertical shear (1 kN) on the beam cross-section, it was found that the horizontal web-post shearing forces were 0.19, 0.34 and 0.4 kN in the three specimens respectively. These results will also be discussed in Chapter 5.

2.8.2 Flexural Tests

Specimens 4 and 5 were tested to investigate the flexural behaviour of composite castellated beams. An approximately central load was applied on spans of approximately 5940 mm. The behaviour of both beams was very similar, and this is described for Specimens 4 and 5 in Tables 2.8 and 2.9 respectively.

The first major distress in the beam comprised yielding of the bottom tee-sections at the openings nearest the mid-span. A few localized whitewash cracks were visible at the upper low moment (LM) opening corners. Figure 2.13 (a) and 2.13 (b) illustrates yield in the bottom tee-section of Specimen 4 and 5 respectively, both during and after testing. The stiffness rapidly dropped to essentially zero. With increasing deflections one or two studs failed with a loud crack, and shortly afterwards sufficient studs had failed that lateral torsional buckling occurred, Figure 2.14. Subsequent examination of Specimen 4 showed that four out of the five studs had failed in shear, creating a large laterally unsupported length, about 2286 mm, that was vulnerable to lateral torsional buckling. The slab rotated horizontally about the lateral support at the far end (east), resulting in a lateral displacement of about 305 mm at the end support at the west end. The final position of Specimen 5 is illustrated in Figure 2.15. During the test it became evident that the west side was going to fail first because of the large end slip between slab and steel that were occurring at this end compared to those at the east end. A portion of the loading history for both specimens 4 and 5 can be ssen in Figure 2.16.

Strains on the cross-section at the centreline of the opening nearest mid-span are shown in Figure 2.17 for Specimen 4. Steel strains at the load levels represented are less than the yield strain. The theoretical distribution based on normal beam bending theory is also shown. Fairly close agreement exists in concrete and steel above the opening. The measured values in the bottom tee-section are slightly lower than the theoretical values; the smaller strains farther from the neutral axis suggest that the the point of contraflexure corresponding to pure shear behaviour would not be at opening mid-length, but displaced towards the high moment end. Specimen 5 showed very similar results, with the unexpected strain distribution in the bottom tee-section even more pronounced. This effect disappears as the ultimate load is approached.

2.9 Results and Discussion

The ultimate test loads are summarized in Table 2.10, and the load history for all five specimens can be seen in Figure 2.18. The three shear tests demonstrated very similar behaviour, with only small differences between the ultimate loads. This suggests that for shear critical beams, the behaviour is not sensitive to the variables considered. Any difference between the shored and unshored loading would have been exaggerated because of the excessive pre-construction load applied, yet the ultimate strengths and failure modes were very similar. The pre-load applied may have represented a significant proportion of the non-composite web-post buckling load. Similarly, the effect of the eccentric opening on the web-post buckling strength showed no difference from that of the mid-depth opening for these shear critical beams. The strain measurements indicate that the bottom tee-sections carry 10 to 25% of the vertical shear.

The design of the 5940 mm span flexural members was influenced by the shear strength of the web. To ensure a flexural failure a low percentage of shear connection was used. An alternative would have been to strengthen the web, but with a single point load producing constant shear in the half-spans, this would have affected the flexural behaviour. Nevertheless, the bottom tee-sections in openings near mid-span underwent extensive yielding, suggesting that a major proportion of the maximum possible strength was attained. Near ultimate, the magnitude of these strains indicated that the material had just begun to strain-harden ($\varepsilon \approx 11\text{-}12\ \varepsilon_y$). It can be noted that tensile stresses existed in the upper tee-sections, indicating that that the neutral axis was close to the concrete slab. Had the beam shear resistance been greater, and more shear studs provided, it is probable that more strain-hardening in the lower tees and yield in the upper tees would have been developed, thus utilizing more of the available slab capacity, leading to a corresponding increase in bending resistance.

TABLE 2.1: Principal Objectives of Test Specimens

SPECIMEN	LOADING	SPAN	PARAMETERS
1	*Shear*	*2184 mm*	*Unshored; mid-depth opening*
2	*Shear*	*2184 mm*	*Shored; mid-depth opening*
3	*Shear*	*2184 mm*	*Shored; eccentric opening*
4	*Flexural*	*5944 mm*	*Shored; eccentric opening*
5	*Flexural*	*5944 mm*	*Shored; mid-depth opening*

Table 2.2: Nominal and Average measured dimensions of Test Specimens

Parameter	Nominal Dimension	Measured Dimension				
		SPEC 1	SPEC2	SPEC 3	SPEC 4	SPEC 5
	mm	mm	mm	mm	mm	mm
b	*101.6*	*102.4*	*identical for all specimens*			
c	*76.2*	*76.2*				
ho	*351*	*352.4*				
h	*175.5*	*176.2*				
tw	*4.49*	*4.69*				
tf	*5.72*	*5.35*				
S	*355.6*	*355.6*				
dg	*478*	*475.1*				
bf	*77.7*	*77*				
dt	*varies*	*58.7*	*59.5*	*42.9*	*45.3*	*63.5*
db	*varies*	*58.7*	*59.5*	*77.8*	*80.8*	*65.1*
Sweep	*0*	*4.5*	*4*	*4.5*	*4.2*	*2.7*
Camber	*0*	*2*	*1.5*	*1.5*	*3*	*3*
effective slab width	*Varies*	*584*	*584*	*584*	*1092*	*1092*
cover slab thickness	*76.2*	*76.2*	*76.2*	*76.2*	*76.2*	*76.2*
Span	*Varies*	*2184*	*2184*	*2184*	*5944*	*5944*

Table 2.3: Coupon Test Results*

Specimen Type	b (mm)	t (mm)	Area (mm^2)	Fy (Stat.) (MPa)	Fy (Dyn.) (Mpa)	Fu (MPa)	% Reduc. in Area	% Elong. in Length
Web 1	12.6	4.7	58.7	N.A	311	446.8	62	N.A
Web 2	12.6	4.7	58.8	N.A	317.8	445.4	55.6	N.A
Web 3	12.6	4.8	59.7	N.A	311	435.8	58.3	N.A
Web 4	12.6	4.8	59.7	302	316.5	441.3	57.4	N.A
Flange 1	12.6	5.4	68	297.9	307.5	437.8	63.2	34.3
Flange 2	12.7	5.4	68.5	310.3	321.3	450.9	66.7	34.3
Flange 3	12.7	5.4	67.7	302	317.2	439.9	61.3	35.9
Flange 4	12.7	5.4	68.7	311	324.1	450.2	62.3	35.9

* *The web and flange coupon samples were taken from a B12x11.8 Bantam beam; they also conformed with the requirements of CAN/CSA-G40.20-M87.*
N.A. – results not available.

Average Values:

F_y (web) :	314.4 MPa
F_y (flange):	317.8 MPa
F_u (web):	442.6 MPa
F_u (flange):	444.7 MPa

Table 2.4: Concrete Cylinder Test Results

LOAD	CYLINDER AREA	COMPRESSIVE STRENGTH		AVERAGE
lbs	in^2	psi	MPa	STRENGTH
Concrete ~ 22 days old				
157000	28.274	5552.8	38.3	
Concrete ~ 35 days old				
154000	28.274	5447	37.6	*5565 psi*
161000	28.274	5694	39.3	*(38.4 MPa)*
157000	28.274	5553	38.3	
Concrete ~ 39 days old				
160468	28.516	5627	38.8	*5571 psi*
157714	28.382	5557	38.3	*(38.4 MPa)*
155552	28.141	5528	38.1	

TABLE 2.5: Specimen 1 Test Observations

LOAD STEP	LOAD (kN)	OBSERVATIONS - SPECIMEN 1
26	105.8	* slight cracking sounds were heard and hairline cracks were observed at corners of the ribs closest to mid-span.
30	122.8	* preloading threaded rods became loose and voltameter reading was almost zero, indicating that complete load transfer had occurred.
32	132.1	* some cracks developed at the bottom of the ribs closest to mid-span due to separation of the concrete rib from the encasing steel deck. * yield lines began to appear on the white wash in the upper low moment (LM) corners of the openings.
40	163.7	* beam unloaded and reloaded to correct tilting of the specimen.
49	186.3	* ultimate load was reached when buckling occurred on the east side of the beam in the web-post between openings 2 & 3.
End of Test		* the buckling patterns and yield lines are clearly established on the whitewash. * both posts on the east side buckled, with that between holes 2 & 3 exhibiting more lateral deformations than the one between holes 1 & 2. * a diagonal crack occurred at the rib above the critical web-post, indicating rib separation caused by different settlements between the rib and steel beam at the this location. * yield lines are particularly visible on the white wash at the upper LM corners of the openings; however, these vary in intensity: yield line patterns decrease with distance from the support. This is contrary to those that occur at the bottom high moment (HM) corners, which increase the further we are from the support.

TABLE 2.6: Specimen 2 Test Observations

LOAD STEP	LOAD (kN)	OBSERVATIONS - SPECIMEN 2
14	79.2	* a crack occurred in the rib above the mid-span stiffener.
20	104.5	* yield lines appeared on the upper LM corners of holes 1,2,5 & 6.
28	141.5	* yield lines were visible on the weld of the web between holes 1 & 2.
31	153.9	* more yield lines at the upper LM and new ones at the bottom HM corners of holes 1,2,5 & 6. * a diagonal crack on the LM side of the rib above opening 1.
36	175.5	* ultimate load was reached. * buckling occurred in the web-post between openings 4 & 5 (opposite to the intended failure side).
End of Test		* buckling occured in the south side, opposite to the intended failure side. * the two web-posts between openings 4, 5 & 6 had buckled but with that closest to mid-span (bet. holes 4 & 5) exhibiting more severe buckling. * diagonal cracks were visible on the rib above the mid-span stiffener. * other diagonal cracks occurred at the rib above the buckled critical web-post (bet. holes 4 & 5). * yield lines were vissible on the whitewash at the upper LM corners of openings 1, 2, 5 & 6; however, the patterns decrease with distance from the supports. * additional yield lines also developed at the bottom HM corner of opening 4.

TABLE 2.7: Specimen 3 Test Observations

LOAD STEP	LOAD (kN)	OBSERVATIONS - SPECIMEN 3
13	74.3	* yield lines were visible on the white wash at the upper low moment (LM) corner of opening 6.
17	89	* new yield lines occurred at the upper LM corners of holes 1, 2 & 5.
20	99.6	* the rib located at mid-span began to exhibit diagonal cracks in both the north and south directions. * with increasing applied load, more yield lines began to appear on the upper LM corners of the holes mentioned earlier and the size of the crack also increased.
39	173.7	* the maximum (ultimate) load was reached. * buckling occurred in the web-post between openings 2 & 3. * after load step 39, the load began to fall gradually with increasing deflections, indicating that buckling had occurred. * buckling was clearly defined on the white wash. * after buckling, a large diagonal crack formed in the second rib from mid-span above the buckled web-post.
End of Test		* it was clear that buckling had occurred on the northern-half of the beam in the first and second web-posts (between openings 2 & 3 and 1 & 2, respectively), with that closest to mid-span exhibiting more severe buckling. * the upper LM corners of the openings showed signs of yielding. The extent increased closer to mid-span. * on the northern half of the beam (failed side), yield lines were also visible on the HM bottom corner of the hole 3.

TABLE 2.8: Specimen 4 Test Observations

LOAD STEP	LOAD (kN)	OBSERVATIONS - SPECIMEN 4
9	37.8	* load was removed and re-applied due to tilting caused by unbalance loading. * yield lines were visible at the upper LM corners of opening no. 1 & 16.
24	75.6	* load was again adjusted due to unbalanced loading.
27	81	* a diagonal crack developed in the rib above the mid-span stiffener.
29	85.4	* switched from load to deflection control because of reduction in stiffness. * new yield lines developed at the upper LM corners of holes 2, 7, 10 & 15. * yield lines appeared at the bottom HM corner of holes 7, 8, 9 & 10.
35	88.4	* maximum load was reached.
39	85.4	* beam was unloaded due to tilting caused by unbalanced loading. * another crack appeared in the rib above the mid-span stiffener.
41	83.6	* by this time the bottom tees and flanges at holes 7, 8, 9 & 10 were exhibiting complex yielding patterns (fully yielded).
55	86.7	* two consecutive loud bangs were heard resembling the failure of two studs.
57	68.1	* more studs failed causing the steel beam to fail by lateral torsional buckling as it disengaged from the slab from the west support to a point near the centre. * failure occurred on the west side, which was opposite to the intended failure side.
End of Test		* yield line patterns on the whitewash and the cracks in the concrete ribs were almost identical on both halves of the beam, except that the patterns on the failed west side were more pronounced. * diagonal cracks had developed in the concrete ribs between openings 8 & 9. * the top and bottom tees and flanges at holes 7, 8, 9 & 10 were fully yielded, with the bottom portions undergoing more yielding (denser crack patterns) than the upper ones. * signs of yielding were apparent at the upper LM corners of holes 1, 2, 15 & 16, with those on the eastern side (holes 1 & 2) being more pronounced. Additional yield lines were also seen on the bottom tee of hole 1. * at least four of the five studs in the western side of the beam (opposite to the intended failure side) had failed in shear. * the studs that failed were those closest to the western support.

TABLE 2.9: Specimen 5 Test Observations

LOAD STEP	LOAD (kN)	OBSERVATIONS - SPECIMEN 5
5, 8, 16 & 19	29.4, 38.3, 69.4 & 77.8	* specimen was unloaded due to tilting caused by unbalanced loading.
bet. 14 & 19	bet. 60.9 & 77.8	* yield lines appeared on the white wash at the bottom portion of the webs just north and south of the mid-span stiffener. * additional yield lines were visible on the upper LM corners of openings 1 & 16. * diagonal cracks developed in the rib above the mid-span stiffener.
21	80.5	* switched to "Deflection Control". * more yield lines were visible and new ones developed at the bottom tees and flanges of holes 7 & 8 (opposite to the loaded side).
24, 30, 41 & 46	81.4 ~ 83.6	* beam was unloaded three times due to tilting and unbalanced loading.
30	84.6	* maximum load was attained.
44	84.6	* sounds were heard. * cracks developed in the two ribs between holes 7 & 8 and between holes 9 & 10.
46	84.6	* the LVDT at mid-span was substituted with a dial gauge because of excessive deformation and for fear of damage.
53	84.6	* more sounds were heard.
71	84.6	* a loud noise was heard resembling the failure of a stud.
77	84.6	* the jig was removed for fear of damage. * soon afterwards, after a little more loading, more studs failed with loud sounds, accompanied by the overall failure by lateral torsional buckling (as was the case for specimen 4).
After Test Completion		* at least four of the five studs in the southern half of the beam (opposite to intended failure side) had failed. * the studs that failed were those closest to the southern support. * the fourth stud from the southern support failed by pulling out of the top steel flange leaving a circular hole in it. The remainder of the studs failed in shear. * yield lines could be seen on the upper LM corners of holes 1,6,9,10,11,15 & 16. * yield lines also developed at the LM corners of openings 6,7,8,9,10,11,16. * bottom tees and flanges at openings 6,7,8,9,10,11 were fully yielded * more yield lines are visible at the upper HM corners of holes 9 & 10 of the failed south side. * the top flange had yielded at the the LM side of hole 11. * diagonal cracks developed in the ribs between holes 7 & 11. * more cracks developed in this specimen, with mid-depth openings, when compared with those of specimen 4, with eccentric openings.

Table 2.10: Ultimate Test Loads

SPECIMEN	1	2	3	4	5
Measured (kN)	*186.3*	*175.5*	*173.7*	*88.4*	*84.6*
Self-weight (kN) *	*3.2*	*3.2*	*3.2*	*8*	*8*
Ult. load (kN)	*189.5*	*178.7*	*176.9*	*96.4*	*92.6*

* *allowance for self-weight in the form of an equivalent concentrated mid-span load.*

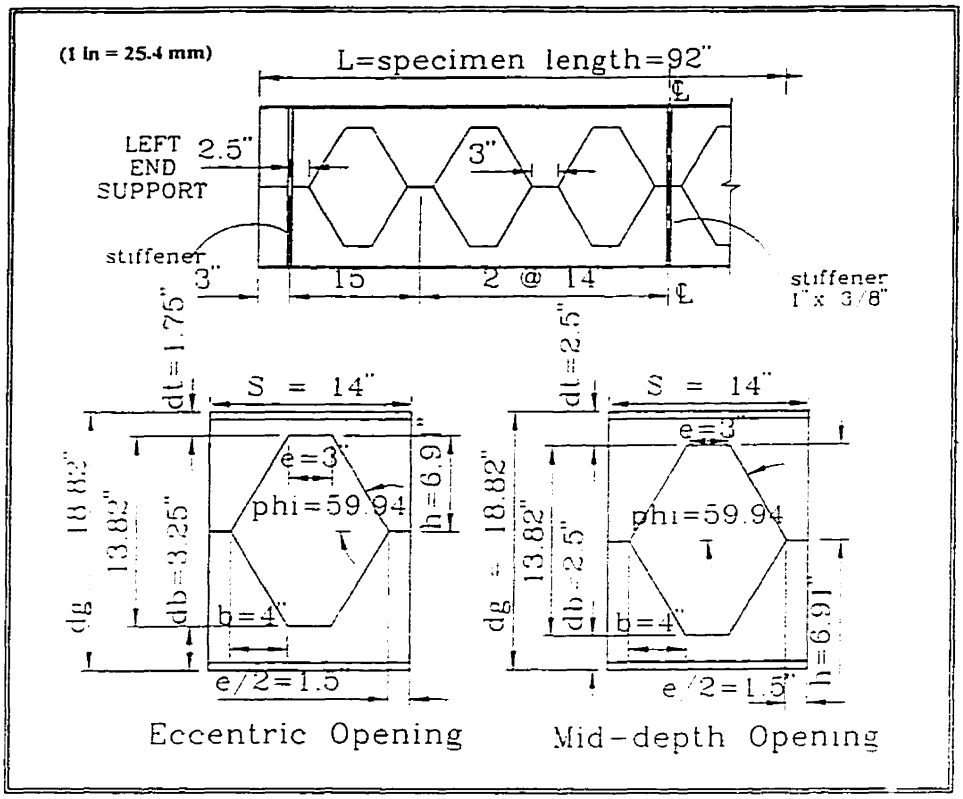

Figure 2.1: Details of non-composite shear specimens

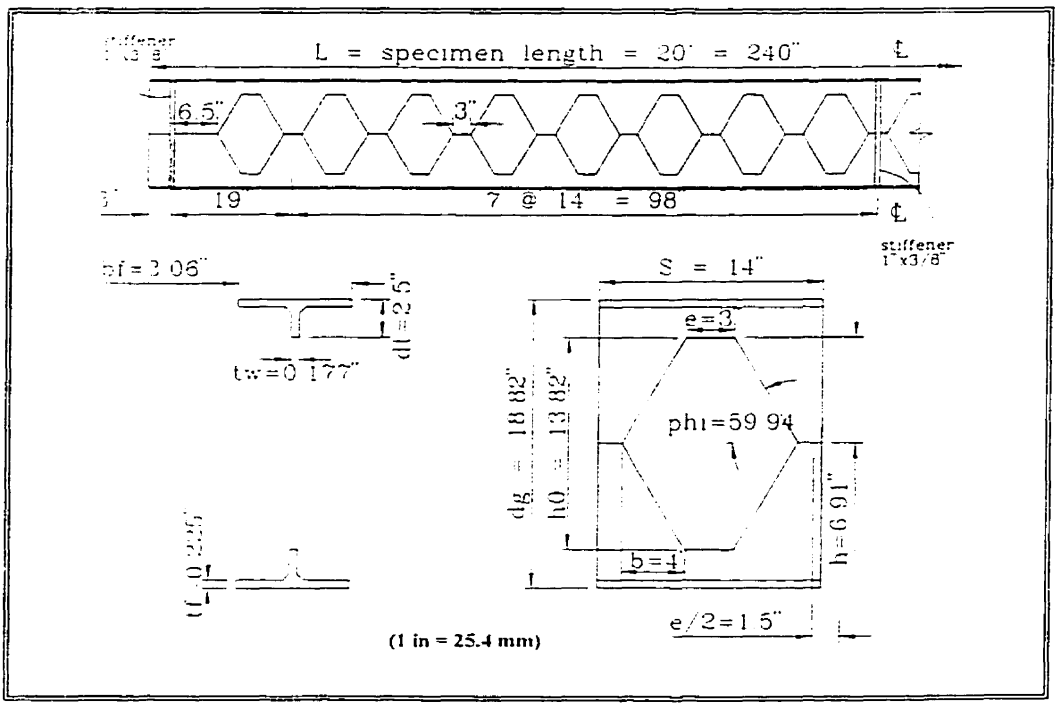

Figure 2.2: Details of non-composite flexural specimens

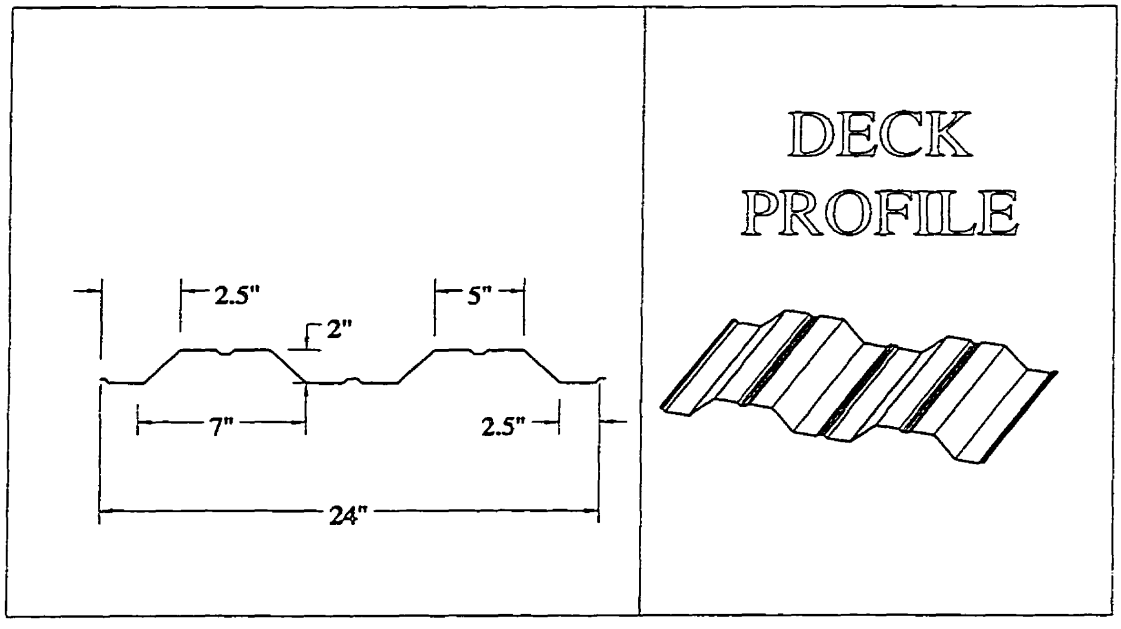

Figure 2.3: Deck profile

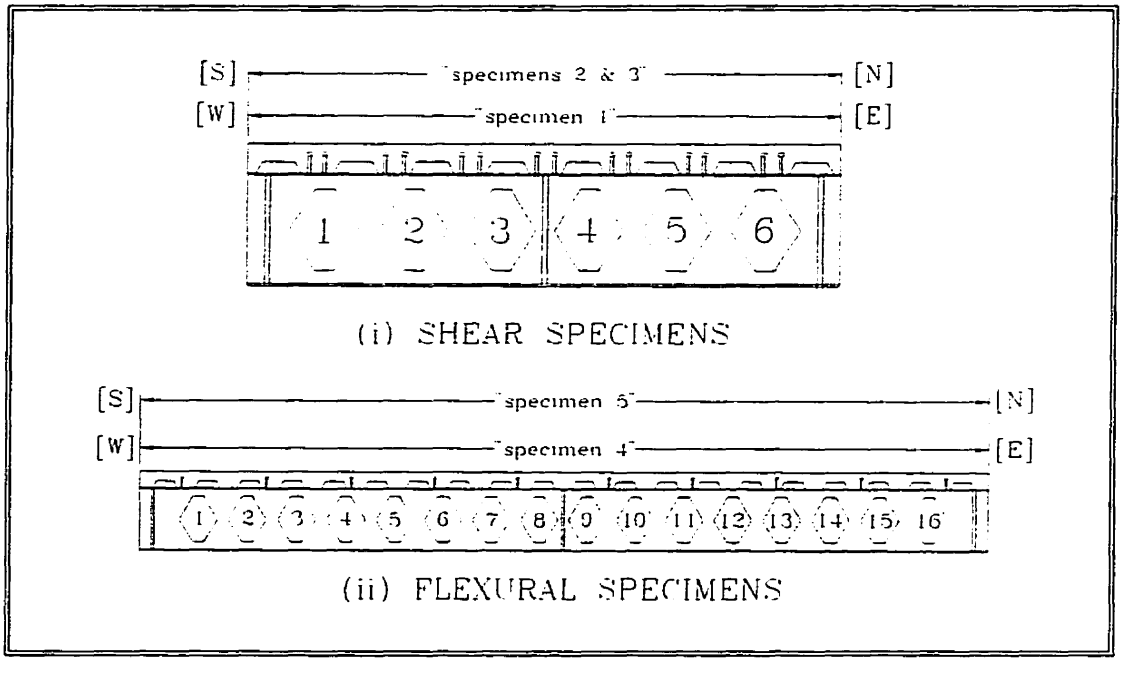

Figure 2.4(a): Stud Layout

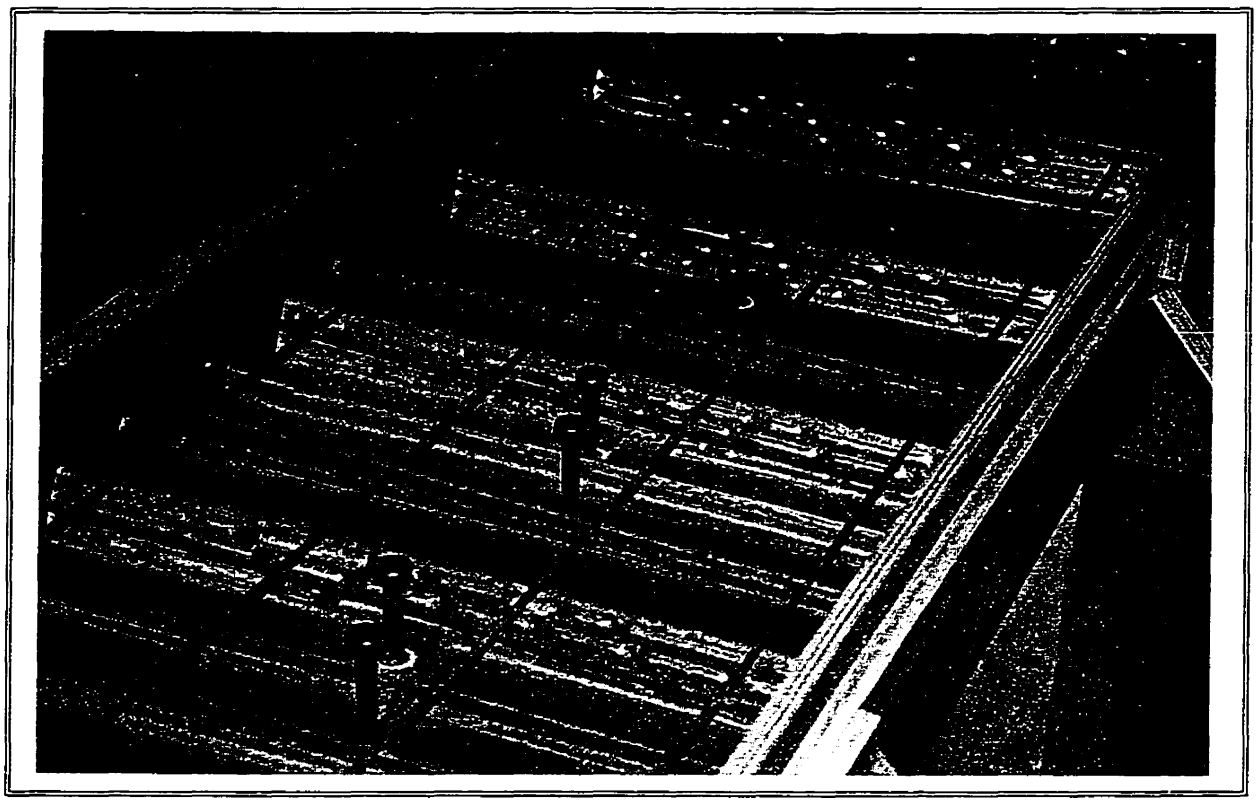

Figure 2.4(b): Shear specimen prior to casting

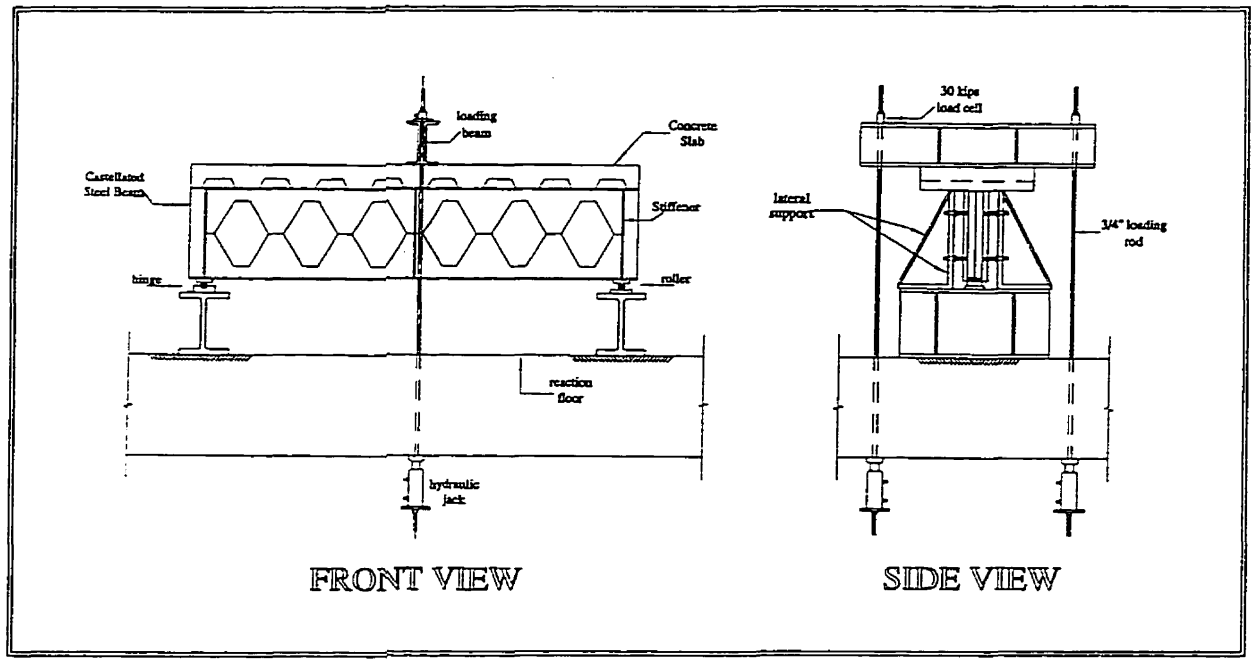

Figure 2.5: Test Apparatus

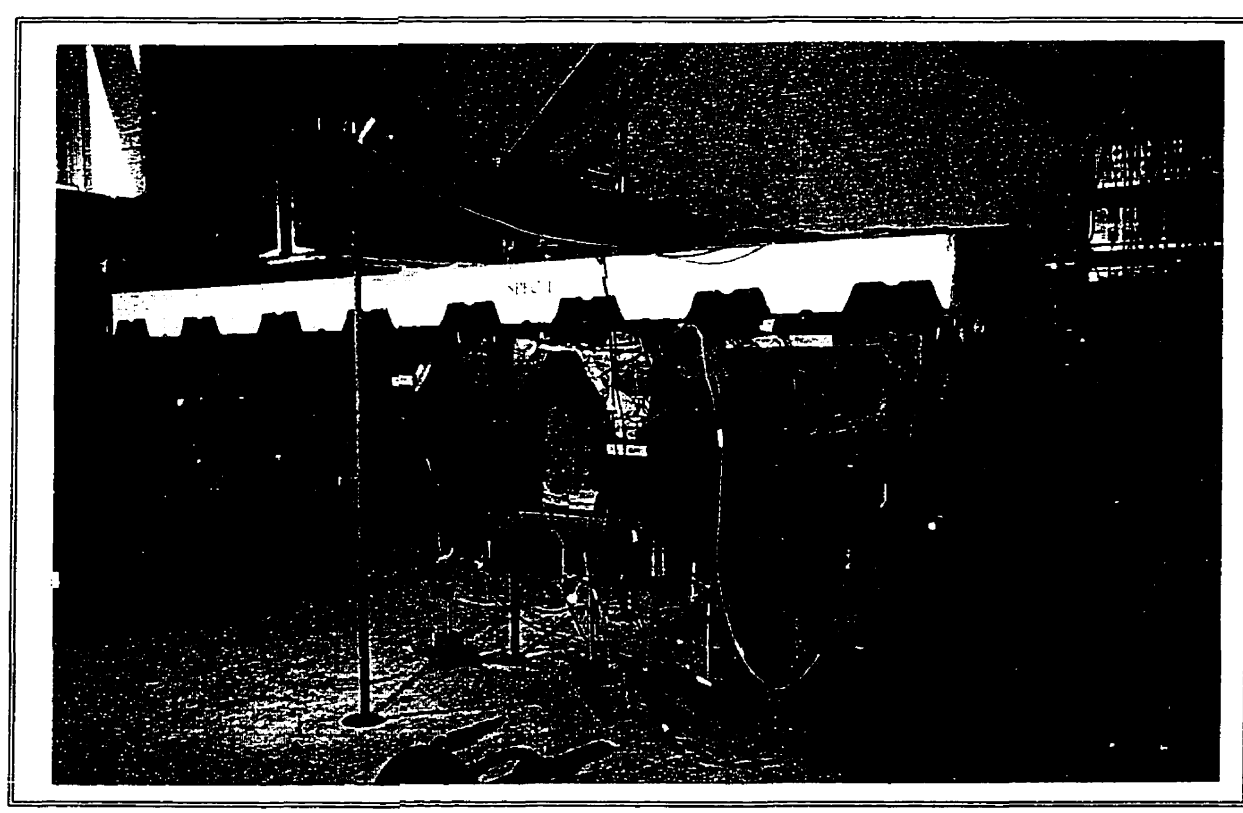

Figure 2.6: General test arrangement (Specimen 1)

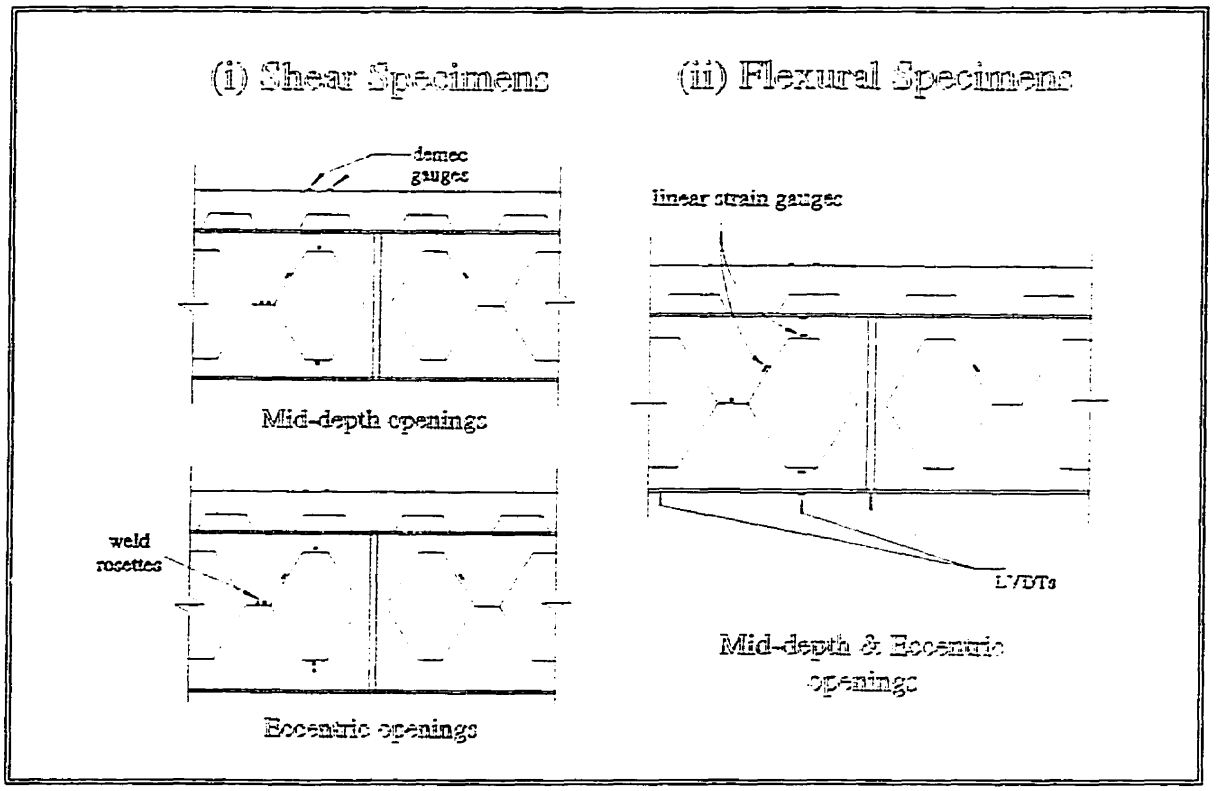

Figure 2.7: Location of strain gauges

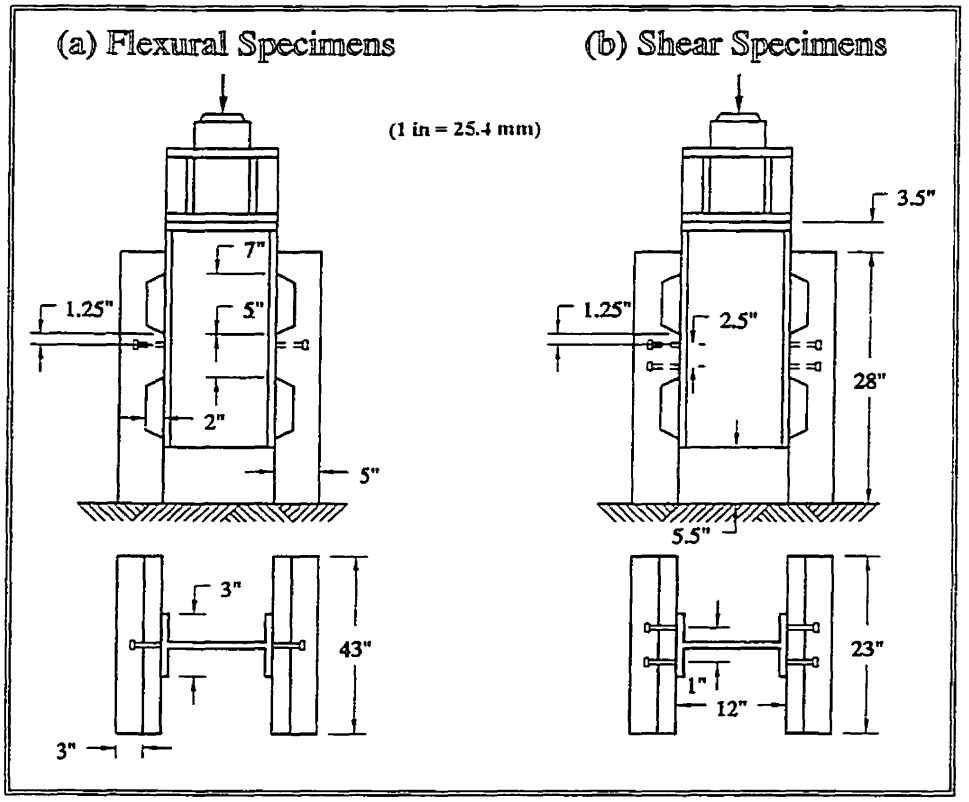

Figure 2.8(a): Push-out test arrangement

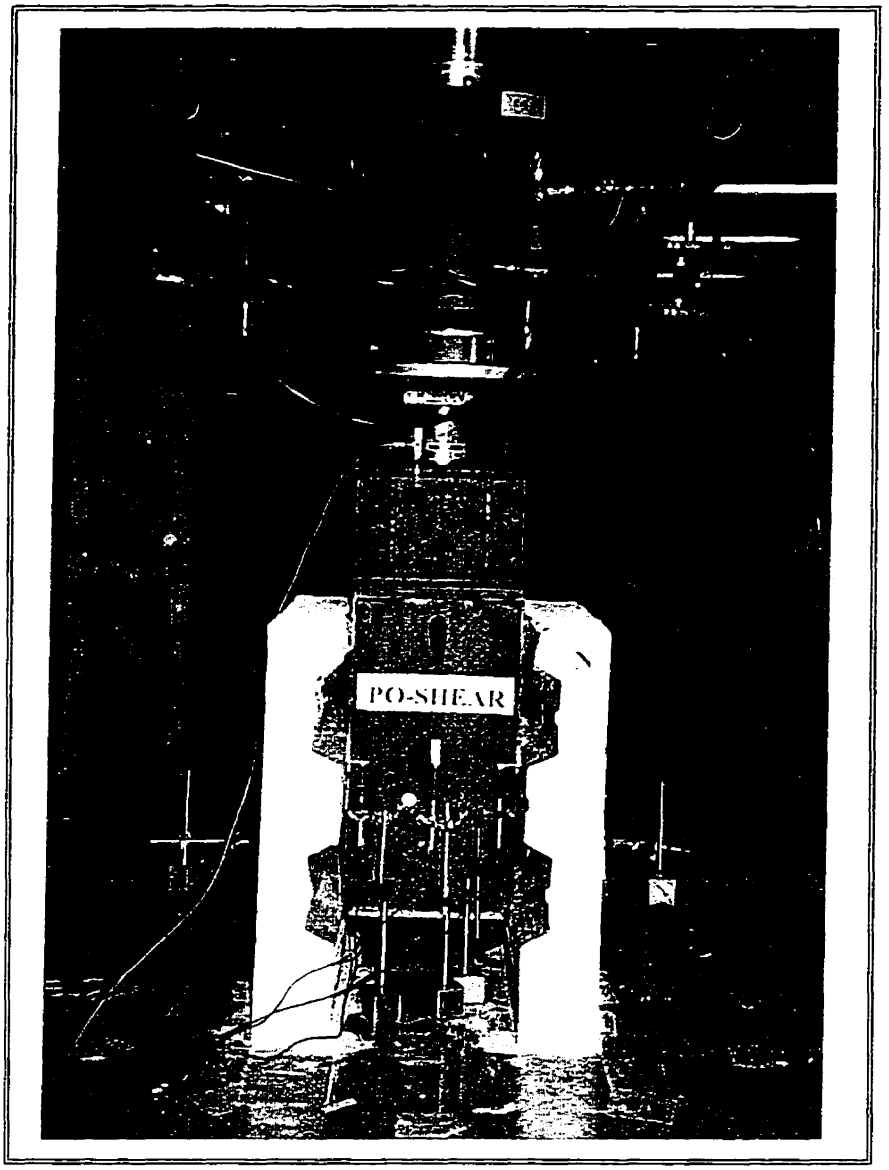

Figure 2.8(b): Push-out test (Shear specimen)

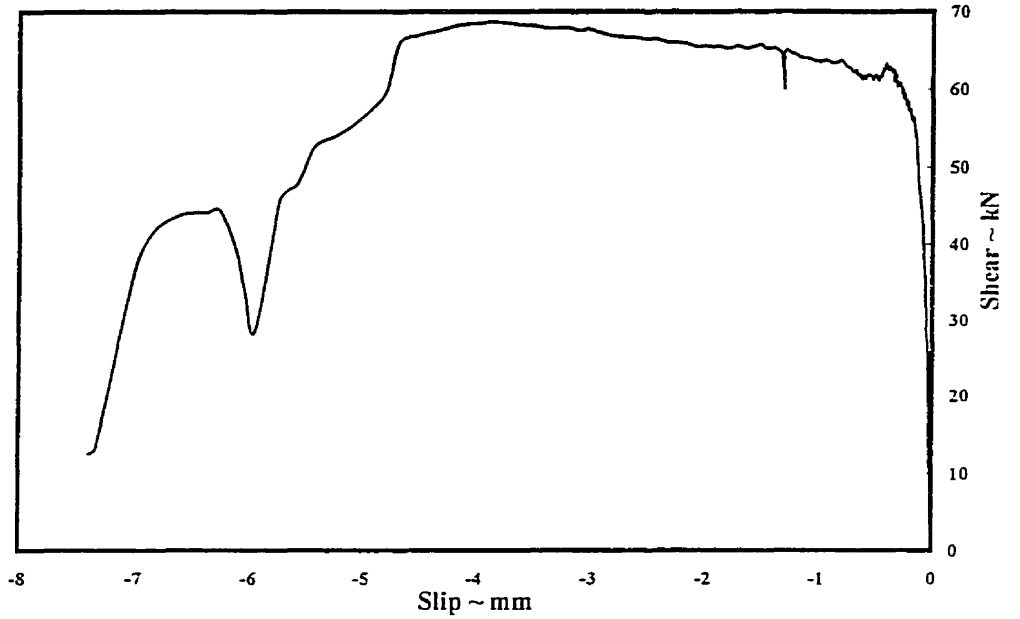

Figure 2.8(c): Shear vs. Slip ~ Push-out test for flexural specimens (1 stud/rib)

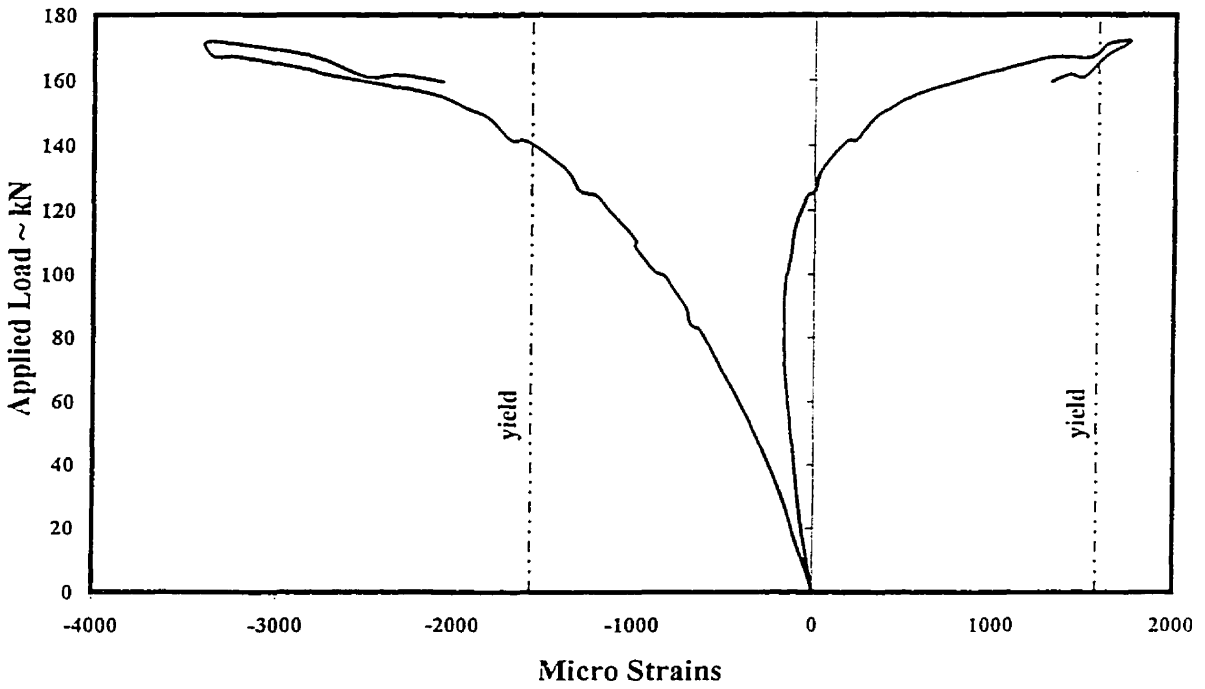

Figure 2.9: Applied load vs. Web strains (Specimen 3)

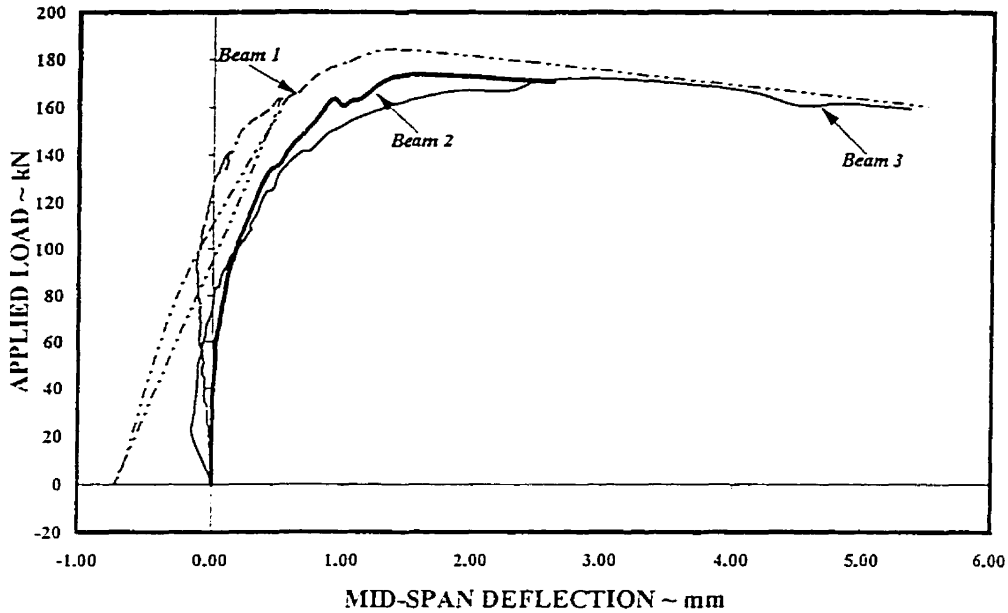

Figure 2.10: Load-deflection curve for shear specimens (Specimens 1, 2 and 3)

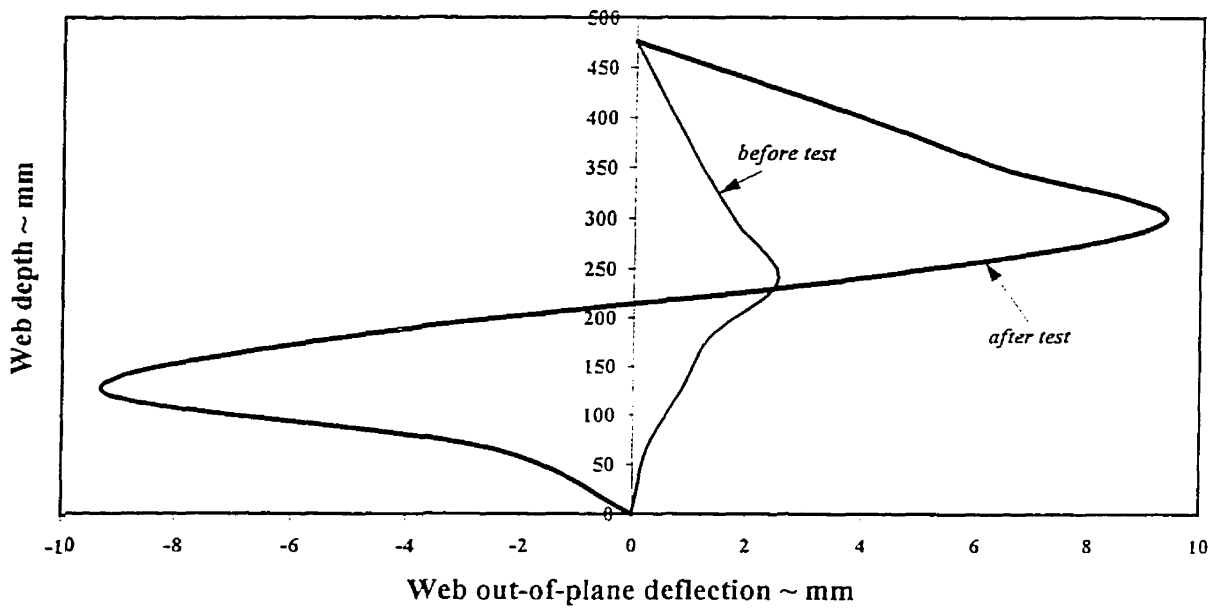

Figure 2.11: Web-post profile before and after testing (Specimen 1)

Figure 2.12(a): Web-post buckling (Specimen 1)

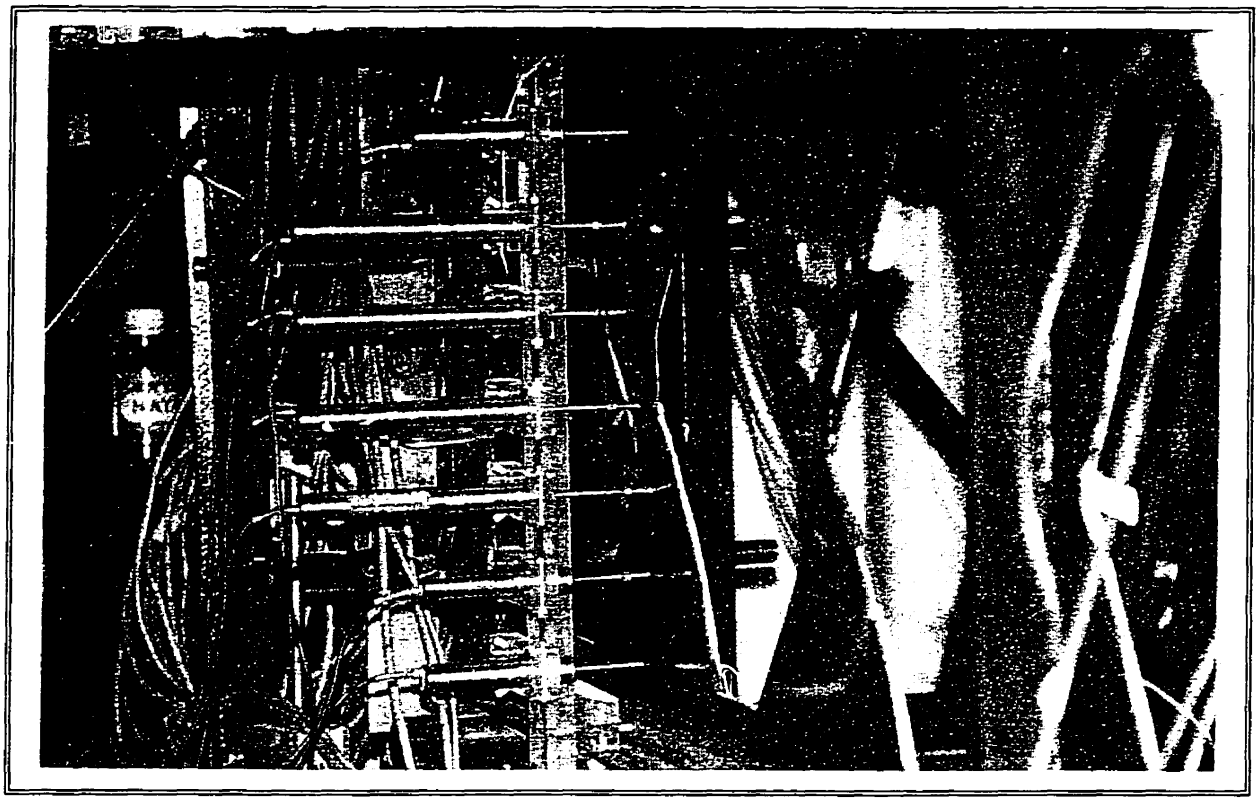

Figure 2.12(b): Web-post buckling (Specimen 2)

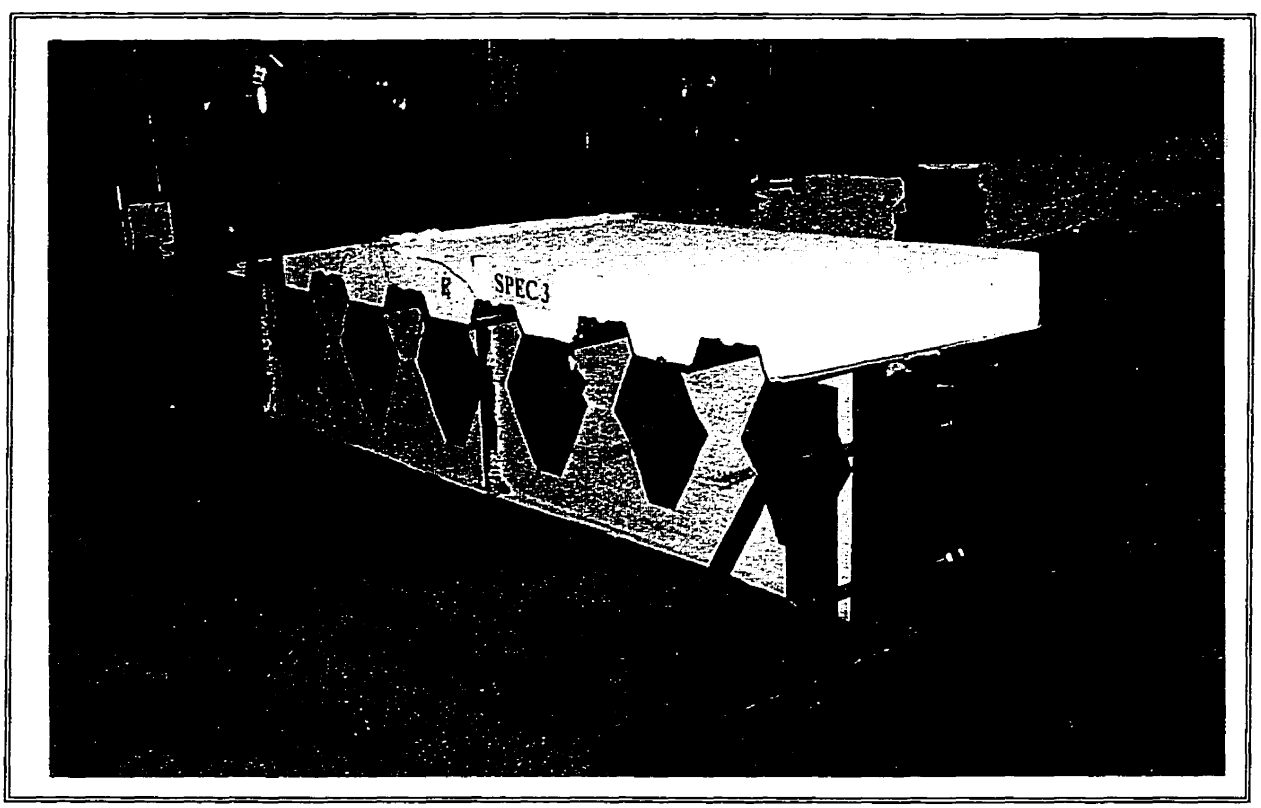

Figure 2.12(c): Web-post buckling (Specimen 3)

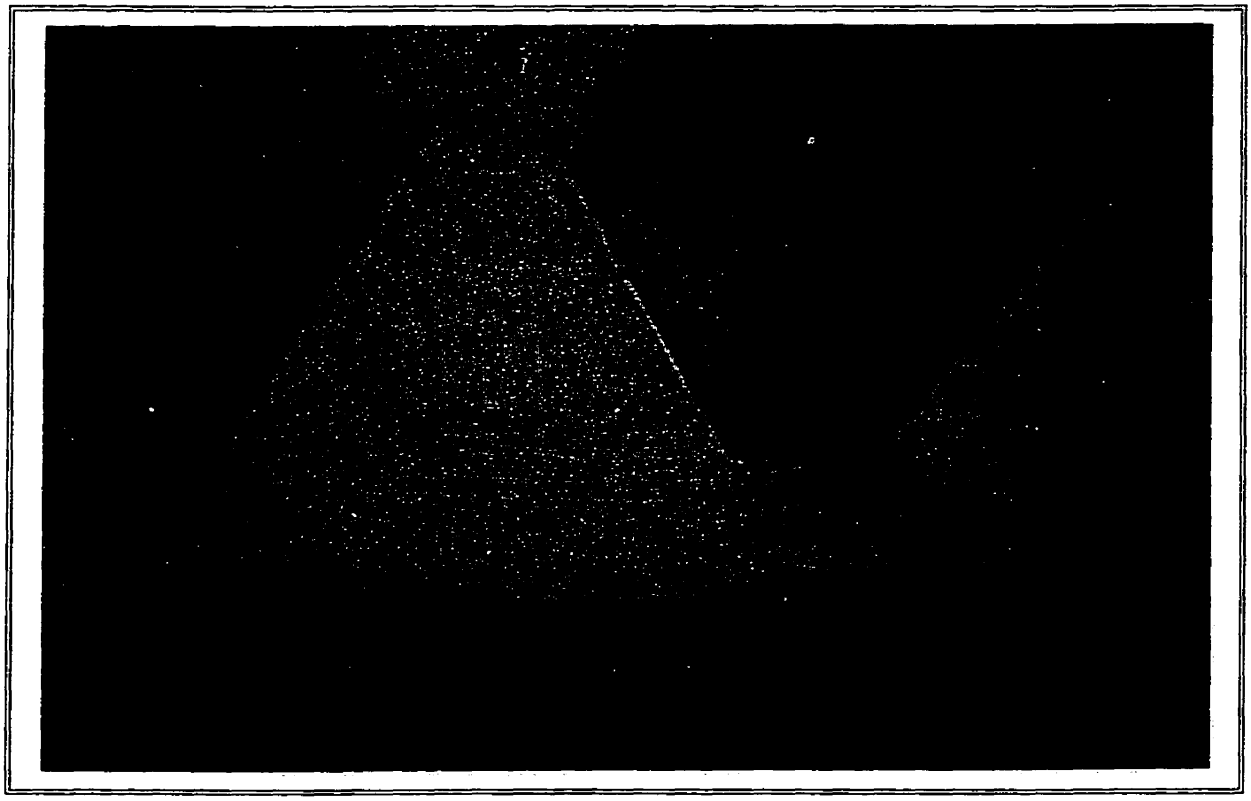

Figure 2.13(a): Bottom tee-section yield during test (Specimen 4)

Figure 2.13(b): Bottom tee-section at ultimate (Specimen 5)

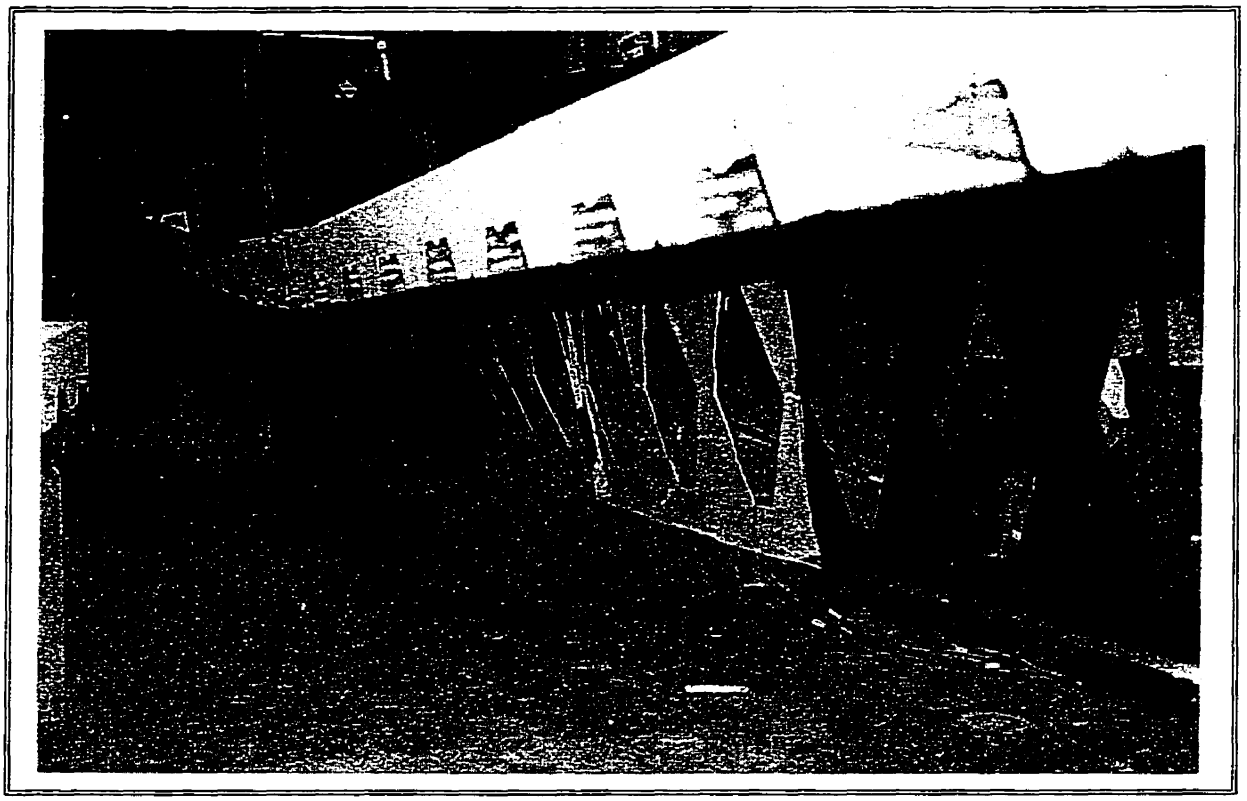

Figure 2.14: Specimen 5 after failure

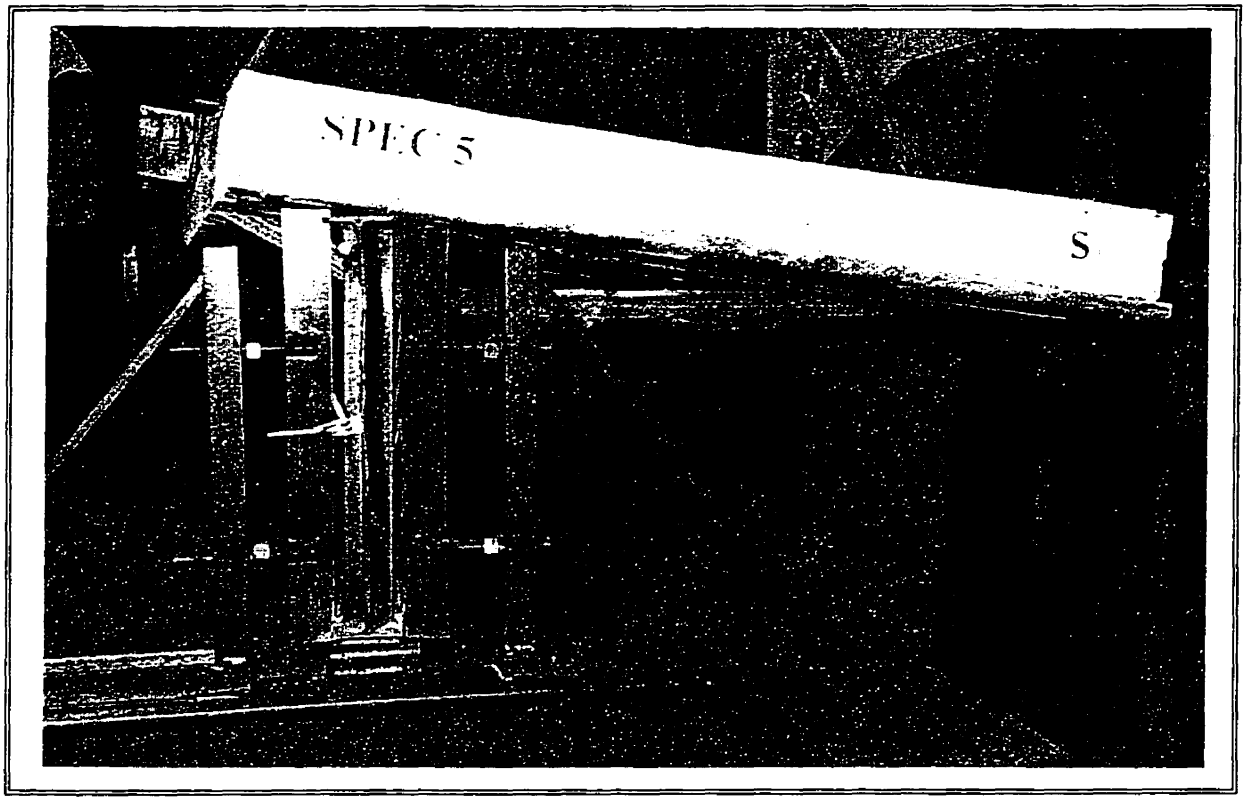

Figure 2.15: Final position of specimen 5 after failure (South end)

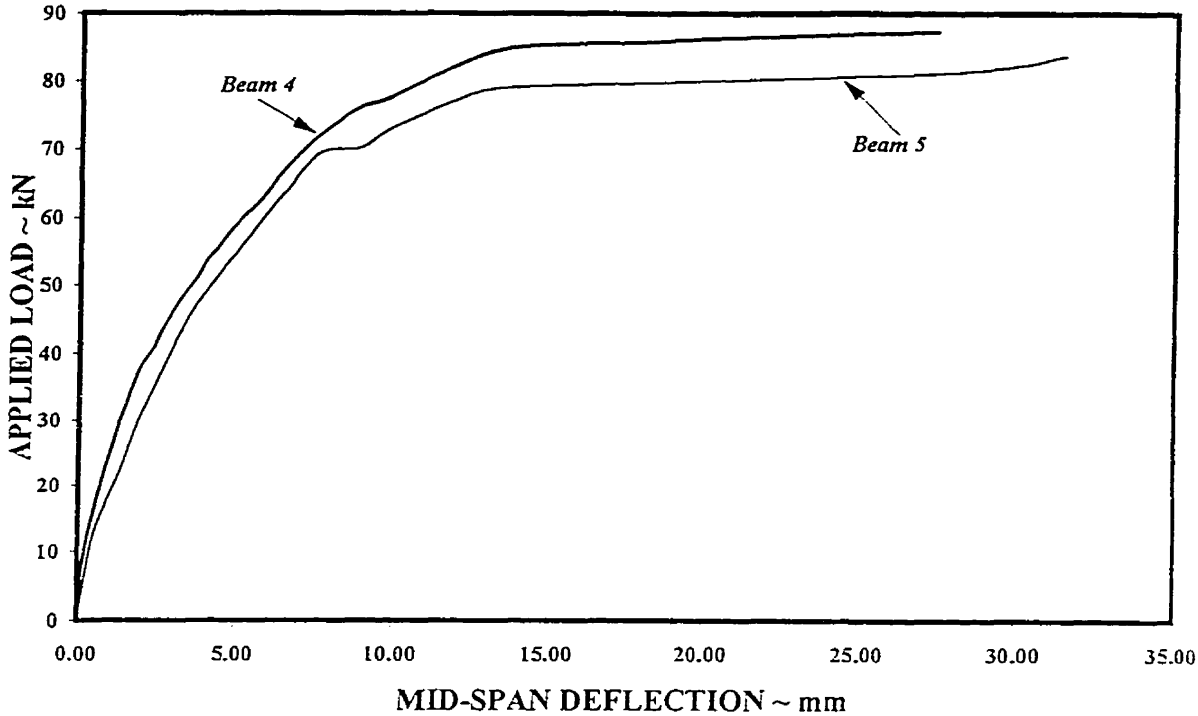

Figure 2.16: Load-deflection curve for specimens 4 and 5

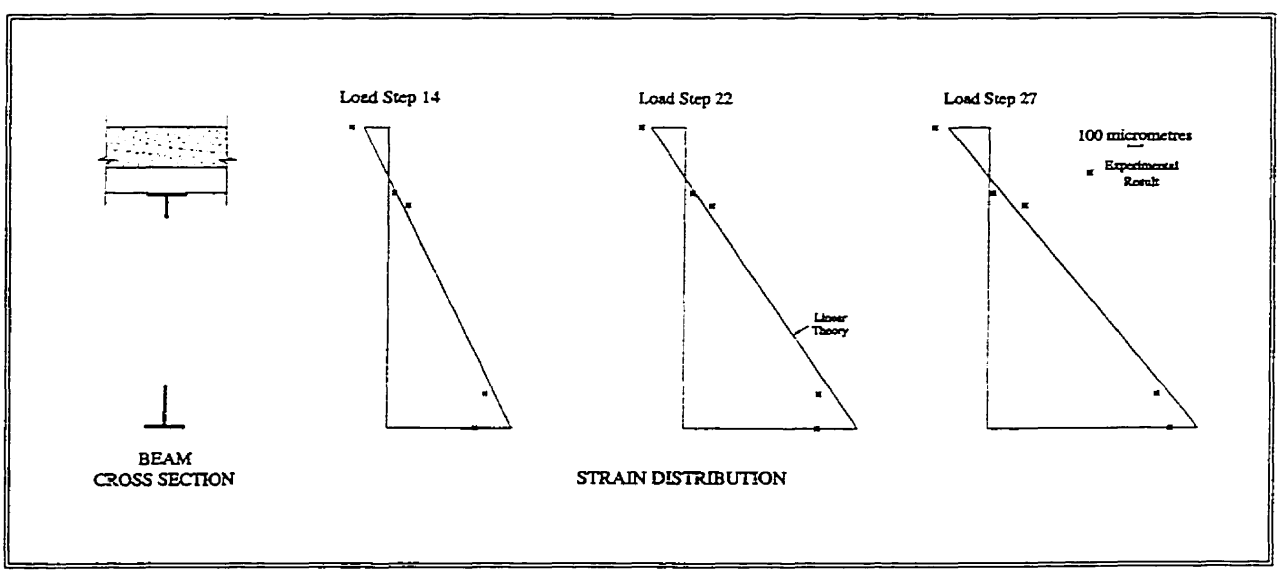

Figure 2.17: Strain distribution through the depth of Specimen 4 (at centreline of Hole 8)

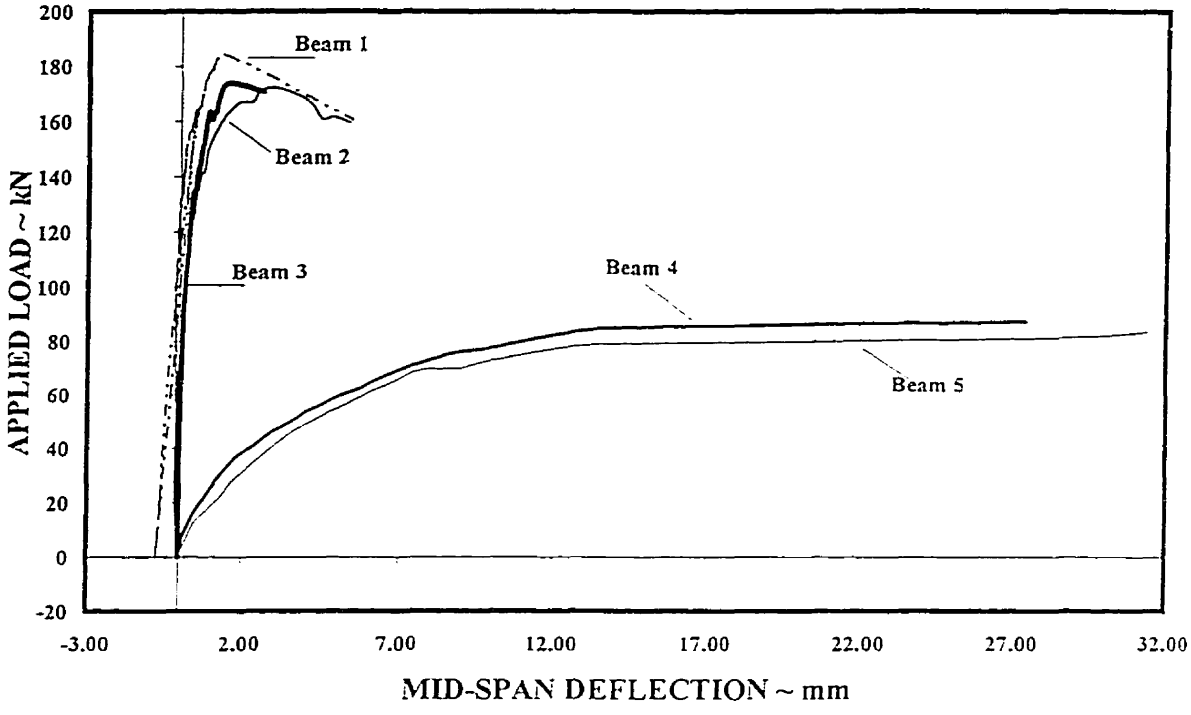

Figure 2.18: Load-deflection curve for all five test specimens

CHAPTER THREE

FINITE ELEMENT ANALYSIS

3.1 General

The goal behind using the Finite Element Method (FEM) is first to simulate the experimental work described in the previous chapter. Moreover, it was also desired to verify whether one could perform numerical analysis on composite castellated beams using the FEM, where quick, reliable and cost effective results could be realized.

This chapter describes the different aspects of the finite element model and the various parameters considered in modeling the composite and non-composite specimens. The finite element package, MSC/NASTRAN, developed by *The MacNeal Schwindler Corporation*, was used in this study. One of the main reasons behind choosing the MSC/NASTRAN package is its nonlinear analysis and buckling capabilities. Moreover, in the previous work by Zaarour and Redwood (1996), acceptable results were obtained using the NASTRAN package, where it was successfully used in modeling the shear buckling failure of web-posts in non-composite castellated beams. A brief description of generating a NASTRAN input file as well as the performing of non-linear stress and buckling analysis is provided in Appendix A.

3.2 The Finite Element Model

In the previous work by Zaarour and Redwood (1996), FEM studies on the buckling of the web-posts in non-composite castellated beams were based on the modeling of a single web-post and parts of the beam in the immediate vicinity, Figure 3.1. A bifurcation analysis was performed, where the material was modeled as elastic-perfectly plastic.

Due to the need to investigate partial shear connection in the composite models, the limited region modeled in the previous work was no longer adequate. Consequently, a length of beam comprising two openings was employed, Figure 3.2. The model was based on the composite castellated shear specimens, which spanned 2184 mm and housed six hexagonal openings as shown in Figure 3.3. This same model was also used in investigating the effect of opening eccentricity, in relation to the beam mid-depth, on the nonlinear buckling behavior of web-posts and on the shear distribution in both composite and non-composite castellated beams. Figures 3.4(a) and 3.4(b) show the two finite element models used in the composite and non-composite cases.

Nominal dimensions were used in generating the finite element models. The loading and boundary conditions were selected such that the actual conditions of the experimental work, described in the previous chapter, could be simulated. The finite element model chosen in this study was based on the shear specimens, from the experimental program, which failed by lateral-torsional buckling of the web-posts. In these shear specimens, the critical posts are those on either side of mid-span, where moment is a maximum, Figure 3.5. However, the effect of moment on the web-post behavior is known to be small, and it was therefore decided to model only the first web post instead of the two posts, Figure 3.2, for reasons of computing economy. The two posts buckled simultaneously during the testing operation. This notion was also reported by Kerdal and Nethercot (1984), who state that in most cases all the web-posts in a span under a shear force of constant magnitude could buckle more or less simultaneously, as was the case in our experimental observations. Another advantage of modeling the shear beams in this way is that the same boundary conditions and support conditions as those used in the test program can be retained.

Symmetry was used to reduce the size of the finite element model. The finite element model was first developed for non-composite castellated beams, and then it was enhanced to model composite castellated beams. The grid point and element numbering schemes were specifically chosen to facilitate changes in the model, pertaining to hole geometry, opening eccentricity, slab dimensions, and shear connector stiffness.

3.3 Mesh Description and Element Allocation

3.3.1 The non-composite castellated beam finite element model

A three-dimensional finite element model of length (2S), twice the opening pitch, was used in representing the non-composite castellated beams, as shown in Figure 3.4(a). In this model, the web, flanges and stiffeners were modeled using two-dimensional, isoparametric, membrane-bending quadrilateral elements. The web shell elements were oriented in the x-y plane, while those of the stiffeners lay in the y-z plane. On the other hand, the flange plate elements were oriented in the x-z plane, as indicated in Figure 3.4(a).

These elements were defined in MSC/NASTRAN using the CQUAD4 input card. Their material properties are defined using the PSHELL input card. The CQUAD4 Nastran card defines the element number, material property number, and the four grid points whose physical location determines the length and width of the individual element. Meanwhile, the PSHELL Nastran card relates to the material property cards MAT1 & MATS1, which are used in conjunction to define the material properties for non-linear analysis, as in our case. These material cards together define the following: element thickness, elastic modulus, yield stress, poisson ratio, type of material nonlinearity, hardening rule, and yield function criteria.

The material properties allocated to these steel elements are based on coupon tests previously performed on samples taken from the web and flanges. These properties are summarized in Table 3.1. The actual Nastran material cards containing the above properties can be found in the sample input file supplied at the back of this report in Appendix B.

This study was concerned with investigating the shear buckling failure of the web-posts and also with the shear distribution in the upper and lower tees at an opening as well as in the concrete slab, in the composite case. As a result, a fine mesh was assigned to these zones, as can be seen in Figure 3.6, to better model their behavior and also to obtain more accurate results. This is particularly important for modeling

the web-post buckling and for good representation of the buckled mode shapes. This can usually be accomplished by assigning at least five nodes per half a sign wave of a deformed shape, Caffrey and Lee (1994). A sample model and its buckled shape can be seen in Figure 3.6.

A total of eight finite element models of different geometries was used in the investigation of non-composite castellated beams. Table 3.2 lists the different parameters relevant to these non-composite models, while Figure 3.7 illustrates these parameters.

3.3.2 The composite castellated beam finite element model

The finite element model used here to model the composite castellated beams is identical to that used in modeling the non-composite specimens, except for the introduction of the steel shear connectors and the concrete slab elements shown in Figure 3.4(b). Here the shear connectors and the concrete slab are modeled using one-dimensional beam elements with nonlinear capabilities. The shear connectors are defined in MSC/NASTRAN using the CBEAM card, while its material properties are supplied in the PBEAM card.

The original composite model devised here was based on specimen 2 of the experimental program. This shear specimen had a clear span of 2184 mm (86 inches) and each rib housed two studs to achieve the appropriate degree of connectivity. The steel deck profile used to support the slab had a height of 51 mm (2 inches) and is shown in Figure 2.3. Consequently, each shear specimen contained 7 ribs and 14 studs, which ultimately provided partial shear connection, as was explained earlier in the experimental work. On the other hand, since the finite element model spanned only 712 mm (28 inches), twice the opening pitch *(2S)*, this meant that only 2 ribs (4 studs), representing partial shear connection, could be accommodated in the NASTRAN model.

The concrete slab modeled here corresponds to that of the actual shear specimens, which had an effective cross sectional area of 44516 mm^2 (76 mm thickness and 584 mm wide). The concrete slab was modeled using one dimensional beam elements, defined via the CBEAM & PBEAM Nastran cards. In addition, it was modeled as a nonlinear-elastic material conforming to the stress-strain curve shown in Figure 3.8(a). The curve is defined in the first and third quadrants to accommodate the concrete ultimate compressive strength as well as its reduced tensile strength; this is done through the MATS1 and TABLES Nastran cards, as shown in the sample input file in Appendix B.

The concrete slab had an ultimate compressive strength of 38.5 MPa, as determined from the concrete cylinder compressive tests in the experimental program. Normal weight concrete was assumed. The modulus of elasticity was obtained from the concrete cylinder compressive test (29,430 MPa), and was then compared with that from the well known formula (A23.3 formula):

$$E_c = w_c^{1.5} \cdot (0.043)\sqrt{f_c'} \quad , w_c = 2300\ kg/m^3$$

Other relevant parameters used to define the slab parameters are shown below:

- *Moment of Inertia in Plane 1* = $I_1 = I_{zz} = b.h^3/12$
- *Moment of Inertia in Plane 1* = $I_2 = I_{yy} = h.b^3/12$
- *Torsional Constant* = $J = bh^3\{1/3-0.21(h/b)(1-h^4/12b^4)\}$; *b=long side, h=short side*

An orientation vector of (0,1,0) was used to orient the slab element local y-axis, which is an important feature in interpreting the Nastran results. As a result of modeling the concrete slab as beam elements, connecting the top steel flange to the neutral axis of the effective slab area, via the shear connectors, had to by means of studs having a length of 89 mm (3.5 inches) instead of their original 76 mm (3 inches). This is indicated in Figure 3.8(b).

As mentioned earlier, since the chosen finite element model spanned only 712 mm, twice the opening pitch *(2S)*, only 2 ribs (4 studs), representing partial shear connection, could be accommodated in the NASTRAN model. The studs are modeled as a frame beam element with fixed-pined end connections capable of transferring shear and moments, as was the case with slab elements. Thus, the stiffness of these BEAM

elements were modeled as $k = 12EI/l^3$. The steps taken to model the shear connectors are as follows:

- The stiffness of the actual studs were obtained from the results of the shear specimen push-out test (2 studs/rib), Figure 2.8(a), where the initial stiffness of each stud was found to be 175 kN/mm. This stiffness was then kept constant.

- The total stiffness for the original four studs is computed and then distributed to each of the nodes along the web-flange junction of the Nastran model according to the node spacing (a total of 25 nodes were used), Figure 3.4(b).

It was practical to model the stiffness of the studs by keeping the modulus and length constant while varying the inertia. This allowed for the possibility of modeling partial shear connection. The area and torsional factor for the modeled studs were also determined accordingly. A spreadsheet was developed to perform the appropriate calculations for the different beam models in this research program. A yield stress of 345 MPa and a modulus of elasticity of 200,000 MPa was used for the studs based on the manufacturer's specifications. An orientation vector of (0,0,1) was used to orient the y-axis of the studs, and an elasto-plastic material nonlinearity was also employed.

In all, eight different element models were utilized in the study of composite castellated beams; their properties are summarized in Table 3.3.

3.3.3 Boundary Conditions

The simplest boundary conditions were adopted in both composite and non-composite models to prevent rigid body movement. The boundary conditions assumed in both models are shown in Figure 3.9. The x, y, and z notations represent translation constraints in the specified directions.

In the non-composite cases, at the right hand side (RHS) of the model, translation constraints in the x-direction at the upper and lower flanges, Figure 3.9, were provided to prevent rigid body rotation about the z-axis. This will also serve to indirectly

impose the appropriate moment at the RHS of the model via the coupling system developed by the horizontal constraint forces and the lever arm separating them. The statics resulting from these loading and boundary conditions were verified for each analysis and were considered to satisfactorily represent the conditions at the end of the beam. The left hand side (LHS) of the model was constrained in the y-direction at the mid-depth of the web in order to represent a roller support. The z-translational constraints in the model are used to prevent the model's rotation about the x-axis.

It should be noted that even though the grid points define the corners of the CQUAD4 web, flange and stiffener elements, each element is elastically connected to only five of the six degrees of freedom at each of its grid points. Hence, the element does not provide direct elastic stiffness to the sixth degree of freedom, i.e. rotational degrees of freedom about the normal have zero stiffness. Unless precaution is taken, this zero stiffness will result in a singularity matrix. Consequently, measures were taken in the finite element model to suppress these singularities. This was done by constraining all the grid point D.O.F. normal to the plane, except for the nodes at the web-flange junction and the web-stiffener junction, because these have components with rotational stiffness.

The composite model, Figure 3.9, incorporates the same boundary conditions as those used in the non-composite model, with the addition of an x-translational constraint to the RHS node of the concrete slab. This was done to insure that the slab will have the same boundary conditions as that of its steel counterpart, and also for it to contribute to the over all acting moment on the RHS of the finite element model.

3.3.4 Load Application

The actual test specimens were simply supported and were loaded at mid-span with a single monotonic point load. As a result, beam and load symmetry was used in modeling the experimental work. The finite element model used represented only half of the a simply-supported beam, and hence was subject to a uniform shear. The shear force was divided into two vertical loads acting on the RHS of the model, Figure 3.2;

these were exerted on the upper and lower flanges to avoid local instabilities from a single concentrated load, and to take into account the role of the stiffener.

3.4 Results and Discussion

3.4.1 Non-Composite Beams

In castellated beams, in regions of high shear, web-posts between openings may prove to be the critical factor governing the ultimate carrying capacity of a beam: in the case when the beam has mid-depth perforations, a web-post is acted upon by two equal and opposite moments and the resulting shearing forces may cause the web-post to fail by lateral buckling out of the beam plane (Aglan and Redwood 1974).

A finite element numerical study was performed on eight non-composite castellated models using the MSC/NASTRAN package; this consisted of performing non-linear stress and buckling analyses using the modeling shown in Figure 3.4(a). A summary of the dimensions used in these models is presented in Table 3.2. Beams 1A and 1F correspond to the end section of the non-composite version of Beams 2 and 3 of the experimental program, with mid-depth and eccentric openings. In all FE models, Figure 3.10, failure occurred by lateral-torsional buckling of the web-post between the two hexagonal openings. The finite element model used captured the non-linear buckling behaviour of the web-posts in the shear critical castellated beams. The double-curvature buckled shape of a web-post is clearly noticed in Figure 3.11. Plots of the principal stresses in Figure 3.12 illustrate the tension and compression regions, in red and violet respectively, that correspond to the double-curvature action discussed by Aglan and Redwood (1974).

Specimen 12-1 of Zaarour and Redwood (1996), from which the configuration of the composite beams considered in this study originated, provides an experimental result representative of a non-composite version of Beam 2, since the material properties of both beams are very similar. The shear force at buckling, from the FEM, was found to be 59 kN for Beam 1A, while the ultimate strength of Specimen 12-1 was 57.4 kN.

Hence, good agreement between the FEM and this one experimental result was realized (2.7 % difference).

Five finite element models (1A, 1F, 1X, 1Y and 1Z) were used to investigate the effect of opening eccentricity on the buckling behaviour of web-posts in non-composite castellated beams. In addition, three other configurations (2A, 3A and 4A) were employed to address the effect of opening geometry on the shear strength of non-composite castellated beams. In the following sections results for the eight analyzed non-composite castellated beams are compared and discussed. Essential features of the behavior were extracted from the numerical results as follows:

(i) Elastic stress distributions were first examined to determine the distribution of vertical shear above and below an opening, and the shear force and bending moments in the web-post. These were established using the free-body diagram of a portion of the beam, spanning between the centerlines of two adjacent openings, as illustrated in Figure 3.13. This free-body diagram was also utilized in performing equilibrium checks to verify the adequacy of the finite element models. Several spreadsheets were developed to interpret the NASTRAN output and to perform the appropriate calculations. This involved computing stress resultants from the output stresses at element centroids; in some cases this required interpolation, for example to obtain stresses on the vertical section through the mid-length of the openings. The horizontal shear in the web-post was computed at the centroids of the elements on one side of the hole mid-depth. For the configuration of the hole in these beams, the web-post width at this level was between 20 and 30% greater than the minimum web-post width. While this provides an accurate assessment of the shearing force predicted by the FEM, it will lead to an overestimate of the shearing force which will cause yield at mid-depth of the web-post (i.e. the welded-joint). A summary of these results, concerning the non-composite cases, is presented in Table 3.4.

(ii) From the above parameters the following were derived, and are given in Table 3.5:

(a) the ratio of horizontal web-post shear to vertical shear on the beam, V_h/V_v.

(b) the web-post shear, V_{hcr}, corresponding to the beam shear at failure, V_{cr}, is given, assuming the ratio found in (a) is applicable.

(c) the ratio of V_{hcr} to the web-post shearing force which would cause yield at the mid-depth of the web-post, V_{ph}, (based on the width at the level of the CQUAD4 elements centroids).

(d) the ratio of the moment at the top of the web-post to that at the bottom, M_1/M_2.

It should be noted that the results in Table 3.4, which refer to the free-body diagrams in Figure 3.13, are based on an applied beam shear (V_v) of 10 kN. This beam shear was selected as a common value for all the finite element models; this was justified by the fact that the overall stress distribution did not change significantly as buckling was approached, indicating the minor role played by inelastic action. A similar treatment is given for composite sections (Table 3.6 and Figure 3.16).

3.4.1.1 Effect of Opening Eccentricity (Non-composite beams)

Five finite element models (1A, 1F, 1X, 1Y and 1Z) were used to investigate the effect of opening eccentricity on the buckling behavior of web-posts in the non-composite beams. The opening configuration shown in Figure 3.14 was utilized in this study, and opening eccentricity was varied between 0 and 40 mm; Table 3.2 summarizes the properties of these models.

Figure 3.15(a) shows that for the maximum possible eccentricity, the shearing force carried by the top and bottom tee-sections is in the ratio of 35:65; nevertheless, the horizontal shearing force carried by the web-post changes only slightly, as can be deduced from Figure 3.15(b). There is also a change in the moments produced by the stress resultants at the top and bottom of the critical post; the variation of moment ratio ($M1/M_2$) with opening eccentricity is illustrated in Figure 3.15(c). The maximum change is from 1.0 to 0.74. The effect of this is to reduce the double-curvature bending in the post, thus causing a more severe condition affecting the lateral buckling of this region. However, beam theory suggests that the effect of such a change would

be small. Figure 3.15(d) shows the variation of shearing force in the beam when buckling takes place. Due to this effect as well as due to the change in the shear force in the post, it can be concluded that opening eccentricity has only a minor impact on the buckling behavior of web-posts in non-composite castellated beams.

3.4.1.2 Effect of Opening Geometry (Non-composite beams)

Three finite element models with different opening configurations (2A, 3A and 4A) were studied to determine the effects of hole geometry (angle of cut, opening pitch, and welded joint length), on the buckling behaviour of web-posts in non-composite castellated beams. For these models, the opening configurations and finite element results are presented in Tables 3.2 and 3.5, while results pertaining to the free-body diagram mentioned earlier are summarized in Table 3.4. It should be noted that no experimental results are available for these sections; the finite element results obtained here are compared with those of the original non-composite section (Beam 1A).

From the FEA results of 2A, it can be noticed that 33% reduction of the welded joint length, from 76.2 mm to 50.8 mm, caused virtually no change in the vertical shear carrying capacity (0.2%). The configuration of 2A resulted in a lower shearing force in the web-post (88% of that in 1A) for the same vertical shear; this lower force together with the changed configuration led to virtually the same vertical shearing force when the post buckled.

In 3A, reduction of the angle of cut from 59.9° to 52.5° increased the web-post width at the top and bottom ends while maintaining the same minimum width as in 1A (76.2 mm). The beam shear carrying capacity increased by 4%. For the same vertical shear, this beam had 18% greater shear in the web-post than 1A.

Beam 4A had a 16.6% reduction in opening height and 33.3% reduction in welded-joint length compared with 1A, and the ratio of horizontal to vertical shear was 86% of 1A. The vertical beam shear capacity increased by 25%. This increase in strength is clearly due both to shorter height of the web-post and the lower shear in it for a given

beam shear. It should be noted that although the configuration of Beam 4A resulted in improved buckling behavior, the smaller opening height means that the web-post is more shear critical, and the reduced welded-joint length also limits the amount of shear that can be carried by the web-post prior to shear yield on the minimum section. As indicated in Table 3.5, web-post failure in this case coincided with yield along the weld. The ratio of horizontal shear to horizontal yield force was only 0.63 in 1A, compared with nearly 1.0 in 4A.

Overall, it can be concluded that while benefits can be realized from altering the opening geometry by decreasing the angle of cut, reducing the length of the welded joint, or by reducing the opening height, there exists a limit as to selecting these parameters.

3.4.2 Composite Beams

The effect of making a beam composite will be to significantly increase the flexural resistance of the steel section; it is however uncertain what effect this will have on the shear resistance. Redwood and Cho (1993) showed that in a composite beam with one isolated web opening, the concrete slab does significantly increase the shear carrying capacity beyond that of the non-composite section. This is because of the enhanced flexural capacity of the upper part of the beam within the length of the opening; there is no reason to anticipate that the web-post will be less susceptible to buckling in the composite section.

Here, a numerical study, using the FEM, is performed on eight composite sections. The study entails carrying-out non-linear stress and buckling analyses on these sections to investigate their shear carrying capacity as well as determining the shear distribution in the steel and concrete components at the centerline of an opening. The properties of the finite element models are presented in Table 3.3, and a summary of the finite element results is found in Table 3.6. These results are based on the free-body diagram shown in Figure 3.16, and are similar to those described earlier for the non-composite cases. In all cases failure occurred by buckling of the web-post between the two

hexagonal openings; Figure 3.17 illustrates the deformed and undeformed web-post shape for Beam 1B. The double curvature buckled shape can be clearly seen in Figure 3.18, while plots of the major principal stresses in Figure 3.19 demonstrate the tension and compression regions, red and violet respectively, in the web-post associated with the double-curvature action. The following discussion makes use of the same parameters derived from the FEA as used for the non-composite beams, as defined in section 3.4.1. FEM values for the composite beams are given in Tables 3.6 and 3.7.

From the principal results summarized in Table 3.7, it can be seen that in all cases, the shearing force in the web-posts when failure occurred exceeded 90% of the web-post yield capacity, and three cases exceeded 96%. Thus yielding at mid-depth of the post is expected to be more significant than in most of the corresponding non-composite beams (the exception being 4A and 4B). Also, in all cases, the ratio of the web-post shearing force to vertical (or beam) shearing force is lower than in the corresponding non-composite beams.

3.4.2.1 Modeling of Test Beams (Composite beams)

The end regions of Beams 2 and 3 of the experimental program were analyzed using the proposed finite element model (1B and 1G) and were compared with the corresponding non-composite cases (1A and 1F). Web-post buckling modes were evident in both cases. The composite beams were found to have significantly higher ultimate shearing forces than the corresponding non-composite ones; the increase given by FEA was 67% and 48% for beams 2 and 3 respectively. The experimentally determined increase for Beam 2 was 59%.

It is of interest to compare these increases to those expected for bending ultimate capacities. No tests were performed for the long non-composite beams subject to flexural failures. However, the theoretical increase in ultimate bending capacity of the composite beams compared with the non-composite equivalent for Test Beams 4 and 5 was about 60%, that is, very similar to the observed increase in web-post buckling

capacity. This result however pertains only to the sections tested in the experimental program, and no general conclusions can be drawn.

Referring to the FEM results in Tables 3.6 and 3.7 and to Figure 3.16, it can be deduced that composite action reduces the shear acting on the web-post, hence providing it with an extra reserve to carry more load, which explains the increased overall beam shear carrying capacity, Beam 1B versus 1A. The composite action also caused a reduction in the amount of vertical shear carried by the tee-sections due to the slab contribution to carrying some of the shear, hence reducing that to be carried by the steel section. In addition, it is clear that for Beams 1B and 1G, for the same vertical shear, the web-post shearing forces are 87% and 89% of the non-composite values (Beam 1A and 1F), suggesting an increase in strength provided the failure mode is unchanged.

3.4.2.2 Effect of Opening Eccentricity (Composite beams)

Two finite element models (1B and 1G), used to represent Test Beams 2 and 3, are employed here to investigate the effect of opening eccentricity and composite action on the buckling behavior of web-posts in composite castellated beams. The FEA results are given in Tables 3.6 and 3.7. It can be seen that making the beams composite improved the shear carrying capacity by 67% and 48% over that of the non-composite cases (1A and 1E). It was noted earlier from FEA of the non-composite cases, for Beams 2 and 3, that the effect of opening eccentricity was to increase the shear capacity by 6.2 %. Here, on the other hand, while a great improvement is noted in the shear carrying capacity in the composite cases, FEA suggests that opening eccentricity reduces the shear capacity by 5.8%. This can be attributed to the change in the moment stress resultants at the top and bottom of the post, which reduce the double-curvature bending in the post, thus causing a more severe condition affecting the lateral buckling of the region. This is illustrated in Table 3.7, by the reduction in M_1/M_2 from 0.97 to 0.91 for Beams 1B and 1G, and by the increase in the web-shear of 1G by 2.6% over that of 1B; these work together to reduce the web-post shear capacity of 1G compared with 1B.

3.4.2.3 Effect of Opening Geometry (Composite beams)

As for the non-composite cases, the modes of failure in castellated beams are principally influenced by beam slenderness, opening geometry (angle of cut, expansion ratio, length of welded joints), as well as the type of loading. Three beams (2B, 3B and 4B) are considered here to investigate the effect of varying the weld length, cut angle and opening height on the shear carrying capacity of composite castellated beams. The non-composite counterparts of these three models are 2A, 3A, and 4A respectively. The opening geometries are summarized in Table 3.3, and the FEM results are found in Tables 3.6 and 3.7. Web-post buckling was evident in all three models; the double-curvature mode shape of the buckled web-post is illustrated in Figure 3.17.

As with the non-composite sections, no experimental results are available for these composite sections, and thus this analysis will rely on the FEA; results will be compared with those from the original composite section, 1B, as well as with the non-composite sections: 2A, 3A and 4A. From the FEM results it can be concluded that the composite beams, 2B, 3B and 4B, were respectively 45%, 45% and 20% stronger than their non-composite counterparts, 2A, 3A and 4A.

Beam 2B, with weld length reduced from 76.2 mm to 50.8 mm, exhibited a 12.8% reduction in the beam ultimate shear carrying capacity, compared to that of 1B. This is attributed to the more slender nature of the web-post of 2B due to the smaller web-post width and also to the smaller M_1/M_2 ratio. It can also be noted that in Beam 2B, less shear is carried by the concrete slab, which imposes more shear on the steel section, aggravating the problem and enhancing the load on the web-post. It is also clear from Table 3.7 that the weld area of 2B is more highly stressed than in 1B, as indicated by the higher ratio of web-post shear at buckling to plastic shear capacity, 0.98 versus 0.95.

Beam 3B had a smaller cut angle (52.5° compared with 59.9°) which resulted in greater pitch between opening centerlines. 3B had 9.5% lower shear capacity than 1B; on the basis of V_h/V_v ratios, (for 3B this is 19% higher than 1B), 3B might have been expected to be 16% weaker. It is evident from the FEM results that both the concrete

slab contribution in shear, and the ratio of M_1/M_2, are very similar for both beams (1B and 3B). The web-post shear at failure in 3B was marginally closer to the shear yield load than in 1B.

Finally, Beam 4B combines the effects of reducing the opening height and the length of the welded joint. The FEM results are summarized in Table 3.6 and indicate that the beam shear capacity is 10.1% less than that of Beam 1B. The reason for this reduced shear capacity can be related to the increased tee-section depth of 4B, which in turn attracts more shear and reduces the shear carried by the concrete slab, Table 3.6. It can also be noted from Table 3.7 that even though the web-post end-moments are less in this case than in 1B, as can be expected from a shorter post, the M_1/M_2 ratio is more critical in 4B than in 1B (0.89 versus 0.97). In Beam 4B, the increased shear capacity combined with the reduction in length of the weld makes the section more susceptible to yield of the welded joint than that of Beam 2B, see V_h/V_{ph} ratio in Table 3.7.

3.4.2.4 Effect of Varying Stud and Slab Stiffness (Composite beams)

Three finite element models (1C, 1D and 1E) were employed in investigating the effect of varying the stiffness of the concrete slab and of the shear connectors on the shear carrying capacity of composite castellated beams. The three composite models have the same steel cross section as that of Beam 1B; their FEM results can be found in Tables 3.6 and 3.7. All three models underwent web-post buckling failures similar to all the other composite and non-composite models, which exhibited the double-curvature configuration. No experimental results are available for these sections, but conclusions will be drawn from comparing their FEM results with those of Beam 1B, corresponding to Beam 2 of the experimental program.

Beam 1C is identical to Beam 1B except for doubling the effective width of the concrete slab. From the free-body diagram shown in Figure 3.16 and the results in Table 3.6, it can be deduced that doubling the slab width had only a minor impact on the overall results, and the shear carrying capacity of this model was found to be 2% less than that of Beam 1B.

Beam 1D is identical to Beam 1B except for reduced stiffness of the shear connectors as indicated in Table 3.3. This was done in an attempt to represent the effect of partial shear connection. The shear carrying capacity of Beam 1D is about 10% lower than that of 1B; it is still 51% higher than the corresponding non-composite case (Beam 1A). The reduced stud stiffness results in less composite action and hence less horizontal shear transferred between the steel and concrete interface. This explains the reduced axial compressive force and shear force in the slab, as well as the increased stress resultants (axial and shear forces) in the tee-sections above and below the openings. These together increase the shear and slightly increase the end-moments in the web-post of Beam 1D, making it more vulnerable to buckling compared to 1B.

Finally, in Beam 1E, the effective slab thickness is reduced from 76.2 mm to 50.8 mm causing a reduction of the slab stiffness. This results in lowering the level of the neutral axis and reducing the beam flexural capacity. The shear capacity of this beam was found to be 60% higher than the non-composite case (Beam 1A) and 4.2% lower than that of Beam 1B. From Figure 3.16 and Table 3.6, it is clear that the effect of reducing the slab stiffness resulted in reducing the shear contribution from the slab, thus increasing the amount of shear exerted on the tee-sections. It also caused an increase in the resultant stresses at the opening, hence increasing the value of the shear force and end-moments in the web-post and making it more prone to buckling than Beam 1B.

Table 3.1: Material properties used in the FEM

PARAMETER	Thickness (mm)	Yield Stress (MPa)	Poisson Ratio	Material Nonlinearity	Hardening Rule	Yield Criterion
Web	4.69	314.4	0.3	elasto-plastic	isotropic	Von-Mises
Flange	5.35	317.9	0.3	elasto-plastic	isotropic	Von-Mises
Stiffener	9.525	317.9	0.3	elasto-plastic	isotropic	Von-Mises

* *E was taken as 200.000 MPa for Steel and 29.430 MPa for Concrete.*

Table 3.2: Properties of the non-composite FE models

B E A M	1A	1F	1X	1Y	1Z	2A	3A	4A
d_g (mm)	478	478	478	478	478	478	478	453
h_0 (mm)	351	351	351	351	351	351	351	301
ϕ (deg.)	59.94	59.94	59.94	59.94	59.94	59.94	52.5	59.94
e (mm)	76.2	76.2	76.2	76.2	76.2	50.8	76.2	50.8
ecc. (mm)	0.0	+ 19.1	+ 12.7	+ 25.4	+ 38.1	0.0	0.0	0.0
t_w (mm)	4.69	4.69	4.69	4.69	4.69	4.69	4.69	4.69
t_f (mm)	5.35	5.35	5.35	5.35	5.35	5.35	5.35	5.35
d_t (mm)	63.5	44.45	50.8	38.1	25.4	63.5	63.5	63.5
d_b (mm)	63.5	82.55	76.2	88.9	101.6	63.5	63.5	63.5
S (mm)	355.6	355.6	355.6	355.6	355.6	304.2	421	276

Table 3.3: Properties of the composite FE models

B E A M		1B	1C	1D	1E	1G	2B	3B	4B
Opening Eccentricity (mm)		0.0	0.0	0.0	0.0	+19.1	0.0	0.0	0.0
Concrete Slab	Width (mm)	584	1168	584	584	584	584	584	584
	Thickness (mm)	76.2	76.2	76.2	50.8	76.2	76.2	76.2	76.2
Stud Stiffness (kN/mm)		175	175	43.75	175	175	175	175	175
Steel Deck Height (mm)		50.8	50.8	50.8	50.8	50.8	50.8	50.8	50.8
Castellation Properties (*hole geometry*)	h_0 (mm)	351	351	351	351	351	351	351	301
	ϕ (degs.)	59.94	59.94	59.94	59.94	59.94	59.94	52.5	59.94
	e (mm)	76.2	76.2	76.2	76.2	76.2	50.8	76.2	50.8
Model length, 2S (mm)		711.2	711.2	711.2	711.2	711.2	608.4	842	552

Table 3.4: Free-body diagram FEM results (Non-composite Cases)

B E A M	1A	1F	1X	1Y	1Z	2A	3A	4A
Buckling shear, V ~ (kN)	59.0	62.7	63	61.8	54.1	59.2	61.34	73.8
Load at buckling, P ~ (kN)	118.1	125.3	125.9	123.5	108.1	118.4	122.7	147.6
S (mm)	355.6	355.6	355.6	355.6	355.6	304.2	421	276
Opening height, ho ~ (mm)	350	350	350	350	350	350	350	301
H1ts (N)	4001	4015	4011	4035	4043	3435	473	338
y1ts (mm)	46.9	34.6	39.18	30	20	46	46.5	53
V1ts (N)	4998	4643	4774	4491	4026	4999	4999	4998
V2ts (N)	5000	4235	4490	3978	3440	5003	5004	4994
H2ts (N)	12177	12124	12174	12072	11965	10568	14349	10393
y2ts (mm)	43.7	31	35.1	27	19	40.7	44.8	48.5
H1bs (N)	4017	4038	4025	4053	4065	344	4756	3395
y1bs (mm)	46.8	56.5	53.4	59.7	68.2	45.9	46.4	52.9
V1bs (N)	4995	5350	5224	5506	5972	4995	4995	4998
V2bs (N)	4992	5768	5508	6020	6560	4999	4990	4990
H2bs (N)	12209	12153	12167	12095	12015	10589	14343	10406
y2bs (mm)	43.8	58.8	53.5	64.3	75.8	40.7	44.8	48.6
Web-post shear, V_h ~ (N)	8257	8167	8213	8110	8001	7259	9736	7103
M1 (kN.mm)	1433	1342	1377	1301	1181	1249	1683	1055
M2 (kN.mm)	1429	1490	1472	1514	1594	1247	1680	1053
% Shear (top tee)	50	44.4	46.3	42.4	37.3	50	50	50
% Shear (bottom tee)	50	55.6	53.7	57.6	62.7	50	50	50

(Note) values here correspond to a beam shear V_s of 10 kN and are related to the free-body diagram in Figure 3.13

Table 3.5: Non-composite beam finite element results

BEAM	F E M (kN)			$V_p^{\#}$ (kN)	V_{hcr}/V_{ph}	V_h / V_v	V_{cr} / V_p	M_1/M_2
	V_{cr}	V_{hcr}^{+}	V_{ph}^{*}					
1A	59	48.7	77.9	390.1	0.626	0.826	0.151	1.002
1F	62.7	51.2	77.9	390.1	0.658	0.817	0.161	0.9
1X	63	51.7	77.9	390.1	0.665	0.821	0.162	0.935
1Y	61.8	50.1	77.9	390.1	0.644	0.811	0.158	0.859
1Z	54.1	43.3	77.9	390.1	0.556	0.8	0.139	0.741
2A	59.2	43	56.5	390.1	0.761	0.726	0.152	1.002
3A	61.3	59.7	82.3	390.1	0.726	0.974	0.157	1.002
4A	73.8	52.4	54.6	370.1	0.96	0.71	0.199	1.002

\+ V_{hcr} *corresponds to horizontal shear at the weld when buckling occurs*

* V_{ph} *based on web width at centroids of elements nearest to the weld and assuming* $F_y = 314.4\ MPa$

\# V_p *cross section plastic shear strength*

Table 3.6: Free-body diagram FEM results (Composite Cases)

BEAM	1B	1C	1D	1E	1G	2B	3B	4B
Buckling shear, V ~ (kN)	98.5	96.5	89.1	94.4	92.8	85.9	89.1	88.5
Load at buckling, P ~ (kN)	197	193	178.1	188.8	185.5	171.7	178.3	176.9
S (mm)	355.6	355.6	355.6	355.6	355.6	304.16	421	276
Opening height, ho ~ (mm)	350	350	350	350	350	350	350	301
H1ts (N)	465	382	1829	589	443	341	607	393
y1ts (mm)	37.6	34.3	42.6	43.9	31.7	25.7	44.8	34.8
H1tc (N)	2888	2988	1764	2838	2913	2565	3338	2418
ytc (mm)	149.8	149.8	149.8	137	130.8	149.8	149.8	162.3
V1ts (N)	2757	2715	2831	2980	1915	3329	2614	3867
V1tc (N)	3113	3138	2688	2838	3700	2456	3338	2020
V2ts (N)	2881	2766	3022	3102	1924	3378	2701	3789
V2tc (N)	2975	3138	2469	2550	3375	2588	2925	2085
H2ts (N)	1762	1528	6256	2374	2005	1072	2783	1331
y2ts (mm)	40.3	41.7	45.5	37.7	30.9	28.9	43.4	34.1
H2tc (N)	8700	8950	5063	8300	8650	7925	9588	7375
H1bs (N)	3372	3392	3617	3440	3375	2924	3957	2824
y1bs (mm)	47.1	47.4	48.5	46.4	58.9	46.6	45.8	52.8
V1bs (N)	4116	4142	4474	4183	4382	4211	4046	4110
V2bs (N)	4133	4079	4496	4343	4684	4026	4364	4118
H2bs (N)	10482	10504	11341	10702	10671	9012	12401	8731
y2bs (mm)	41.4	41.3	41.8	41.8	53.2	37.9	42.8	46.4
Web-post shear, V_h ~ (N)	7168	7168	7785	7320	7357	6196	8552	5977
M1 (kN.mm)	1161	1146	1257	1227	1142	962	1407	787
M2 (kN.mm)	1192	1189	1296	1228	1244	1048	1420	879
% Shear (concrete slab)	30.6	31.4	25.8	27.0	35.4	25.3	31.4	20.5
% Shear (top tee)	28.2	27.5	29.3	30.4	19.2	33.5	26.5	38.3
% Shear (bottom tee)	41.2	41.1	44.9	42.6	45.4	41.2	42.1	41.2

(Note) values here correspond to a beam shear V_s of 10 kN and are related to the free-body diagram in Figure 3.13

Table 3.7: Composite beams finite element results

BEAM	F E M (kN)			$V_p^{\#}$ (kN)	V_{hcr}/V_{ph}	V_h / V_v	V_{cr} / V_p	M_1/M_2
	V_{cr}	V_{hcr}^{+}	V_{ph}^{*}					
1B	98.5	70.6	77.9	390.1	0.907	0.717	0.253	0.973
1C	96.5	69.2	77.9	390.1	0.889	0.717	0.247	0.964
1D	89.1	69.4	77.9	390.1	0.891	0.779	0.228	0.97
1E	94.4	69.1	77.9	390.1	0.887	0.732	0.242	1.0
1G	92.8	68.3	77.9	390.1	0.877	0.736	0.238	0.918
2B	85.9	53.3	56.5	390.1	0.942	0.62	0.22	0.918
3B	89.1	76.2	82.3	390.1	0.926	0.855	0.228	0.991
4B	88.5	52.9	54.6	370.1	0.967	0.598	0.239	0.895

\+ V_{hcr} *corresponds to horizontal shear at the weld when buckling occurs*

* V_{ph} *based on web width at centroids of elements nearest to the weld and assuming* $F_y = 314.4\ MPa$

\# V_p *cross section plastic shear strength*

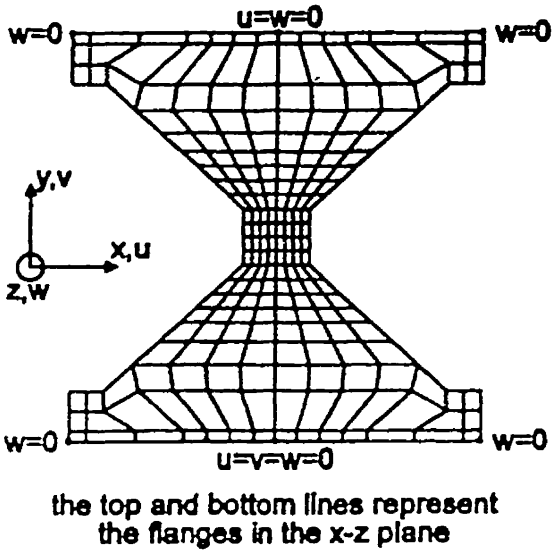

Figure 3.1: Non-composite finite element model used by Zaarour and Redwood (1996)

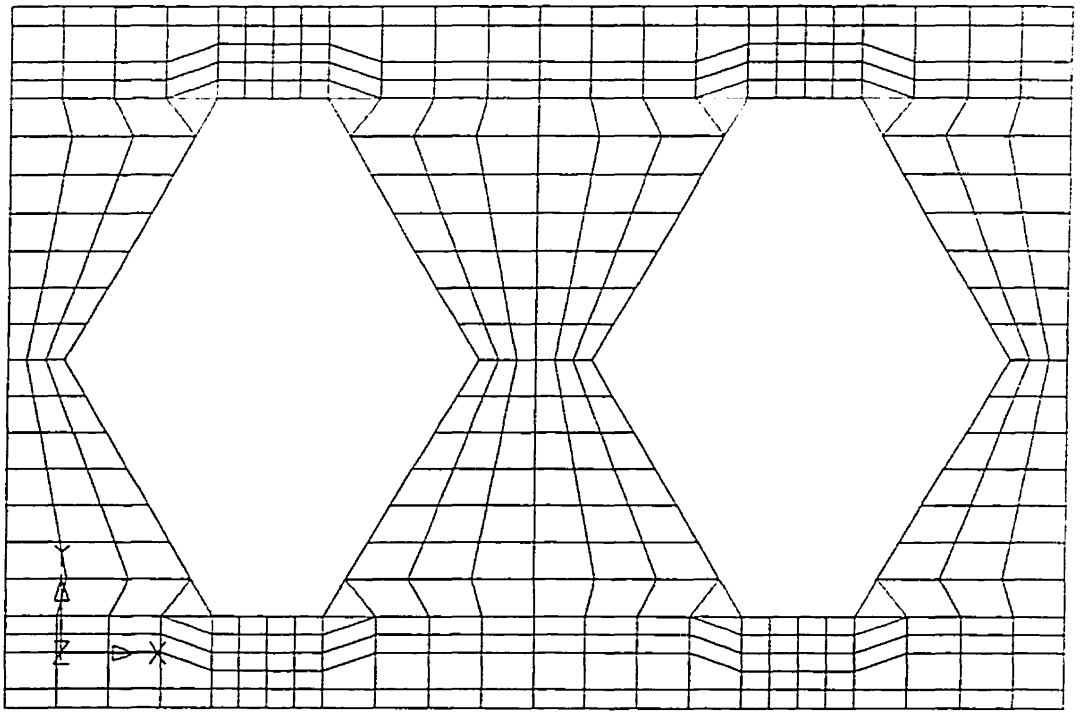

Figure 3.2: Finite element model used in performing the numerical study

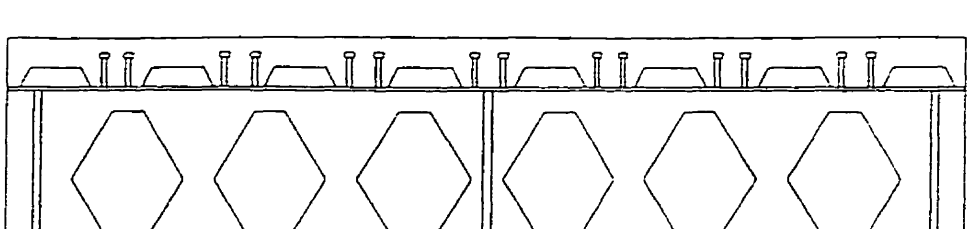

Figure 3.3: Composite castellated beam (Shear specimen)

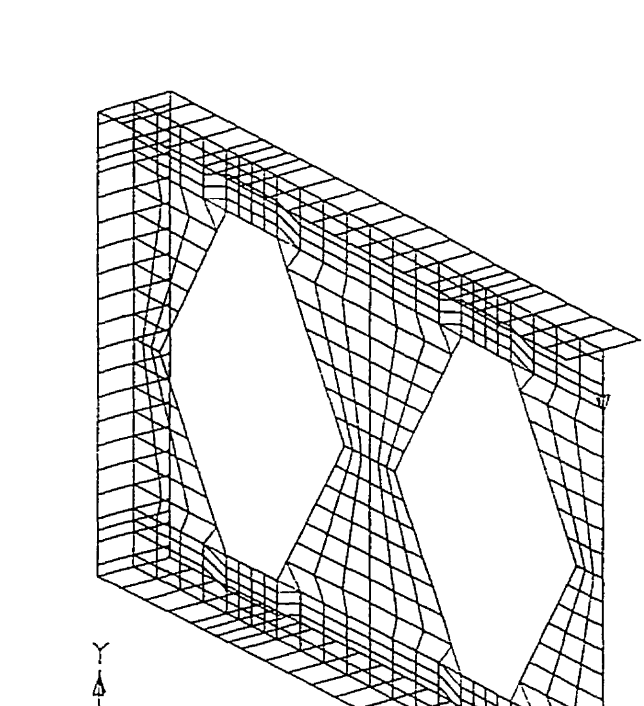

Figure 3.4(a): 3D non-composite castellated beam finite element model

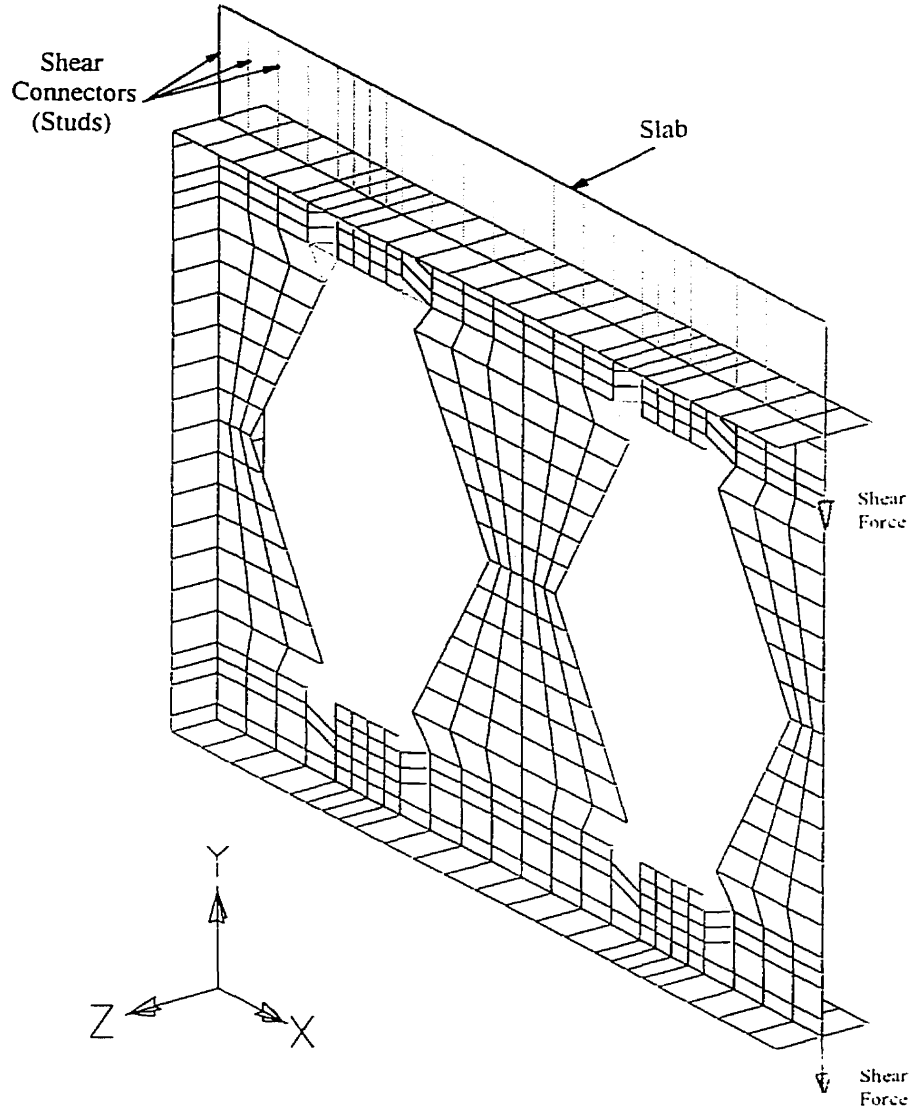

Figure 3.4(b): 3D composite castellated beam finite element model

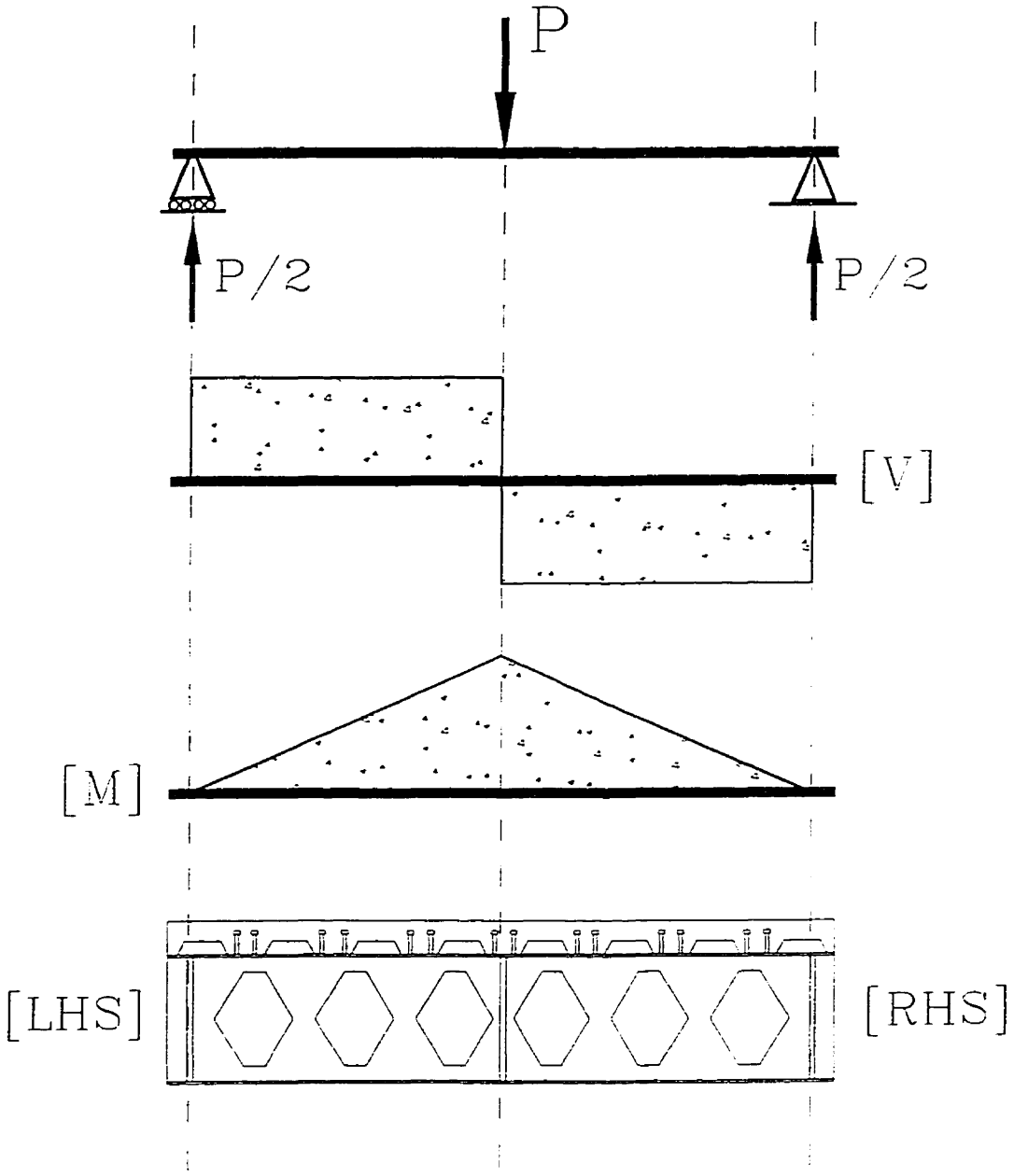

Figure 3.5: Shear and bending moment diagram for a test specimen

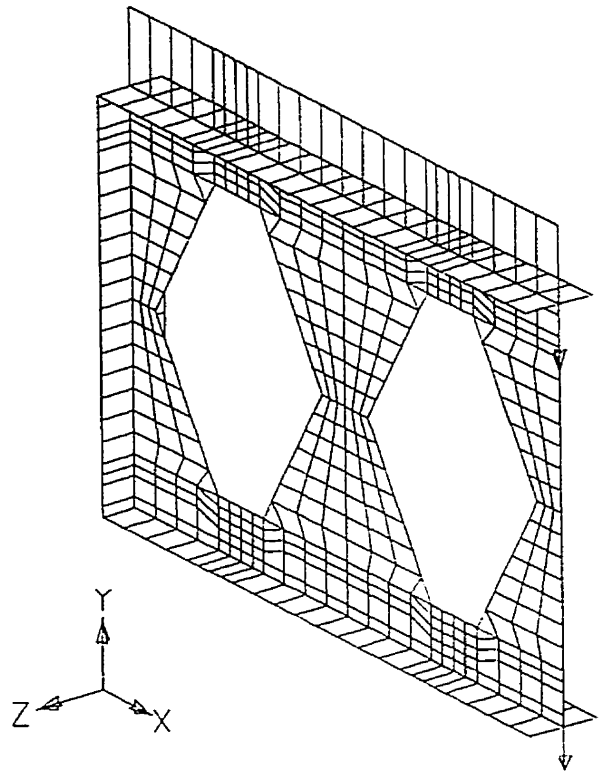

(a) Before

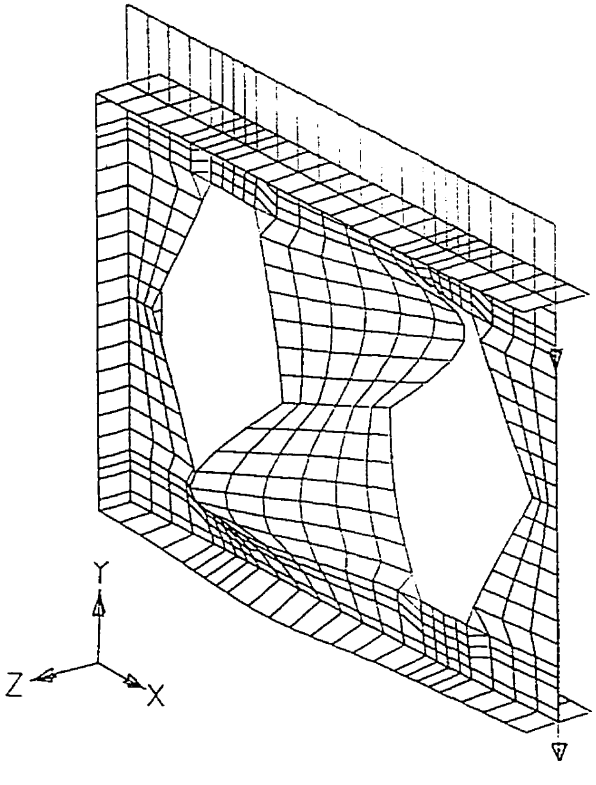

(b) After

Figure 3.6: A web-post before and after buckling using the proposed FEM

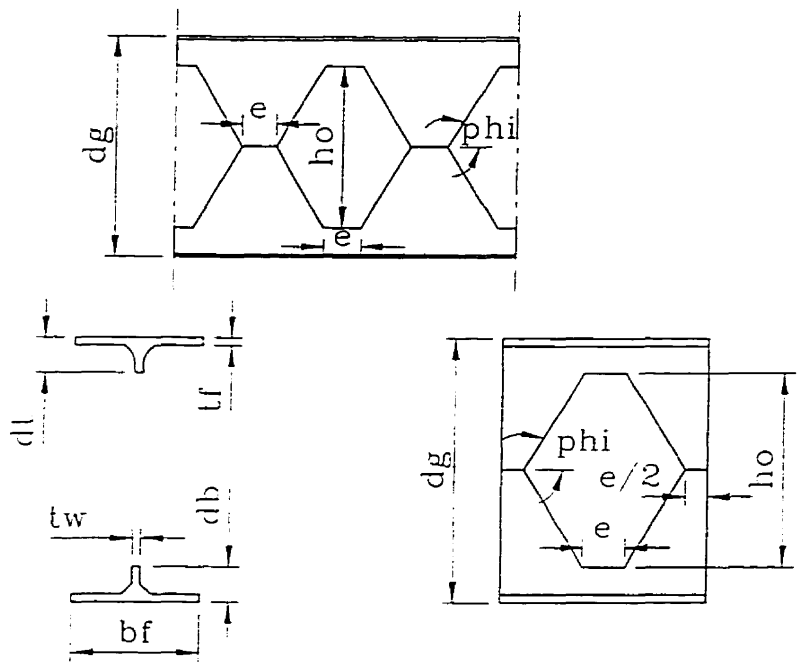

Figure 3.7: Castellation Parameters

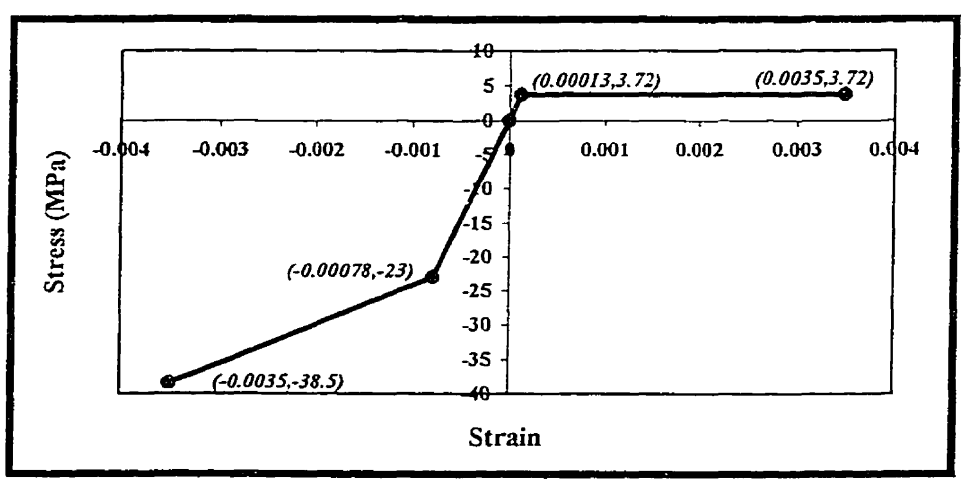

Figure 3.8(a): Concrete slab stress-strain curve assumed in the FEM

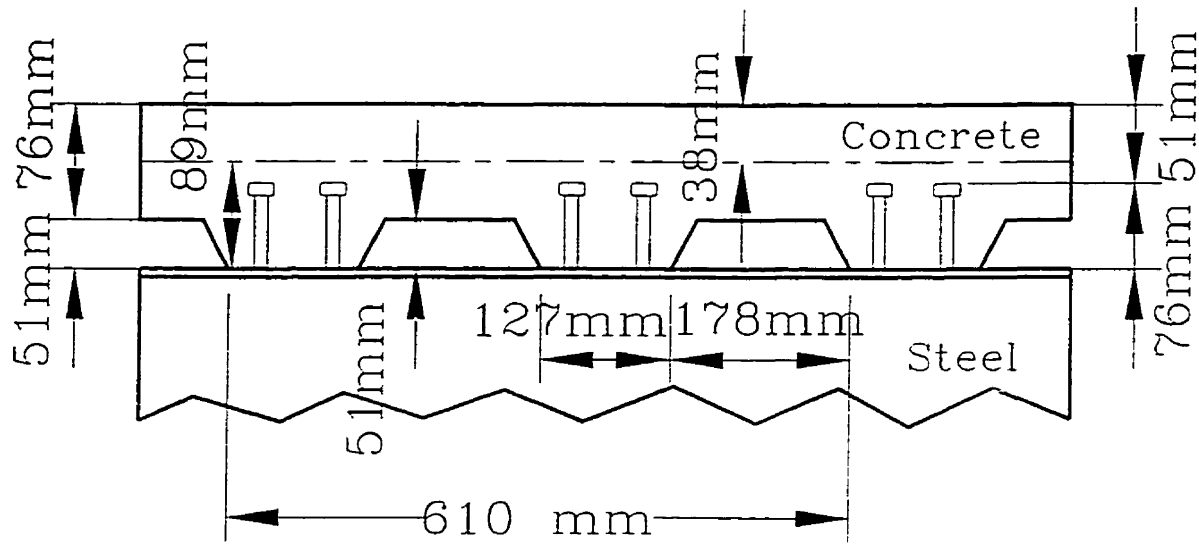

Figure 3.8(b): Stud connection between top steel flange and concrete slab N.A. (Shear connector model)

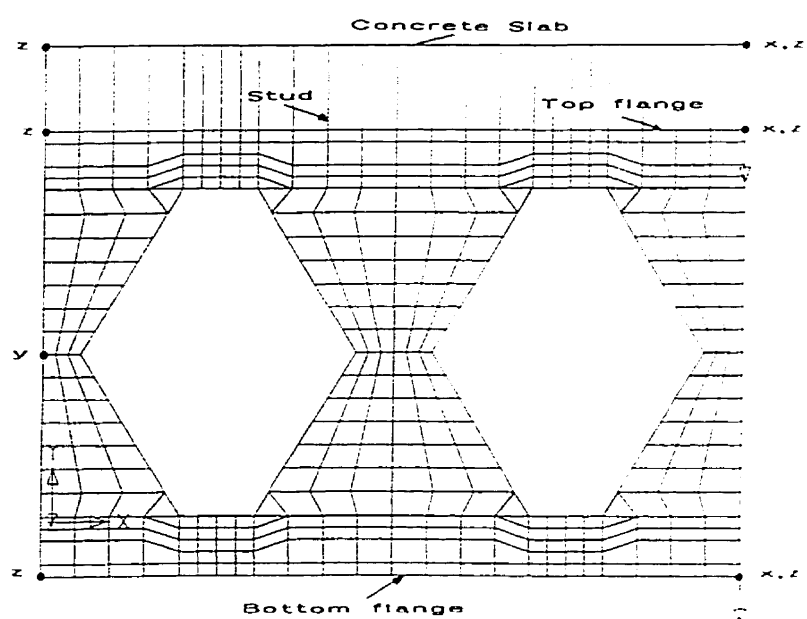

Figure 3.9: FEM boundary conditions assumed in the non-composite and composite models

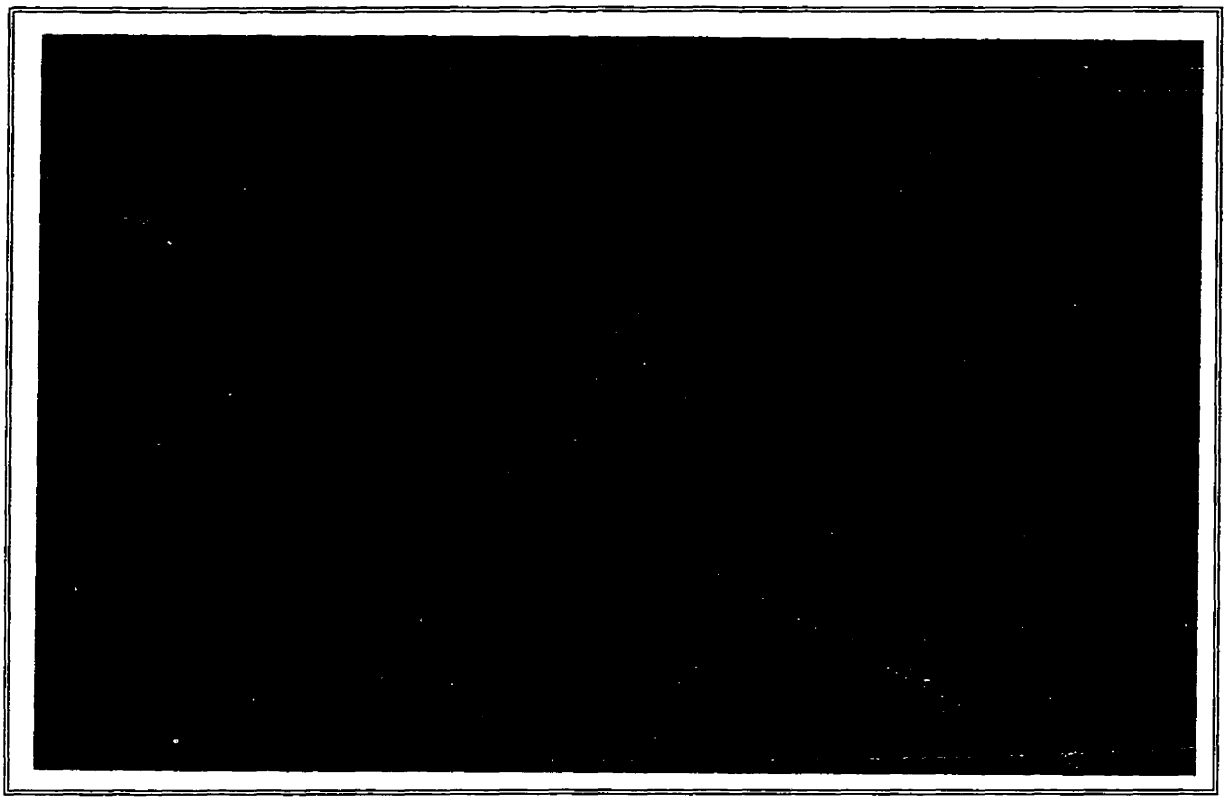

Figure 3.10: Beam 1A undeformed shape (non-composite)

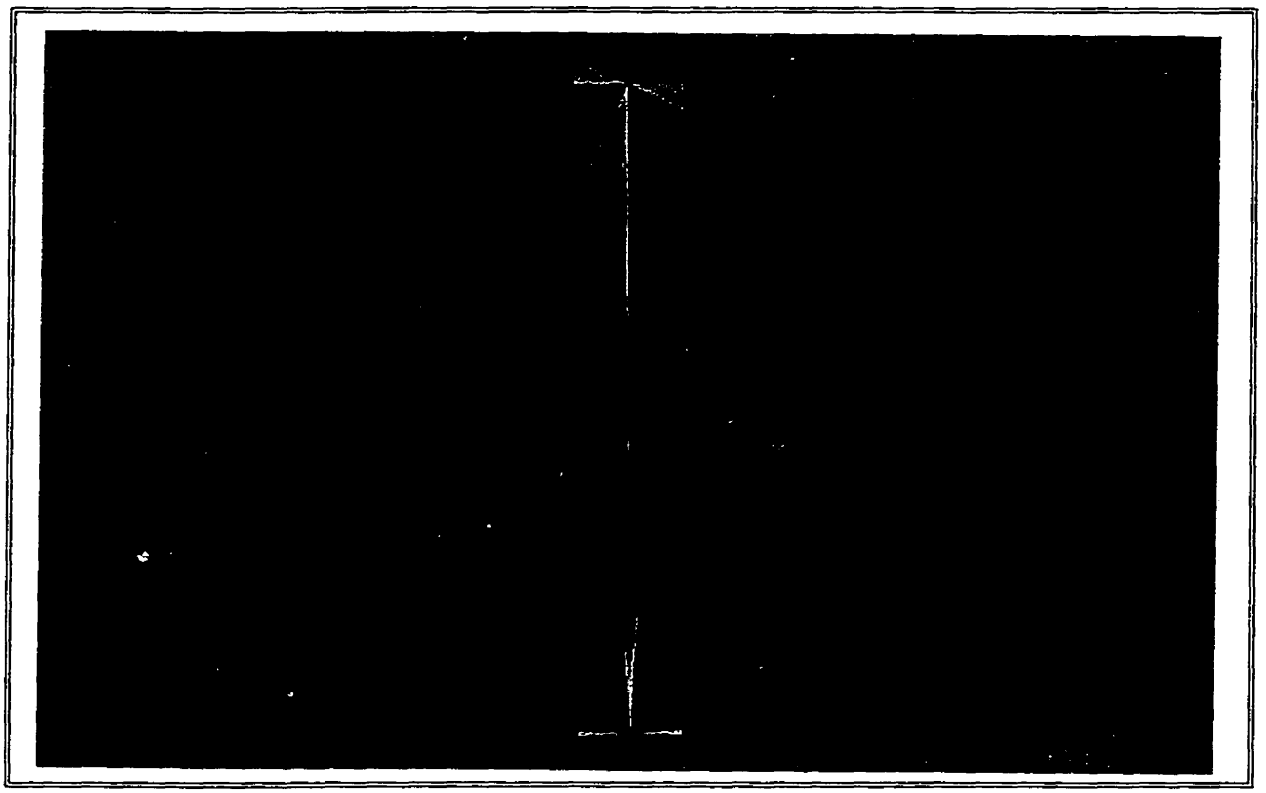

Figure 3.11: Double curvature shape of a buckled web-post in Beam 1A

Figure 3.12: Principal stresses (major) indicating tension and compression zones corresponding to the double curvature effect in the web-post (Beam 1A)

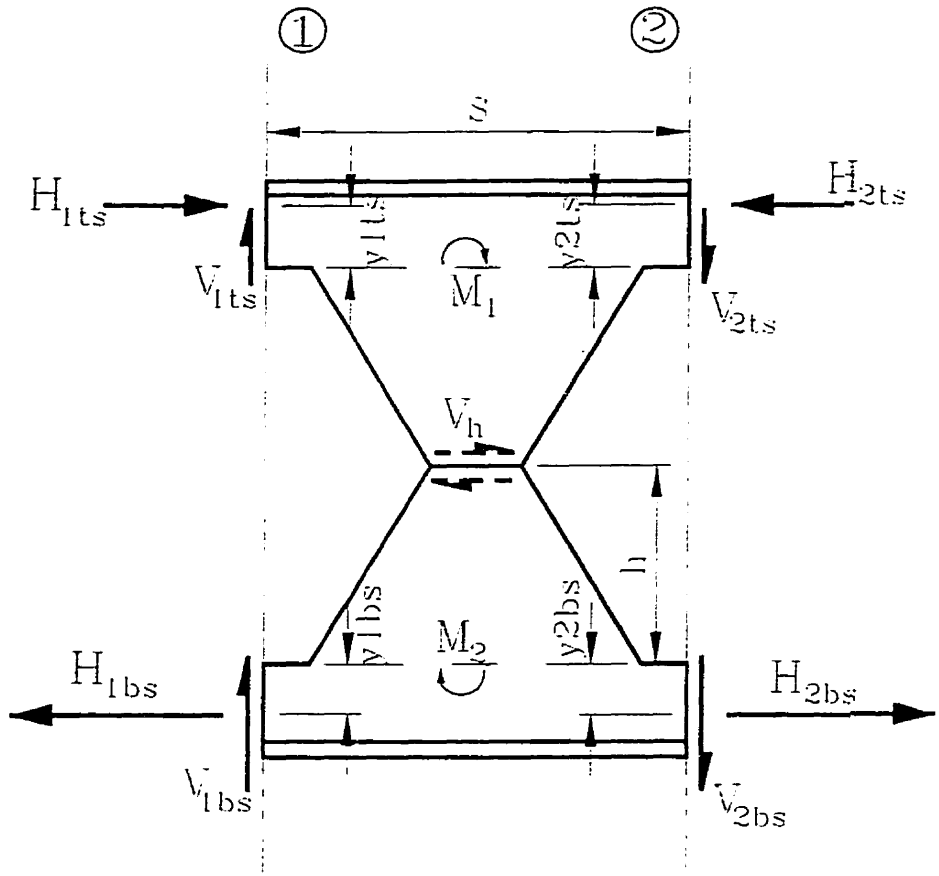

Figure 3.13: The free-body diagram used in the numerical analysis of the non-composite castellated beams

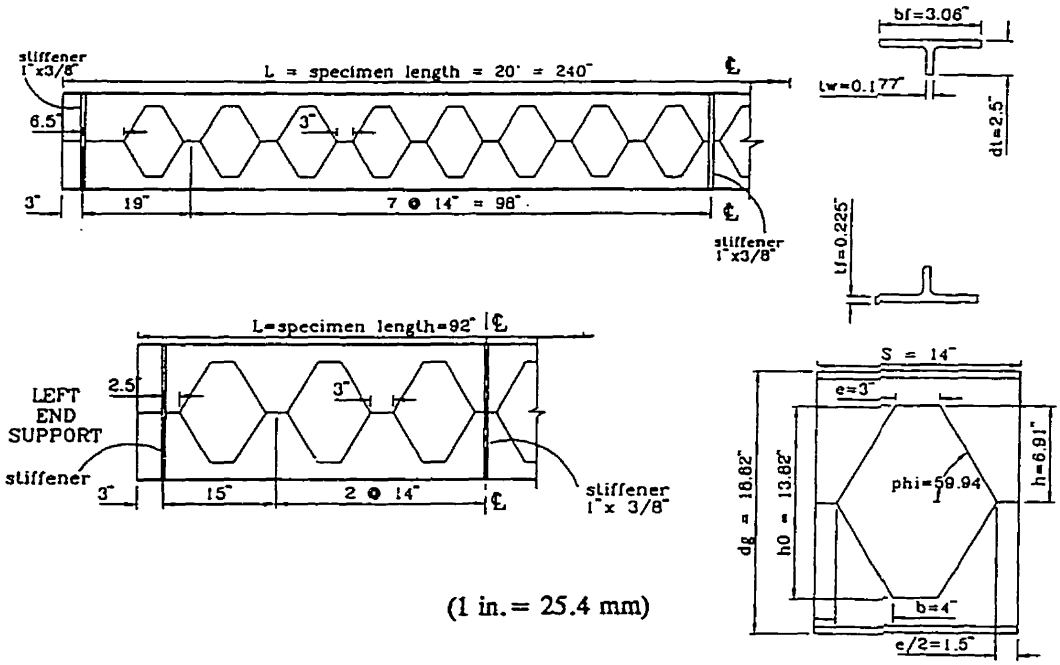

Figure 3.14: Castellated beam configuration used in studying the effect of opening eccentricity on the buckling behavior of the web-posts

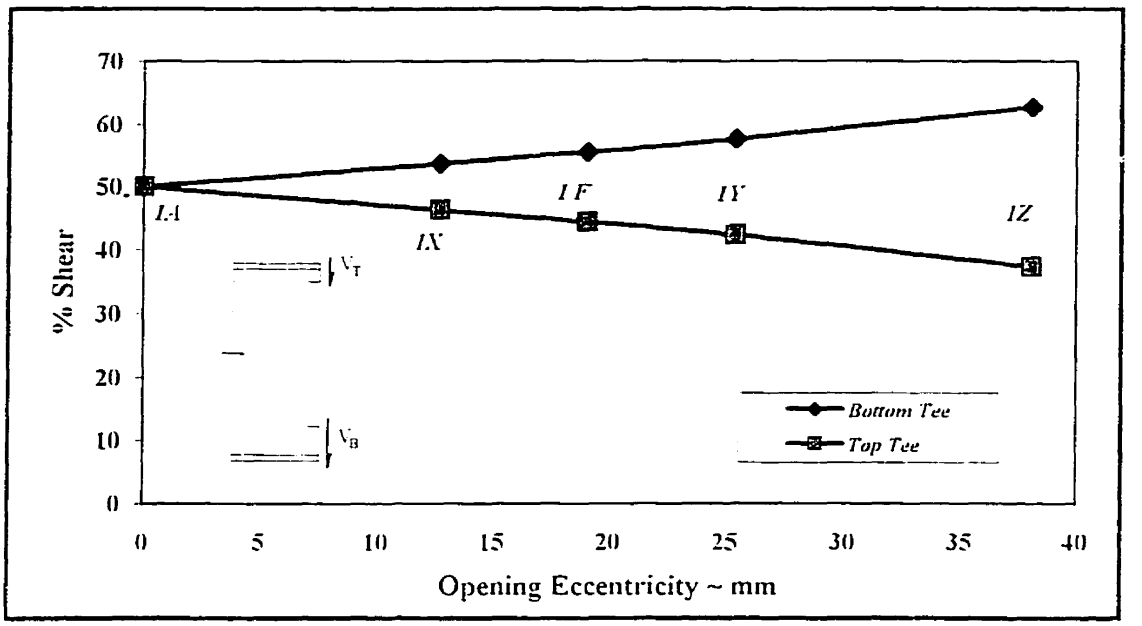

Figure 3.15(a): Shear distribution above and below an opening with varying opening eccentricity

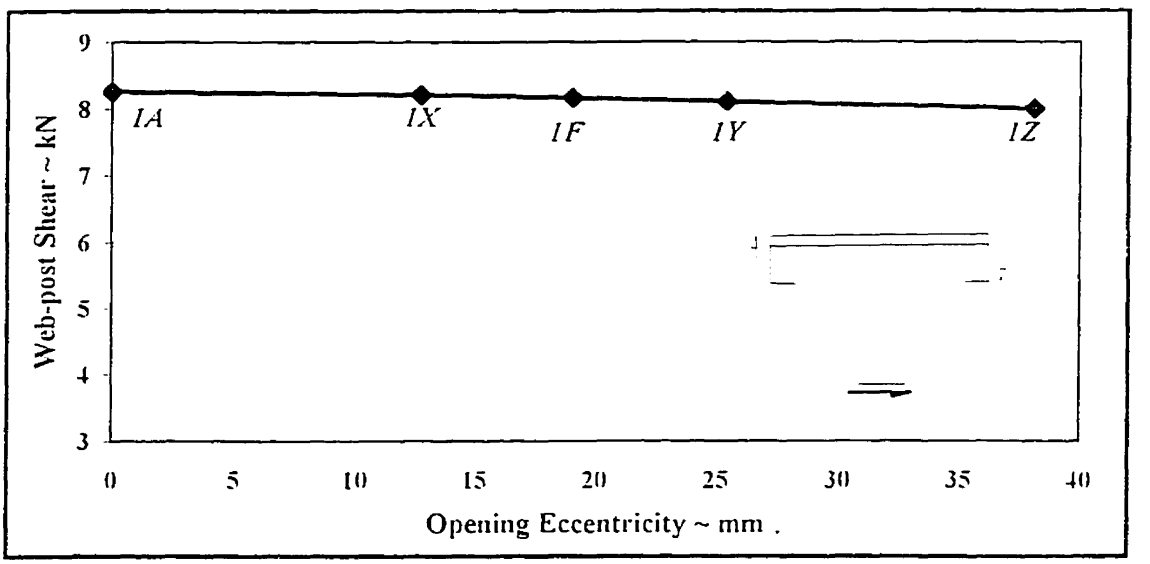

Figure 3.15(b): Variation of web-post horizontal shear force with varying eccentricity

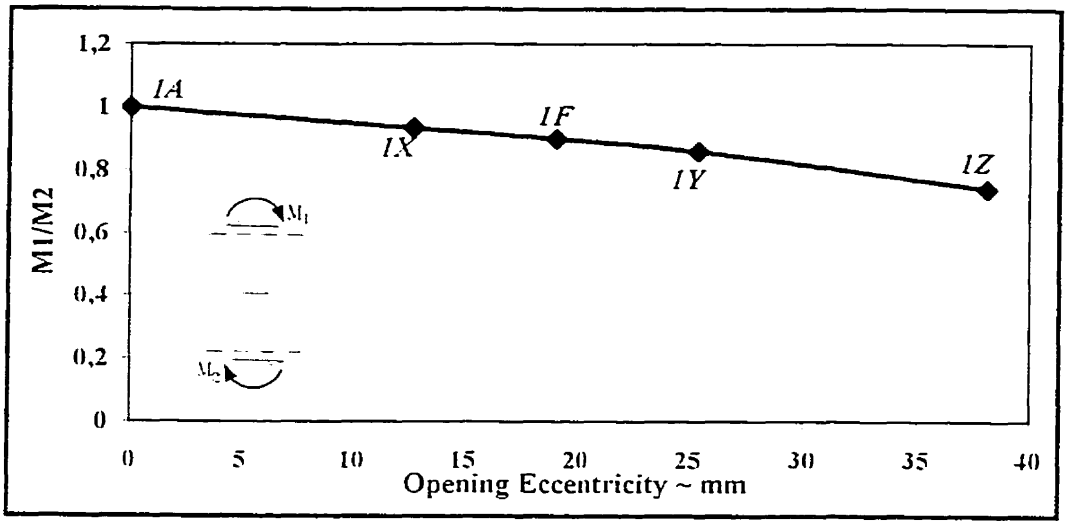

Figure 3.15(c): Variation of moments at top and bottom of the web-post with opening eccentricity

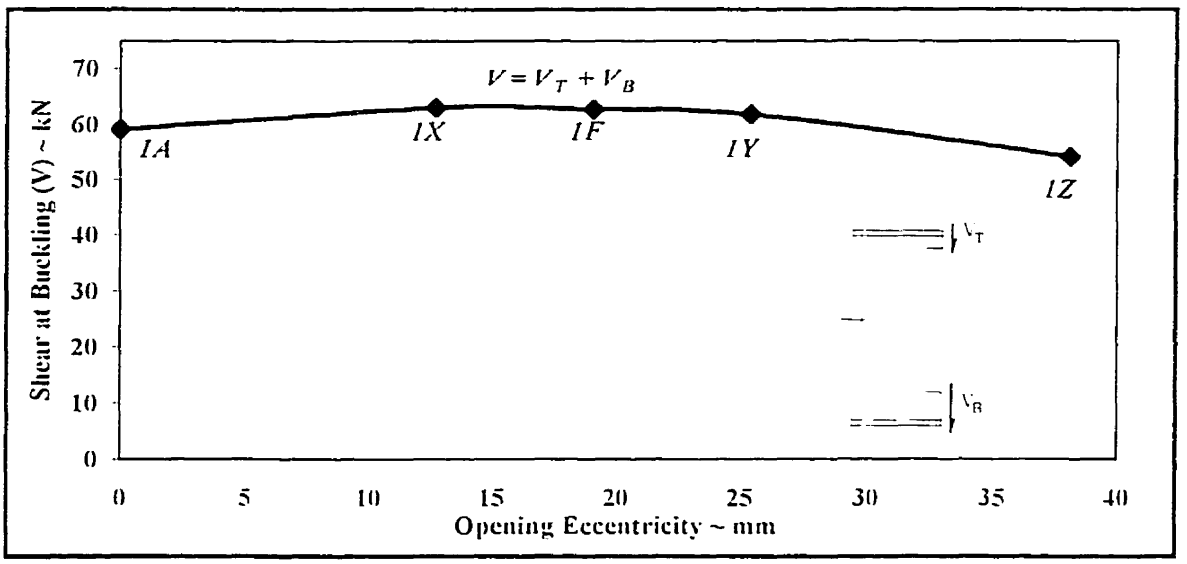

Figure 3.15(d): Beam shear at web-post buckling

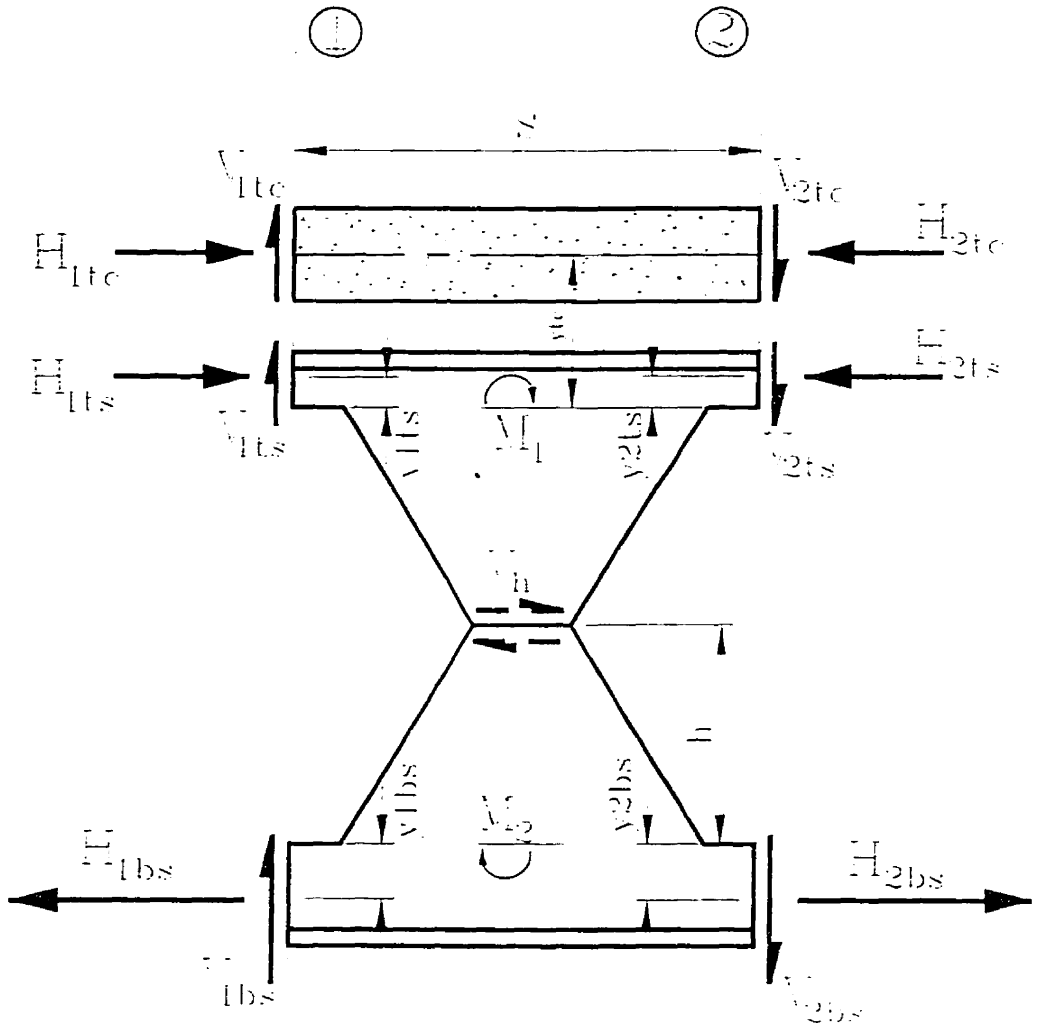

Figure 3.16: The free-body diagram used in the numerical study of the composite castellated beams

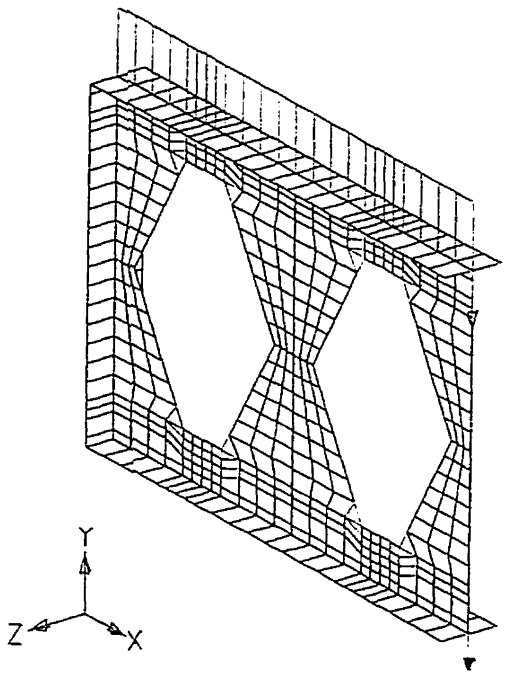

Figure 3.17(a): Beam 1B underformed web-post (composite beam)

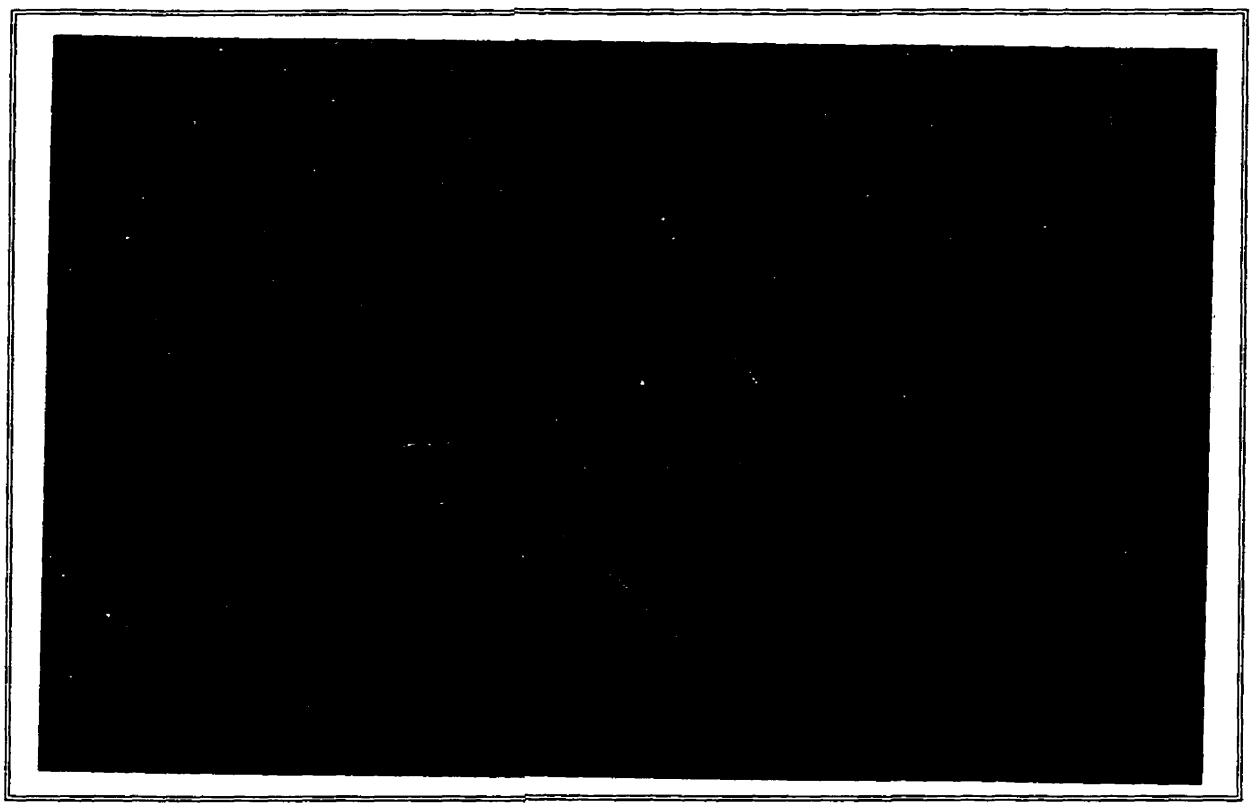

Figure 3.17(b): Beam 1B web-post after buckling (composite beam)

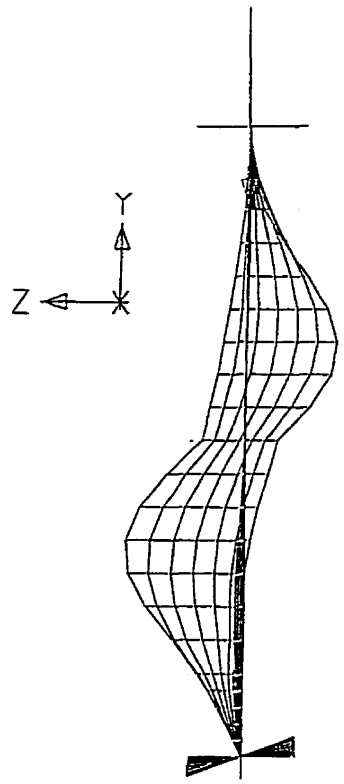

Figure 3.18: Double curvature effect in a buckled web-post (composite beam 1B)

Figure 3.19: Principal stresses (major) distribution in composite beam 1B

CHAPTER FOUR

YIELD ANALYSES OF CASTELLATED BEAMS

This chapter describes the yield analysis performed on non-composite and composite castellated beams. In this analysis, the possibility of local or overall buckling is not considered. The methods used herein are largely based in previous research work on non-composite and composite beams with an isolated web opening. These method are described in detail in the works of Redwood (1983) and Redwood and Cho (1993). In addition, research on beams with multiple web openings was also considered in the work of Redwood (1968).

4.1 Mechanism Failure Mode

An isolated web opening is considered to fail after the development of a parallelogram (Vierendeel) mechanism, which is triggered by the formation of four plastic hinges at the re-entrant corners of the opening. At these hinges, the contribution of the axial and shearing forces to the plastic moments must be considered due to their high magnitudes.

In this study the most general case, a composite beam with an eccentric web opening, is analyzed using Eqns (2) and (6) through (15) of Redwood and Cho (1993). These equations are used in constructing moment-to-shear (M/V) interaction diagrams, such as that illustrated in Figure 4.1. An interaction diagram relates the bending moment and shearing force at the centerline of an opening, and is constructed by computing values of M_o, M_1, and V_1, as indicated in Figure 4.1. These values are then non-dimensionalized by dividing by the plastic moment (M_p) or plastic shear (V_p) value of the unperforated steel beam section.

The Vierendeel, or four-hinge mechanism, assumes the presence of a shearing force; however, as this approaches zero, the solutions converge to values corresponding to pure bending: that is, the bending moment pertaining to slab compression failure, with

the steel cross-section fully yielding in tension and compression. A parabolic curve is used in representing the moment-shear relationship between points 0 ($0,M_o/M_p$) and 1 ($V_1/V_p,M_1/M_p$).

The solutions obtained using the equations of Redwood and Cho (1993) are dependent on the number of shear connectors between the high moment end of the opening and the nearest point of zero moment, as well as on the number of shear connectors located between the ends of the opening considered. Due to the short length of the openings in the tested castellated beams, the latter value has conservatively been taken as zero. The point "O" can be based on the assumption of a large number of connectors; however, for a given opening, a reduced value of the pure bending capacity, based on the actual number of connectors, should be implemented. An approximate solution can be obtained by using this reduced value to provide a horizontal cut-off on the interaction diagram, as can be seen in Figure 4.1. Alternatively, a parabolic variation between the pure bending value and point 1 may gives a slightly better result.

The solution described above were implemented in all the beams considered in this study. The hexagonal or octagonal holes of castellated beams are treated as being rectangular with a length equal to the horizontal length of the top and bottom hole edges, and a height equal to the full depth of the opening. The coordinates of points "0" and "1" on the interaction diagram for all these beams are given in Table 4.1. Values of the plastic moment and shearing forces are also provided in this table; these are based on the nominal dimensions and material properties. Table 4.2 illustrates the effect on the pure bending capacity of Beam 1B, for varying numbers of shear connectors, between the support and the high moment end of an opening, on the pure bending capacity, according to Redwood and Cho (1993).

4.2 Web-post Yield Mode

Due to the closely spaced openings in castellated beams, a yield failure may occur in the web-post. This will frequently occur before the Vierendeel failure mechanism develops, particularly in cases where the moment-to-shear ratio is low. This mode of failure is analyzed in the following:

Figure 4.2 shows the stress resultants acting on the various parts of a short length of beam, between the centerlines of adjacent openings. The tensile forces below the openings will be different due to the moment gradient (i.e. the shear), and this difference is equal to the horizontal shearing force in the web-post. The forces T_1 and T_2 relate to the bending moments at the two sections, and to the line of action of these forces, defined by y_1 and y_2, when measured from the extreme tension fiber.

$$V_h = T_2 - T_1$$

There is some uncertainty regarding the magnitudes and the line of action of these forces; as a result, several different approaches have been taken:

(a) If the bottom tee-sections are yielding in tension, and points of contraflexure exist at opening mid-length, the forces would pass through the centroids of the tee-sections.

(b) Redwood (1968) suggested for non-composite beams using the web-flange interface, i.e. $y_1 = y_2 = t_f$.

(c) If inelastic action does not predominate, the lines of action can be based on elastic flexural analysis of the cross-section, again assuming points of inflection at opening centerlines.

(d) Stresses from the finite element analyses can be summed to give the resultants T_1 and T_2. Alternatively, the shear stresses can be summed to give V_h directly.

When dealing with web-post buckling, the shearing force will be high, while the beam bending moment will be small, and so the extent of plastic action in the tees will also be small. Consequently, method (a) is considered inappropriate, and method (b), while it

gives a reasonable approximation for non-composite beams, it is not applicable to composite beams. Methods (c) and (d) are hence the only methods considered in analyzing web-post yielding in this study; results of these two methods are given in Table 4.3.

Results given for Method (c) assume a fully effective slab, whereas the partial shear connection prevents full participation. One way of accounting for this is by raising the modular ratio "n_e", in the above computations, thus reducing the effectiveness of the slab in compression. Table 4.4 shows how V_h/V for Beams 1B and 1G changes as the modular ratio increased up to a factor of 10 times the initial value. For the beams, about nine studs are needed to provide full shear connection to the slab, and it is hypothesized that if there is, for example, one stud between the support and the first web-post, then the modular ratio could be increased by a factor of 9/1. This is the case for the beams used in the flexural tests, Beams 4 and 5, whereas for the short test beams, there were 3 or 4 studs. These low degrees of shear connection affecting the shear critical region of a beam are not untypical of practical details.

Assuming web-post yield will occur when the minimum web-post area is subjected to the shear yield stress $F_y/\sqrt{3}$, the web-post yield load (V_{hp}) will then be equal to $(et_wF_y/\sqrt{3})$. Using this result, the vertical beam shear which would produce horizontal shear yield of the web-post, V_3, can be found using one of the methods listed above. Using method (c), this beam shear, V_3, can be expressed as a fraction of V_p, as follows:

$$\frac{V_3}{V_p} = \frac{V_{hp}}{V_p} \quad \frac{1}{(V_h/V)}$$

Values of V_3 are given in Table 4.1. It can be seen that in all cases the value of V_3/V_p is less than V_1/V_p, and this represents a cut-off on the M-V interaction diagram. If partial shear connection is included in the this analysis, the values in Table 4.4 can be used. For example, if three studs are present, and n_e is increased by a factor of 3, V_3/V_p is reduced from 0.256 to 0.247 for Beam 1B, and from 0.251 to 0.244 for 1G.

4.2.1 Shear Critical Holes

The interaction diagrams for Beams 1A and 1B are plotted in Figure 4.3; the vertical broken line represents the onset of web-post yield. It can be seen that the capacity of the composite beam is significantly reduced by yielding of the web-post, whereas the non-composite one is only slightly reduced below that for the four-hinge mechanism. Near the ends of a beam, the moment-to-shear ratio will be low, and a radial line representing the loading on the holes near the support will normally intersect the vertical cut-off, indicating that web-post yield is the likely mode of failure for these holes (buckling is not considered in this analysis). In Figure 4.4(a) the three lines closest to the x-axis represents the holes of the short test beams (1, 2 and 3), as indicated in Figure 4.4(b), where hole 1 in nearest the support.

4.2.2 Flexural Critical Holes

Figure 4.4(a) also represents the M-V interaction diagram for a longer span beam containing a total of 16 holes, Figure 4.4(c), which corresponds to Beam 5 of the test program. The radial lines represent the loading path (M/V) for each opening in one half span. The points shown at the intersection of these lines with the interaction diagram represent the failure condition for each hole. Because the test specimens were simply-supported and subjected to a point load at mid-span, the web-openings were in a uniform shear span; as a result, the intersection providing the lowest V/V_p value represents the limiting behavior of the beam. Since the openings have different number of studs between their high moment ends and the nearest support, different horizontal cut-offs apply to different openings, as illustrated in Figure 4.4(a). This graph shows that failure of this beam is associated with deformations at hole 8, given by the intersection with the line corresponding to five studs (n=5) between the support and the critical hole.

For the particular beam configuration used for Figure 4.4(a), it can be seen that the resulting interaction diagram becomes rectangular: there is no interaction between bending and shear because the four hinge mechanism is not mobilized prior to either flexural failure due to partial shear connection or web-post yielding. This is due to the

very short opening length, and it can be anticipated as being applicable to many castellated beam configurations.

4.3 Conclusions

Interaction diagrams for the ultimate shearing force and bending moments were generated for castellated beams using methods developed for isolated web openings. These solutions are based on the occurrence of full yield or concrete failure, and do not consider buckling. It is shown that the mechanism failure will only occur under high M/V ratio; at a low M/V, the web-post will yield at its mid-depth. A simple elastic flexural analysis of the cross section can be used to determine the web-post shearing force. This uses the elastic modular ratio ($n_c = E_s / E_c$). This mode of failure is represented by a vertical cut-off on the interaction diagram. Table 4.1 gives coordinates of the interaction diagrams for all beams studied, assuming full shear connection.

At low M/V, partial shear connection reduces the effectiveness of the slab in carrying compression, thus increasing the shearing force in the web-posts, and in effect, reducing V_3. Near the beam end, few studs will typically be placed between the support and the first web-post resulting in a low degree of shear connection. For this case, the modular ratio has been multiplied by a factor equal to the ratio of the number of studs required for full shear connection to the actual number available. This reduced value of V_3 is then represented as a vertical cut-off, see Figure 4.1.

At high M/V, the capacity may be limited if there is a small number of shear connectors between a potentially critical hole and the nearest point of zero bending moment. Such partial shear connection can be incorporated as horizontal cut-offs on the interaction diagram. Table 4.2 gives the coordinates for various numbers of studs for Beam 1B. Web-posts at successively greater distances from the support will have greater degrees of shear connection available, and thus different cut-offs may be appropriate to each. These results will be compared with test and FEM results in Chapter 5.

Table 4.1: Interaction Diagram Coordinates ~ Yield Analysis

BEAM	M_p (kN.m)	V_p (kN)	V_{ph} (kN)	M_{po}/M_p	M_1/M_p	V_1/V_p	V_3/V_p
1A	143.6	390.1	62.2	0.708	0.295	0.218	0.203
1B	143.6	390.1	62.2	1.098	0.382	0.411	0.256
1C	143.6	390.1	62.2	1.116	0.428	0.595	0.262
1D	143.6	390.1	62.2	1.098	0.382	0.411	0.256
1E	143.6	390.1	62.2	1.019	0.386	0.334	0.245
1F	143.6	390.1	62.2	0.645	0.283	0.218	0.203
1G	143.6	390.1	62.2	1.156	0.359	0.419	0.251
2A	143.6	390.1	41.5	0.708	0.338	0.241	0.158
2B	143.6	390.1	41.5	1.098	0.4	0.434	0.2
3A	143.6	390.1	62.2	0.708	0.295	0.218	0.171
3B	143.6	390.1	62.2	1.098	0.382	0.411	0.216
4A	132.3	370.1	41.5	0.767	0.353	0.314	0.171
4B	132.3	370.1	41.5	1.241	0.416	0.513	0.221

* *M_p and V_p are the plastic moment and plastic shear values, respectively, of the unperforated steel section.*

Table 4.2: Influence of number of studs (n) on Pure Bending Resistance (Beam 1B)

n	≥ 9	8	5	4	3	2	1
M_{po}/M_p	1.098	1.075	0.954	0.911	0.866	0.816	0.758

Table 4.3: Web-post Shears as a proportion of Beam Shear

BEAM	V_h / V	
	CROSS-SECTION ANALYSIS *	FINITE ELEMENT METHOD +
1A	*0.787*	*0.826*
1B	*0.622*	*0.717*
1C	*0.609*	*0.717*
1D	*0.622*	*0.779*
1E	*0.651*	*0.732*
1F	*0.787*	*0.817*
1G	*0.634*	*0.736*
2A	*0.673*	*0.726*
2B	*0.532*	*0.620*
3A	*0.932*	*0.974*
3B	*0.738*	*0.855*
4A	*0.656*	*0.71*
4B	*0.507*	*0.598*

* Method (c) assuming full shear connection

+ Method (d)

V_h = horizontal shear in web-post

V = vertical shear on beam

Table 4.4: Effect of partial shear connection on web-post shearing force

multiplier (x)	modular ratio	V_h / V	
		1B	1G
1	7.2	0.622	0.634
2	14.4	0.636	0.646
3	21.6	0.646	0.655
4	28.8	0.655	0.663
5	36	0.662	0.669
6	43.2	0.668	0.675
9	64.8	0.684	0.689
10	72	0.689	0.693

V_h = *shearing force in web-post*

V = *vertical shear in beam*

n_c = *modular ratio (200,000/27900 = 7.2)*

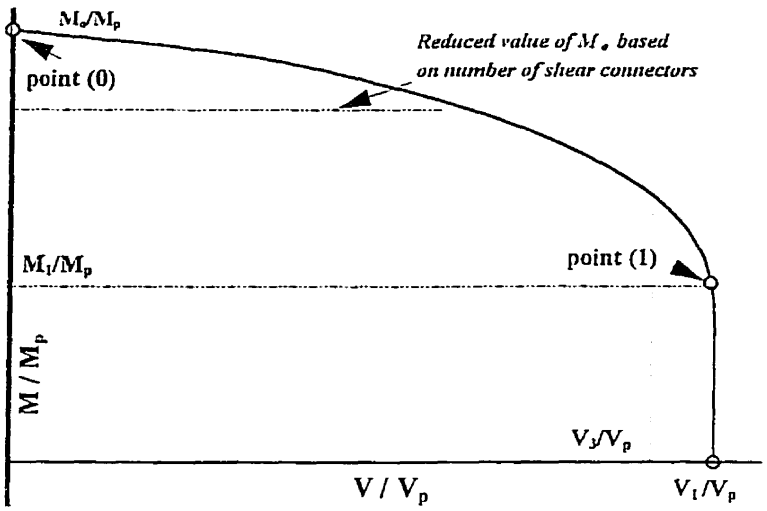

Figure 4.1: A sample moment to shear (M/V) interaction diagram (Yield Analysis)

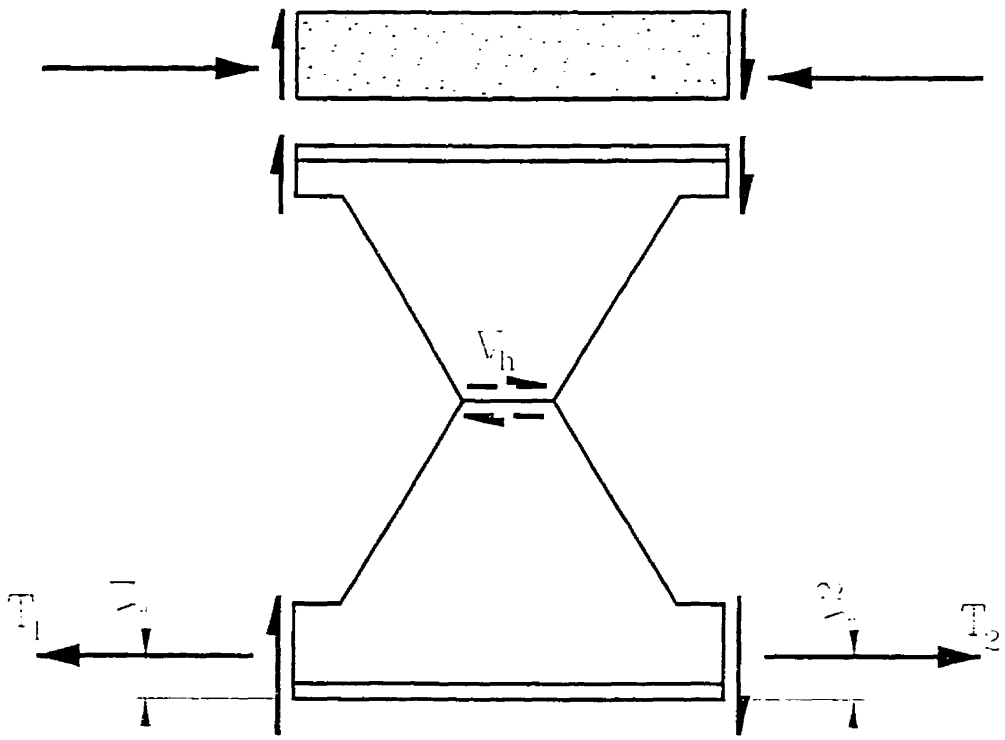

Figure 4.2: Forces in a composite castellated beam segment

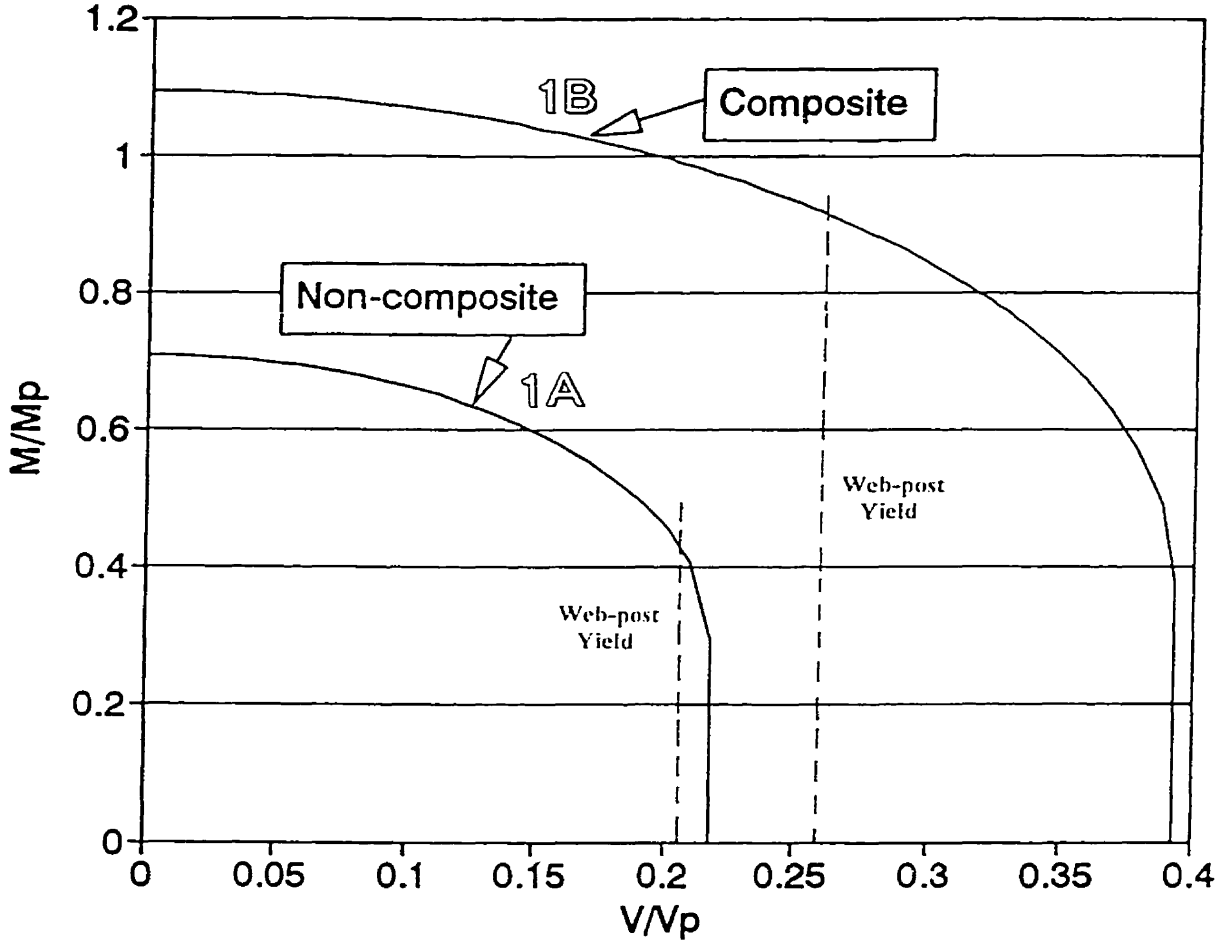

Figure 4.3: Interaction diagrams for composite and non-composite beams

(Mid-depth openings)

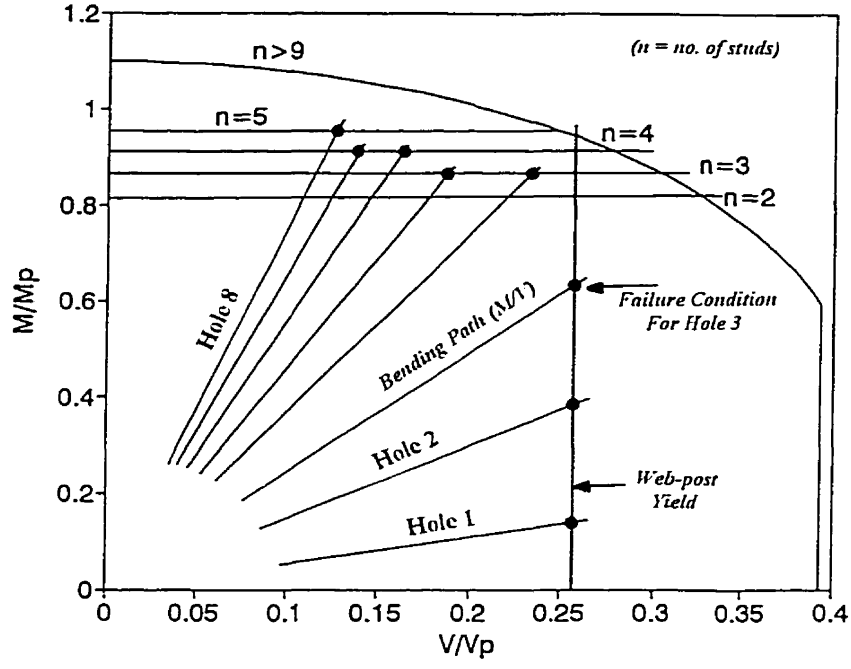

Figure 4.4(a): Yield Analysis: M/V interaction diagrams for shear and flexural specimens (Mid-depth openings)

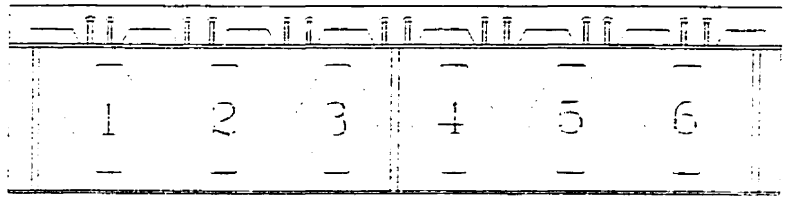

Figure 4.4(b): Shear specimens

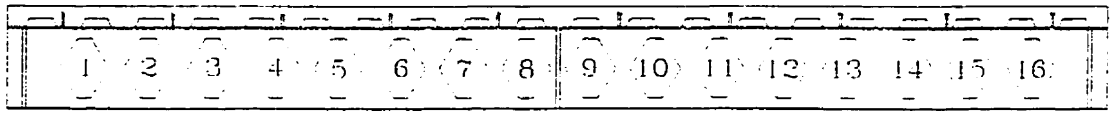

Figure 4.4(c): Flexural specimens

CHAPTER FIVE

RECONCILIATION OF TESTS AND THEORIES

5.1 Web-post Shearing Force

The web-post shearing forces, obtained from the FEM stress analysis in Chapter 3, prior to buckling, have been compared with those obtained from the elastic analysis of the cross-section, as summarized in Table 4.3. While the trends are identical in all cases, the finite element method predicts greater web-post shearing forces, expressed as a fraction of the shearing force on the beam, than the elastic cross-sectional analysis (Table 5.1).

This discrepancy may be attributed in part to the fact that method (c) on which the cross-sectional analysis was based assumes points of inflection at mid-length of opening centerlines, whereas the finite element results and the test observations clearly illustrate that the latter point is in general not at mid-length of the opening, but varies in position from one opening to the next, depending on the degree of connectivity achieved between the steel section and the composite deck. Another possibility for the discrepancy can be attributed to the fact that method (c) in Chapter 4 assumes full composite action, while the finite element results were based on a model which attempted to simulate the partial shear connection that was used in the test beams; the use of partial shear connection increases the horizontal shear force in the web-post because of the reduced horizontal shear transferred between the steel and concrete interface, as indicated in the FEM results for 1B and 1D in Table 4.3.

In the experimental program, strains measured by rosette strain gauges, placed near the web-post mid-height, were used to estimate the horizontal shear force in the web-posts of Beams 1, 2 and 3 in the elastic range. For a unit vertical shear of 1 kN acting on the composite beam cross-section, it was found that in the elastic range the horizontal web-post shearing forces were 0.19, 0.34 and 0.4 kN in the three test beams respectively. On the other hand, the theoretical values, based on equilibrium of the

free-body diagram shown in Figure 3.16 with a composite concrete slab, and the assumptions of "strength of materials" (a parabolic shear stress distribution along the weld rectangular cross-section), were 0.622, 0.622 and 0.634 respectively for Beams 1, 2 and 3, as indicated in Table 4.3. Thus the test measurements are from 30 to 60% lower than those obtained from linear theory, and even lower when compared with the FEM results.

5.2 Distribution of Vertical Shearing Forces

To determine the shearing stresses in the tee-sections above and below the openings in Beams1, 2 and 3, some strain rosettes were placed on an opening centerline. The measured shear strains in the lower tee were used to estimate the shear force carried below the opening. This was done using the "strength of materials" solution relating shear stresses to shear forces in a prismatic beam. The percentage of shear force in the tee-sections and concrete slab, as obtained from the experimental results, are summarized in Table 5.2. These suggest that most of the shear force will be carried by the upper portion of the beam above an opening; however, the reliability of the specific values is questionable, particularly because it could have been anticipated that Specimen 3 with the deeper bottom tee-section would have carried more than Specimen 2. In addition, it is unlikely that the concrete slab would have been able to carry so much vertical shear with the low degree of shear connection provided, and when no yielding is anticipated in the tees while being in the elastic range.

The finite element results corresponding to Beams 1, 2 and 3 are also indicated in Table 5.2. Model 1B was used to simulate test Beams 1 and 2 with mid-depth openings, while 1G represents Beam 3 with a 19.1 mm opening eccentricity. It is clear from the finite element results that in the mid-depth cases, the bottom tees will carry less than 50% of the vertical shear, with the upper tee and slab together sharing the balance, see Table 5.2 for the specific ratios. The opening eccentricity further increases the amount of vertical shear in the concrete slab due to the decreased upper tee-section depth and increases that carried by the bottom tee; this is to be expected because of the increased depth of the tee-section below the opening.

There is a large discrepancy between the vertical shear force distribution determined from the FEM and that obtained from the test strain measurements. While both methods indicate that more vertical shear will be carried above an opening, the percentages are quite different. The test results can be considered inconclusive because there is no explanation as to why the bottom tee-section in Beam 3 carries less than Beam 2, when it must be expected to carry more because of the greater stiffness. In addition, there is no reason to anticipate the observed changes in the vertical shear force distribution between Beams 1 and 2, unless the preload in Beam 1 affected the results. A possible cause for these incompatible results might be due to the inappropriate use of the "strength of materials" solution in deriving forces from measured strains; also in most cases, the limited web depth permitted only one strain gauge which was located quite near the hole edge, thus recording a low magnitude of shear strain and magnifying any error. The shear forces obtained from the measured strains are so consistently lower than expected that some systematic error is suspected. Exhaustive examination of the procedures followed has not identified the problem.

5.3 Flexural Failure Loads

Because the test beam dimensions differed slightly from the nominal values used in Figure 4.4, the yield interaction diagram for Beam 5, with mid-depth openings, is redrawn in Figure 5.1. It can be seen from Table 5.3 that the beam failed at a load very close to the predicted value; this is indicated by the M/M_p ratio. In Beam 5, the ratio of test to predicted loads was 1.01; here buckling did not occur. If a parabolic curve is used instead of the assumed horizontal cut-off to account for partial shear connection, the ratio rises to 1.03.

A similar result was obtained for Beam 4 with eccentric openings, as indicated in Figure 5.2. In this situation the ratio of test to theory was 0.983 (using the horizontal cut-off) for Beam 4, which collapsed in flexure after the failure of the shear connectors.

As can be seen from Table 5.3, the results based on yielding failures are in good agreement with the test failure loads for the longer test beams which failed in flexural modes corresponding to those predicted by the analyses.

From the yield analysis performed in Chapter 4, and referring to Figures 4.3 and 4.4 with a horizontal cut-off at (n=5 studs), it is clear that the composite test beam (Beam 5) is 42% stronger in flexure than its non-composite counterpart.

5.4 Web-post Failure

As with the flexural specimens in the previous section, the test beam dimensions differed slightly from the nominal values used in Figure 4.4, the yield interaction diagram for Beams 2 with mid-depth openings, is redrawn in Figure 5.1. Table 5.4 shows that Beam 2 failed at a load lower than the predicted value based on yield, as indicated by the V_u/V_p ratio. The ratio of test ultimate load to yield load was 0.895; this difference can be attributed to the buckling failure, which is not considered in the yield analysis. A similar result was obtained for Beam 3 with eccentric openings, as indicated in Figure 5.2. The ratio of test to theory was 0.898 for the short beam, Beam 3, which failed by web-post buckling, not yield.

Referring to the FEM stress results of 1B and 1G in Table 3.7, which correspond to test beams 2 and 3 respectively, it can be concluded from comparing the V_{cr}/V_p ratios with those from the test in Table 5.5 that while the trends are similar in both cases, the finite element method predicts greater web-post shearing forces, 0.252 and 0.238 for beams 2 and 3 compared with 0.221 and 0.219 as obtained from the test results; this is also illustrated in figures 5.1 and 5.2.

The predicted load causing web-post buckling in Beams 2 and 3, using the finite element analysis, was found to be 7% and 5% greater than that predicted from the test results.

5.5 Composite versus Non-composite Beams

When referring to the FEM results of 1A and 1B in Table 4.3, one can notice that the horizontal shear in the web-post is greater in the non-composite case than in the composite one. This is indicated by the V_h/V ratio, which is 0.826 for 1A (non-

composite) and 0.717 for 1B (composite). Hence the ratio of horizontal shear in the post for the composite case to the non-composite one ($V_{h.comp}/V_{h.noncomp}$) is 0.868.

When using the "strength of materials" approach described in the previous chapter, it is noticed that by increasing the modular ratio n_c by a factor of nine (i.e. reducing the slab stiffness to represent partial shear connection), the $V_{h.comp}/V_{h.noncomp}$ ratio will reach the same value obtained using the FEM (i.e. 0.868); this notion is illustrated in Table 5.6.

A similar result was also obtained for the cases with eccentric openings (i.e. 1F and 1G). Referring back to Table 4.3, the FEM $V_{h.comp}/V_{h.noncomp}$ ratio was found to be 0.901. The $V_{h.comp}/V_{h.noncomp}$ ratio based on the "strength of materials" approach is shown in Table 5.7. It is clear that had a multiplier of around 12 been used, there would be excellent correspondence between the two approaches.

Table 5.1: Web-post Shears as a proportion of Beam Shear

BEAM	V_h / V	
	CROSS-SECTION ANALYSIS *	FINITE ELEMENT METHOD +
1B (Specimen 2)	*0.622*	*0.717*
1G (Specimen 3)	*0.634*	*0.736*

* Method (c) assuming full shear connection. Chapter 4

\+ Method (d). Chapter 4

V_h = horizontal shear in web-post

V = vertical shear on beam

Table 5.2: Shear distribution in the tees and concrete slab at an opening centerline

PARAMETER		Shear Distribution (%)		
SPECIMEN		1 *,+	2 *,+	3 *,#
TEST	*Concrete slab & Top tee*	*89*	*75*	*81*
	Bottom tee	*11*	*25*	*19*
FEM	*Concrete slab*	*31*	*31*	*35*
	Top tee	*28*	*28*	*19*
	Bottom tee	*41*	*41*	*46*

* *Test results based on "strength of materials" solution*

\+ *based on finite element model 1B*

\# *based on finite element model 1G*

Table 5.3: Test/Theory(yield) ratios for flexural specimens

BEAM	M_u / M_p		Test/Theory Ratio
	Test	Theory (yield analysis)	
4	*0.985*	*1.002*	*0.983*
5	*0.947*	*0.937*	*1.011*

* *(M_u/M_p) corresponding to an (n_c) value of 21.6, see Chapter 4*

Table 5.4: Test/Theory(yield) V_u/V_p ratios for shear specimens

BEAM	V_u / V_p		Test/Theory Ratio
	Test	Theory (yield analysis)*	
1	*0.234*	*0.247*	*0.947*
2	*0.221*	*0.247*	*0.895*
3	*0.219*	*0.244*	*0.898*

* *(V_u/V_p) corresponding to an (n_c) value of 21.6, see Chapter 4*

Table 5.5: Test/Theory(FEM) V_u/V_p ratios for shear specimens

BEAM	V_u / V_p		Test/Theory Ratio
	Test	Theory (FEM)	
1	*0.234*	*0.252*	*0.929*
2	*0.221*	*0.252*	*0.877*
3	*0.219*	*0.238*	*0.92*

* *(V_u/V_p) corresponding to an (n_c) value of 21.6, see Chapter 4*

Table 5.6: Composite/Non-composite web-post shear ratio using the "strength of materials approach": Mid-depth openings (1A and 1B)

multiplier (x)	1	2	3	4	5	6	9	10
modular ratio	7.2	14.4	21.6	28.8	36	43.2	64.8	72
V_h/V^*	0.622	0.636	0.646	0.655	0.662	0.668	0.684	0.689
$V_{h,comp} / V_{h,noncomp}^+$	0.79	0.808	0.821	0.832	0.841	0.849	0.869	0.875

* *based on "strength of materials" approach*

\- $V_{h,comp}$ *(1B) = 0.787* $V_{h,noncomp}$ *(1A), referring to Table 4.3*

Table 5.7: Composite/Non-composite web-post shear ratio using the "strength of materials approach": Eccentric openings (1F and 1G)

multiplier (x)	1	2	3	4	5	6	9	10
modular ratio	7.2	14.4	21.6	28.8	36	43.2	64.8	72
V_h/V^*	0.634	0.646	0.655	0.663	0.669	0.675	0.689	0.693
$V_{h,comp} / V_{h,noncomp}^+$	0.806	0.821	0.832	0.842	0.85	0.858	0.876	0.881

* *based on "strength of materials" approach*

\- $V_{h,comp}$ *(1G) = 0.787* $V_{h,noncomp}$ *(1F), referring to Table 4.3*

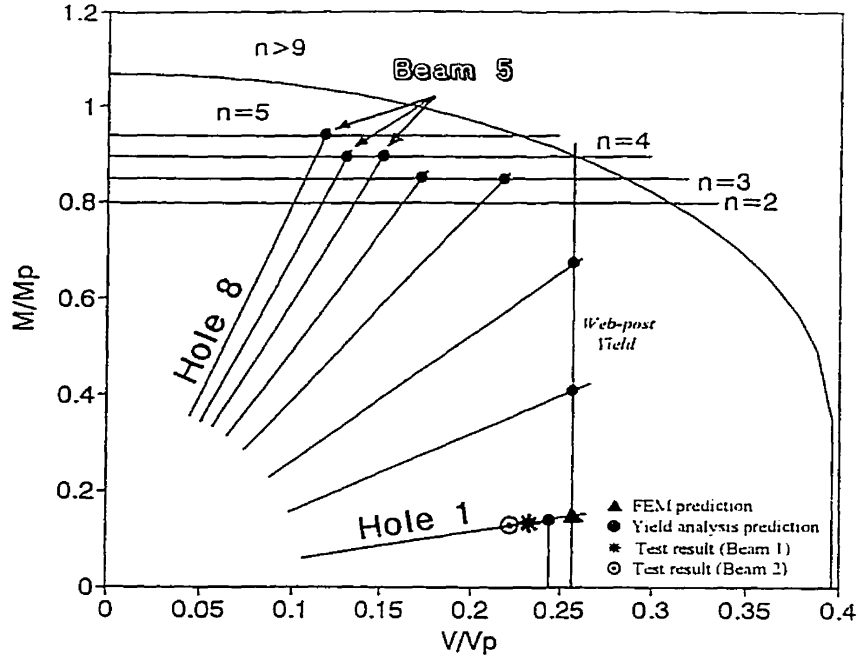

Figure 5.1: M/V interaction diagram for test beams 1, 2 and 5 with mid-depth openings (Yield Analysis)

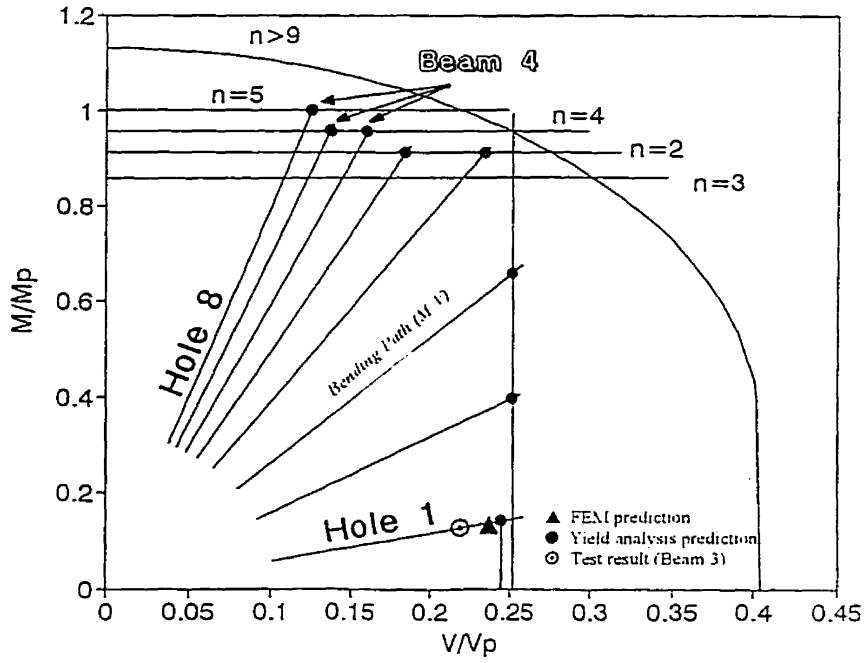

Figure 5.2: M/V interaction diagram for test beams 3 and 4 with eccentric openings (Yield Analysis)

CHAPTER SIX

CONCLUSIONS

Several concluding remarks, pertaining to non-composite and composite castellated beams, can be drawn from the experimental program, finite element analysis, and yield analysis incorporated in this research program.

6.1 General Conclusions

6.1.1 Experimental Program

- Ultimate failure of the three shear critical composite castellated test beams (Specimens 1, 2 and 3) was associated with lateral-torsional buckling of the web-posts. The longer flexural test beams (Specimens 4 and 5), on the other hand, failed when most of the studs in one half of the span failed, resulting in lateral-torsional buckling of the suddenly unconstrained compression flange. Before this occurred, high strains ($\approx$ 10 times the yield strain) had developed following tensile yield of the lower part of the steel beam, while tensile strains had also developed above the opening indicating that the neutral axis was close to the concrete slab.

- Opening eccentricity was found to have little effect on the buckling behavior of the web-posts in the shear critical test specimens; for the flexure critical beams, it may account for the slight improvement in the strength of Beam 4 compared with Beam 5.

- From the test program, the effect of unshored construction was found to be insignificant in governing the buckling behavior of the shear critical castellated beams.

6.1.2 Numerical Study (Finite Element Analysis)

- In the numerical study using the finite element method, web-post buckling was the dominant mode of failure observed in all composite and non-composite models; however, the composite beams were found to have significantly higher ultimate shear carrying capacities than their non-composite counterparts. This was attributed principally to the reduced horizontal shear force in the web-posts as a result of the composite action, hence providing the posts with an extra reserve to carry more load.

- The web-post buckling capacity of non-composite and composite castellated beams, in which openings are eccentric with respect to the beam mid-depth, is shown by the finite element analysis to be only slightly affected by the magnitude of the opening eccentricity.

- The finite element model proposed in this study captured the nonlinear buckling behavior in both composite and non-composite castellated sections.

- The FEM results suggest a 67% and 48% increase in the shear carrying capacity of Beam 1B (with mid-depth openings) and Beam 1G (with eccentric openings), respectively, compared with their non-composite counterparts (Beams 1A and 1F).

- In the non-composite cases, FEA showed that reducing the throat distance had little influence on the beam shear capacity, as long as the weld had sufficient strength to transmit the force. However, the reduction in throat distance resulted in reduced horizontal shear in the post and increased the weld susceptibility to rupture as indicated in the V_{hcr}/V_p ratio for 2A. Reducing the angle of cut and opening height for the studied section resulted in increasing the beam shear capacity by 4% and 25% for beams 3A and 4A respectively, compared with 1A.

- In the composite sections studied using FEA, reducing the throat distance, cut angle, and opening height, resulted in decreasing the beam shear capacity and increasing the horizontal shear stress at the welded joint level. Reducing the stiffness of the concrete slab or using partial shear connection resulted in decreasing the composite beam shear carrying capacity, in addition to lowering the level of the neutral axis, thus decreasing the flexural capacity too. These reduce the amount of horizontal force and vertical shear in the concrete slab, leading to an increase in the stress resultants in the tee-sections above and below an opening, thus increasing the horizontal force in the web-post. As a result, the weld area is more vulnerable to rupture, and the web-post is more likely to buckle.

6.1.3 Yield Analysis

- No Vierendeel modes of failure were observed in any of the test specimens or finite element models with different opening geometries because of the short weld lengths adopted in all the beams. In Chapter 4, interaction diagrams for the ultimate shearing force and bending moments, which were originally developed for isolated web openings, have been successfully applied to hexagonal openings in castellated beams. These solutions are based on the occurrence of full yield or concrete failure, and do not consider buckling. It is shown that the mechanism failure will only occur under a high M/V ratio; at a low M/V, the web-post will yield at its mid-depth. In addition, at a high value of M/V, the beam capacity may be limited if there is a small number of shear connectors between a potentially critical opening and the nearest point of zero bending moment.

- It was found from the yield analysis that the shear capacity of a composite beam is significantly reduced by the web-post yield, whereas the non-composite one is only slightly reduced below that for the four hinge mechanism.

- The yield analysis indicates a 42% increase in the flexural capacity of the test beam 5 with mid-depth openings compared with its non-composite counterpart.

6.2 General Comparisons

6.2.1 Comparison of Tests and Theories

- The experimental results from the strain measurements and the FEM results suggest that most of the beam vertical shear will be carried by the upper portion above an opening, be it mid-depth or eccentric.

- The predicted loads causing buckling for the shear critical beams, using the FEM, are in very good agreement with those obtained from the tests.

- Results based on yielding failures are in very good agreement with the test failure loads for the flexural test beams 4 and 5, which failed in flexural modes corresponding to those predicted by the yield analysis. On the other hand, the yield analysis tends to slightly overestimate the failure loads for the shear critical composite beams (1, 2 and 3) by about 10%; this due largely to the buckling failures of the web-posts in the tests, which are not accounted for by the yield analysis.

6.2.2 Comparison of FEM and Yield Approach

- The finite element method predicted a higher horizontal shear force in the web-post than the elastic cross-sectional analysis based upon method (c) in Chapter 4.

- It should be noted that the yield results were initially based on the assumption of full shear connection, and perfect bond (i.e. no slip); as a result, the yield analysis tends to predict slightly lower horizontal shear forces in the web-posts, for the composite and non-composite cases, when compared with those obtained from the FEM. However, it was found that by increasing the modular ratio (n_c) in the "strength of materials" approach to represent partial shear connection, as was used in the FEM, the yield analysis results achieve better agreement with those of the FEM.

- From the FEM and yield analyses, it was found that yielding at mid-depth of the post (i.e. at the welded joint) is expected to be more significant in composite castellated beams than in the corresponding non-composite cases, because the horizontal shear force in the web-posts were found to approach 90% of the web-post yield capacity in most the composite sections, when buckling failure occurred. With the exception of 4A, the shear force in the web-posts of the non-composite beams were also below 76%.

6.2.3 Miscellaneous

- Current design methods for composite beams conservatively choose to ignore any shear contribution from the concrete slab; this notion is, however, negated here as it was found that the concrete slab played an important role in improving the shear capacity of the web-posts by reducing the amount of vertical shear carried by the tee-sections at an opening and reducing the horizontal shear in the post.

REFERENCES

Aglan, A.A., and Redwood, R.G. 1974. Web buckling in castellated beams. Proc. Instn. Civ. Engrs, Part 2, Vol. 57, pp 307-320.

Bazile, A., and Texier, J. 1968. Essais de poutres ajourées (Tests on castellated beams). Constr. Métallique, Vol. 3, pp 12-25.

Caffrey, J.P., and Lee, J.M. 1994. MSC/NASTRAN: Linear static analysis user's guide, V68. The Macneal-Schwendler Corporation, Los Angeles, California, USA.

Canadian Institute of Steel Construction. 1995. Handbook of steel construction, 2nd edition. Universal Offset Limited, Markham, Ontario, Canada.

Canadian Standard Association, 1987. General requirements for rolled or welded structural quality steel. CAN/CSA-G40.20-M87, Roxdale, Ontario, Canada.

Chien, E.Y.L., and Ritchie, J.K. 1984. Design and construction of composite floor systems. Canadian Institute of Steel Construction, Willowdale, Ontario, pp 323.

Deiesques, R. 1968. Stabilité des montants des poutres ajourées (Stability of web posts of castellated beams). Constr. Métallique, No. 3, pp 26-33.

Dougherty, B.K. 1993. Castellated beams: A state of the art report. Journal of the South African Institution of Civil Engineers, **35**:2, 2nd Quarter, pp 12-20.

Giriyappa, J., and Baldwin, J.W. 1966. Behaviour of composite castellated hybrid beams. Univ. of Missouri Engng. Experimental Res. Station, Columbia, Mo, USA.

Halleux, P. 1967. Limit analysis of castellated steel beams. Acier-Stahl-Steel, **32**:3, 133-144.

Hartono, W., and Chiew, S.P. 1996. Composite behaviour of half castellated beam with concrete top slab. Advances in Steel Structures. Proceedings of a conference in Hong Kong, Pergamon. Editors: S.L. Chan and J.G. Teng, pp 437-442.

Hosain, M.U., and Spiers, W.G. 1973. Experiments on castellated steel beams. J. American Welding Society, Welding Research Supplement, **52**:8, 329S-342S.

Jayas, B.S., and Hosain, M.U. 1987. Behaviour of headed studs in composite beams: push-out tests. Canadian Journal of Civil Engineering, **15**:2, 240-253.

Jayas, B.S., and Hosain, M.U. 1989. Behaviour of headed studs in composite beams: full-size tests. Canadian Journal of Civil Engineering, **16**:5, 712-724.

Kulak, G.L., Adams, P.F., and Gilmor, M.I. 1990. Limit state design in structural steel. Canadian Institute of Steel Construction, 358 p.

Kerdal, D., and Nethercot, D.A. 1984. Failure modes for castellated beams. J. Constr. Steel Research, Vol. 4, pp 295-315.

Knowles, P.R. 1991. Castellated beams. Proc. Institution of Civil Engineers, Part 1, Vol. 90, pp 521-536.

Kolosowski, J. 1964. Stresses and deflections in castellated beams. Struct. Engr, **42**:1, 19-24.

Larnach, J.W., and Park, R. 1964. The behaviour under load of six castellated composite T-beams. Civ. Engng. and Pub. Works, **59:**692, 339-343.

Lee, S.H. 1992. MSC/NASTRAN: Handbook for nonlinear analysis, V67. The Macneal-Schwendler Corporation, Los Angeles, California, USA.

Maalek, S., and Burdekin, F.M. 1991. Weld quality requirements for castellated beams. Struct. Engr, **69:**13, 243-254.

Nethercot, D.A., and Kerdal, D. 1982. Lateral-torsional buckling of castellated beams. Struct. Engr, **60B:**3, 53-61.

Okubo, T., and Nethercot, D.A. 1985. Web post strength in castellated beams. Proc. Instn. Civ. Engrs, Part 2, Vol. 79, pp 533-557.

Raymond, M., and Miller, M. 1994. MSC/NASTRAN: Quick reference guide, V68. The Macneal-Schwendler Corporation, Los Angeles, California, USA.

Redwood, R.G. 1968. Ultimate strength design of beams with multiple openings. Preprint No. 757, ASCE Annual Meetings and National Meeting on Structural Engineering, Pittsburgh, Pa, USA.

Redwood, R.G. 1983. Design of I-beams with web perforations. In beams and beam columns- Stability and Strength. Editor: R. Narayanan, Applied Science Publishers, London.

Redwood, R.G., and Cho, S.H. 1993. Design of steel and composite beams with web openings. J. Construct. Steel Research, **25:**1&2, 23-41.

Redwood, R.G., and Wong, P. 1982. Web holes in composite beams with steel deck. Proc. 8th Canadian Structural Engineering Conference, Canadian Steel Construction Council, Willowdale, Ontario, Canada.

Robinson, H. 1988. Multiple stud shear connections in deep ribbed metal deck. Canadian Journal of Civil Engineering, **15**:4, 553-569.

Sherbourne, A.N. 1966. The plastic behaviour of castellated beams. Proc. 2nd Commonwealth Welding Conference. Inst. of Welding, No. C2, London, pp 1-5.

Toprac, A.A., and Cooke, B.R. 1959. An experimental investigation of open-web beams. Welding Research Council Bulletin, Series No. 47, New York.

Ward, J.K. 1990. Design of composite and non-composite cellular beams. The Steel Construction Institute.

Zaarour, W.J., and Redwood, R.G. 1996. Web buckling in thin webbed castellated beams. ASCE Journal of Structural Engineering, **122**:8, 860-866.

APPENDIX A

NASTRAN INPUT FILES

A.1 Generating the Nastran input file

The NASTRAN input file is basically composed of four main sections: File Management Section, Executive Control Section, Case Control Section, and Bulk Data Section. The File Management Section is an optional section and is used for allocating files, control restarts and database operations. In this study, this section was strictly used for nonlinear buckling analysis restart files.

The Executive Control Section contains the first required group of statements in any MSC/NASTRAN input files. The primary functions of the Executive Control Section are as follows:

* *defining the type of analysis to be performed and the solution sequence.*
* *defining general conditions such as time allocation and desired system diagnostics.*

In the input files, NASTRAN was requested to perform nonlinear stress and buckling analysis using a structural solution sequence called SOL 106. This solution sequence is used to perform nonlinear static analysis, which can later be used to perform nonlinear buckling analysis. The main reason behind selecting SOL 106 is the interest in finding out whether NASTRAN can accurately predict the non-linear buckling behavior of the web-posts in composite castellated beams.

The case control section always follows the executive control section and proceeds the bulk data section; it is an essential requirement for any input file. The primary functions of the case control section are:

* *specifying sets of bulk input data that are to be used in the analysis.*
* *specifying output requests such as: ECHO, FORCE, SPCFORCE, STRESS, DISPLACEMENT, etc.*

** selecting certain bulk data conditions such as: type of loads, constraints, and nonlinear parameters to be used, as shown below.*

The bulk data section contains all data necessary for describing a structural model; it was used in the Nastran FEM input file to define the following:

** geometric nonlinearity, which will allow for large displacements.*

** set of parameters for nonlinear static analysis iteration strategies (load increments and stiffness matrix and conversion updates).*

** geometry and constraints: coordinate systems, location of grid points in space and their corresponding degrees-of-freedom, using the input card GRID.*

** element types: one and two dimensional elements (CQUAD4, CTRIA3, CBEAM).*

** material properties, using MAT1 & MATS1 to define nonlinear material properties.*

** element properties, using PSHELL & PBEAM to define element area, inertia, etc.*

** load value and orientation, using the FORCE card.*

It should be noted that, in the input files, the Nastran card PARAM,LGDISP was used to impose geometric nonlinearity, while the card MATS1 was used in conjunction with MAT1 to define material nonlinearity.

It was mentioned earlier that the CQUAD4 elements used in modeling the web, flanges and stiffeners had zero rotational stiffness about the surface normal. One way to eliminate the singularities associated with this lack of normal rotational stiffness is to apply a fictitious stiffness term to the degrees-of-freedom using the PARAM,K6ROT card (Caffrey and Lee, 1994). In the input files, this card was assigned the default value of 100, which is automatically assigned to all nonlinear runs with SOL 106.

In the previous work by Zaarour and Redwood (1996), a fictitious value of 10000 was assigned to the PARAM,K6ROT card of the input file to suppress the singularities associated with the normal D.O.F. Even though this yielded acceptable results, it is

generally recommended that usage of such a high value for K6ROT should be avoided. The value assigned to PARAM,K6ROT directly affects the stiffness of the elements and the overall structural stiffness; hence, it can affect the buckling behavior of the modeled web-posts. It was therefore judged appropriate to use the default value of 100, while constraining the appropriate D.O.F. in the nodal points.

A.2 Reasons for performing Non-linear Analysis using SOL 106

- Buckling is associated with large displacements and rotations; i.e. the displacement transformation matrix is no longer constant as is the case for linear analysis.

- Buckling occurs in the portion of the P-Δ curve where the stiffness matrix is no longer constant; as a result, the stiffness matrix keeps on changing and needs to be updated regularly.

- The kinematics relationships is nonlinear. Both compatibility and equilibrium are satisfied in the perturbed configuration as a result of the inclusion of geometric and differential stiffness.

- Elements may yield; hence, element constitutive relationship is nonlinear (nonlinear-elastic or plastic material).

A.3 Non-linear Stress and Buckling Analysis

In order to perform non-linear buckling analysis using the Nastran FE package, the analysis is subdivided into two stages (or two input files): the Cold start run and the restart run; these are described below

A.3.1 Non-linear Static Analysis (Cold Start Input File)

This is the first step in performing the non-linear buckling analysis; the cold start begins with performing a non-linear static analysis using SOL 106, see the cold start input file in Appendix B. The type of loading imposed on the finite element model is subdivided into different subcases in the case control section. The NLPARM Nastran card is then used to define the number of load increments and iterations to achieve a specific load, the method for controlling stiffness updates, and the convergence criterion. In most cases the default values were used in defining key Nastran parameters; for example, AUTO is the default method for controlling the stiffness update strategy; here the program will automatically select the most efficient strategy based on convergence rates. Another important command used in the nonlinear analysis is the LGDISP parameter which allows for large displacements and rotations in the model. As mentioned previously, all data pertaining to the model geometry, boundary conditions, element type and properties are defined in the bulk data section of the file. For particular descriptions and default values of the various Nastran parameters, please refer to Reymond, M., and Miller, M. (1994).

The algorithm used in performing the non-linear static analysis is illustrated in Figure A.1 and it is summarized in the following nine steps:

- Advancing (Predicting) Phase:

1. *Determine an increment (e.g., load, displacement, or arc length) to move forward along the equilibrium path.*
2. *Determine an estimate of a tangent stiffness matrix.*
3. *Determine the displacement increment to move forward; generally by solving equilibrium equations.*
4. *Calculate the element resulting forces.*
5. *Calculate the unbalanced load and check for convergence.*

(note) if solution converges, then go to step 1, else continue as follows:

- Correcting (Iterating) Phase:

6. *Determine an estimate of the tangent stiffness matrix.*
7. *Determine the displacement increment due to the unbalance load.*
8. *Calculate the element resisting forces.*
9. *Calculate the unbalanced load and check for convergence.*

(note) if solution converges, then go to step 1, else go to step 6.

A.3.2 Buckling Analysis (Restart Run)

This is the second and final stage of the non-linear buckling analysis run. A restart input file uses data stored in the previous run (Cold start) to accomplish the tasks requested in the current one. In the cold start, the load in the nonlinear static analysis keeps on increasing until instability is detected; the buckling analysis is then continued using the restart input file. The instability is signaled by the occurrence of a singularity when a negative determinant of [K] is encountered; a message referring to the singularity is provided by the cold start run output..

In the restart run, the load is initiated two or three load steps (or loopid) before that which caused the instability; this will allow for predicting the buckling load causing the instability using the buckling equations. The key Nastran parameters used in the restart buckling input file are summarized as follows:

SOL 106
PARAM,BUCKLE
PARAM,LGDISP
METHOD & EIGB

The Nastran parameters BUCKLE, LGDISP and METHOD are used in SOL 106 to impose the nonlinear buckling analysis. The EIGB option is then used to provide the necessary information pertaining to bifurcation buckling, such as eigenvalue range, method of eigenvalue extraction, method for normalizing the eigenvectors, etc. A sample restart input file, used in this research, is provided in Appendix B. In the restart input file the INCLUDE statement was used in the executive control section to invoke the file "nlbshape" which contains the necessary PLOT commands to view the

mode shapes of the buckled web-posts. This file is also included in Appendix B; without this file, it would impossible to view the nonlinear buckled mode shapes.

As mentioned earlier, buckling of the web-posts in the castellated beams investigated herein was associated with a bifurcation buckling problem: loss of stability occurs when two or more equilibrium paths intersect in the load-deflection space (Figure A.2); the point of intersection is termed a bifurcation point, and any load beyond this point will cause the structure to buckle. If one is interested in studying the post-buckling behavior, such as in the case of a snap-through buckling problem (Figure A.3), it is recommended to combine the NLPARM with NLPCI arc length increments, which allow tracing the structure behavior beyond the buckling point.

The nonlinear buckling concept associated with the Nastran BUCKLE parameter is illustrated in Figure A.4, while the relevant equations are summarized below:

$$[K_n - \lambda \Delta K]\{\phi\} = \{0\}$$
$$\{u_{cr}\} = \{u_n\} - \lambda \{\Delta u\}$$
$$F_{cr} = \{P_{cr}\} = \{P_n\} - \alpha \{\Delta P\}$$

where,

λ = *eigenvalue*

ϕ = *eigenvector*

$\{u_{cr}\}$ = *critical displacement or displacement at buckling*

$\{P_{cr}\}$ = *critical load or load causing buckling*

$\Delta K = K_n - K_{n-1}$ = *incremental stiffness*

$\{\Delta u\} = \{u_n\} - \{u_{n-1}\}$ = *incremental displacement*

$\{\Delta P\} = \{P_n\} - \{P_{n-1}\}$ = *incremental load*

α = *critical buckling factor* $= \dfrac{\lambda.\{\Delta u\}^T[K_n + 0.5\lambda.\Delta K]\{\Delta u\}}{\{\Delta u\}^T\{\Delta P\}}$. *given by the restart run output*

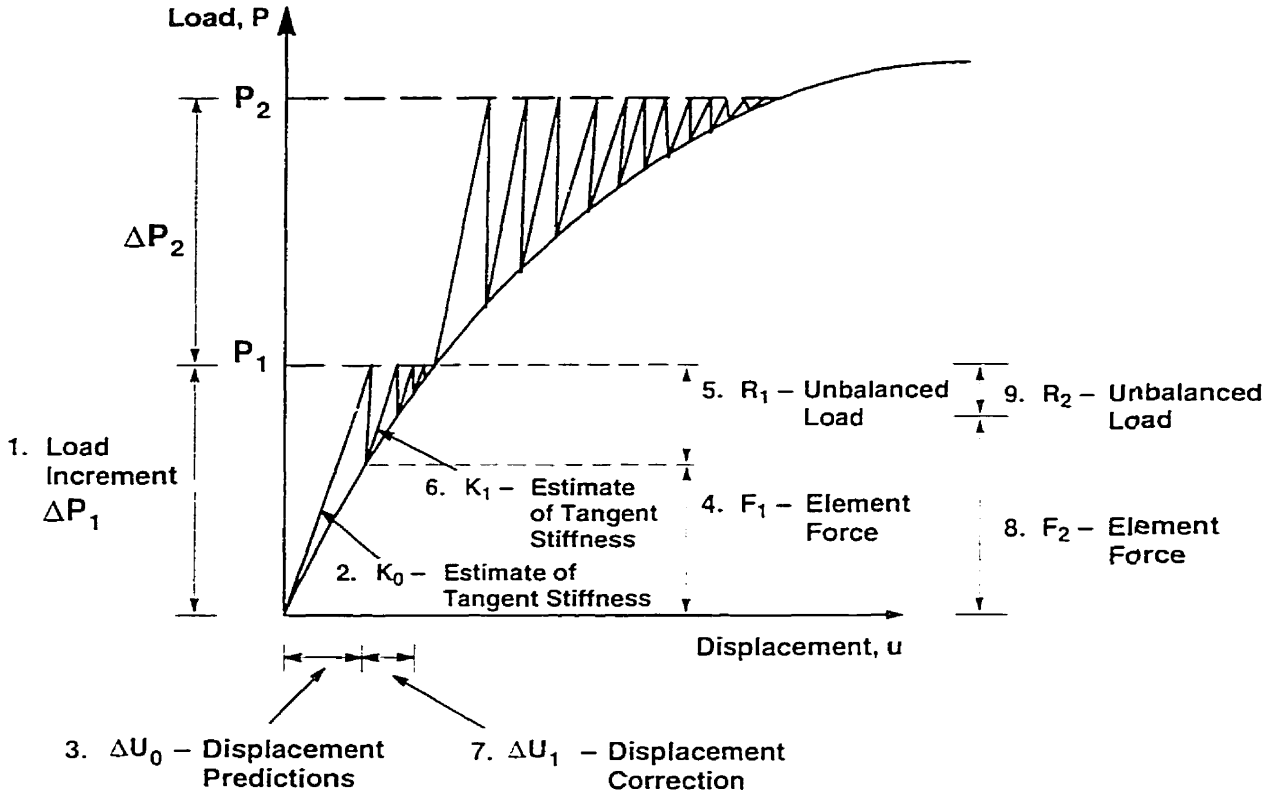

Figure A.1: Concept of non-linear analysis in MSC/NASTRAN

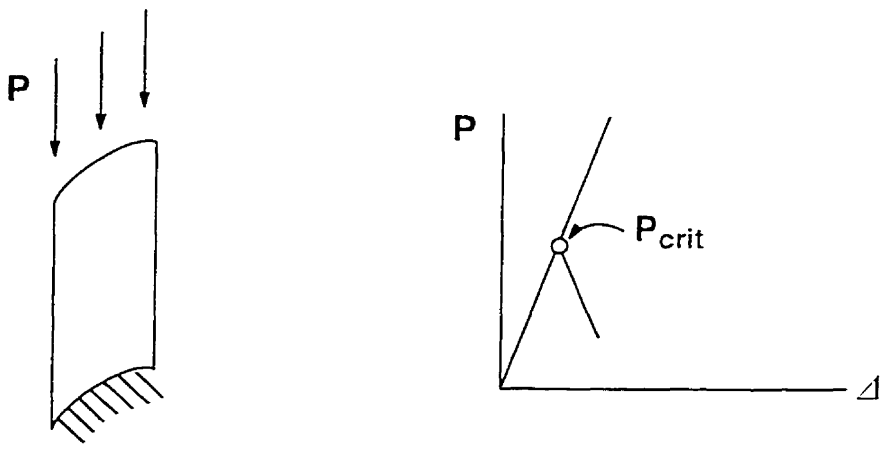

Figure A.2: Bifurcation buckling problem

Figure A.3: Snap-through buckling problem

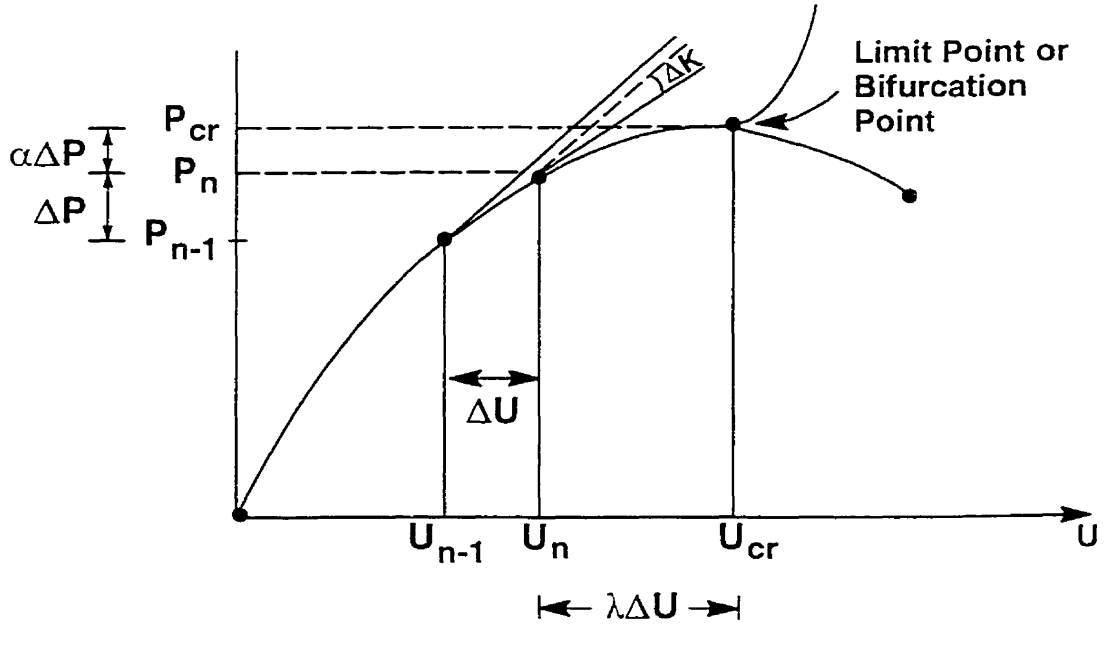

Figure A.4: Concept of non-linear buckling using MSC/NASTRAN

APPENDIX B

SAMPLE NASTRAN INPUT FILES

SAMPLE "COLD START" NASTRAN INPUT FILE

```
$ !!!!!!!!!!!!!!!!!!!!!!!!!!!!!!!!!!!!!!!!!!!!!!!!!!!!!!!!!!!!
$ < A >  E X E C U T I V E   C O N T R O L   S E C T I O N
$ !!!!!!!!!!!!!!!!!!!!!!!!!!!!!!!!!!!!!!!!!!!!!!!!!!!!!!!!!!!!
$
ID MOD6-58, Non-linear analysis of a "Composite Castellated Beam"
SOL 106
TIME=900
CEND
$
$ !!!!!!!!!!!!!!!!!!!!!!!!!!!!!!!!!!!!!!!!!!!!!!!!!!!!
$ < B >  C A S E   C O N T R O L   S E C T I O N
$ !!!!!!!!!!!!!!!!!!!!!!!!!!!!!!!!!!!!!!!!!!!!!!!!!!!!
$
TITLE = TRIAL#4: Mid-depth case; <3"slab; ho=11.85"; phi=59.94; 2"weld>
$
SET 1 = 4,5,6,7,8,9,78,79,90,91,102,103,114,115,126,127,138,139,150,151,
        162,163,174,175,186,187,204,205,206,207,208,209,278,279,290,291,
        302,303,314,315,326,327,338,339,350,351,362,363,374,375,386,387,
        406,407,418,419,430,431,442,443,456,457,468,469,480,481,492,493,
        707,719,731,732,743,744
$
ECHO = NONE
  FORCE = 1
  SPCFORCE = ALL
  STRESS(PLOT) = ALL
  DISPLACEMENT(PLOT) = ALL
$
SUBCASE 1
  LOAD = 10
  NLPARM = 10
SUBCASE 2
  LOAD = 20
  NLPARM = 20
SUBCASE 3
  LOAD = 30
  NLPARM = 30
SUBCASE 4
  LOAD = 40
  NLPARM = 40
OUTPUT(POST)
$
$ !!!!!!!!!!!!!!!!!!!!!!!!!!!!!!!!!!!!!!!!!!!!!!!!
$ < C >  B U L K   D A T A   S E C T I O N
$ !!!!!!!!!!!!!!!!!!!!!!!!!!!!!!!!!!!!!!!!!!!!!!!!
$
BEGIN BULK
PARAM,POST,0
PARAM,DBCCONV,XL
PARAM,LGDISP,1
PARAM,DBDRNL,-1
PARAM,K6ROT,100.0
NLPARM,10,2,,AUTO,,,UPW,YES
NLPARM,20,5,,AUTO,,,UPW,YES
NLPARM,30,10,,AUTO,,,UPW,YES
NLPARM,40,20,,AUTO,,,UPW,YES
$
$ !!!!!!!!!!!!!!!!!!!!!!!!!!!
$ [1] GRID POINTS ALLOCATION
$ !!!!!!!!!!!!!!!!!!!!!!!!!!!
$
$ ******************************************
$ GRID IDENTIFICATION NUMBERS OF WEB'S UPPER HALF
$ ******************************************
$
GRID,1,,0.0,0.0,0.0,,25
GRID,2,,8.5,0.0,0.0,,6
=,*(1),=,*(8.5),==
=(1)
GRID,5,,250.5,0.,0.,,6
=,*(1),=,*(8.5),==
=(1)
GRID,8,,276.0,0.,0.,,6
GRID,9,,284.5,0.,0.,,6
=,*(1),=,*(8.5),==
=(1)
GRID,12,,526.5,0.,0.,,6
=,*(1),=,*(8.5),==
=(1)
$
GRID,16,,0.,21.5,0.,,
GRID,17,,12.614,21.5,0.,,6
=,*(1),=,*(12.614),==
=(1)
GRID,20,,238.158,21.5,0.,,6
=,*(1),=,*(12.614),==
=(1)
GRID,23,,276.0,21.5,0.,,6
GRID,24,,288.614,21.5,0.,,6
=,*(1),=,*(12.614),==
=(1)
GRID,27,,514.158,21.5,0.,,6
=,*(1),=,*(12.614),==
=(1)
$
GRID,31,,0.,43.0,0.,,
GRID,32,,16.761,43.0,0.,,6
=,*(1),=,*(16.761),==
=(1)
GRID,35,,225.717,43.0,0.,,6
=,*(1),=,*(16.761),==
=(5)
GRID,42,,501.717,43.0,0.,,6
=,*(1),=,*(16.761),==
=(1)
$
GRID,46,,0.,64.5,0.,,
GRID,47,,20.909,64.5,0.,,6
=,*(1),=,*(20.909),==
=(1)
GRID,50,,213.273,64.5,0.,,6
=,*(1),=,*(20.909),==
=(5)
GRID,57,,489.273,64.5,0.,,6
=,*(1),=,*(20.909),==
=(1)
$
GRID,61,,0.,86.0,0.,,
GRID,62,,25.057,86.0,0.,,6
=,*(1),=,*(25.057),==
=(1)
GRID,65,,200.8295,86.0,0.,,6
```

```
=,*(1),=,*(25.057),==
=(5)
GRID,72,,476.829,86.0,0.,,6
=,*(1),=,*(25.057),==
=(1)
$
GRID,76,,0.,107.5,0.,,
GRID,77,,29.204,107.5,0.,,6
=,*(1),=,*(29.204),==
=(1)
GRID,80,,188.384,107.5,0.,,6
=,*(1),=,*(29.204),==
=(5)
GRID,87,,464.388,107.5,0.,,6
=,*(1),=,*(29.204),==
=(1)
$
GRID,91,,0.,129.0,0.,,
GRID,92,,33.352,129.0,0.,,6
=,*(1),=,*(33.352),==
=(1)
GRID,95,,175.944,129.0,0.,,6
=,*(1),=,*(33.352),==
=(5)
GRID,102,,451.944,129.0,0.,,6
=,*(1),=,*(33.352),==
=(1)
$
$
GRID,106,,0.,150.5,0.,,
GRID,107,,28.125,150.5,0.,,6
=,*(1),=,*(28.125),==
=(2)
GRID,111,,125.25,150.5,0.,,6
=,*(1),=,*(12.75),==
=(2)
GRID,115,,191.625,150.5,0.,,6
=,*(1),=,*(28.125),==
=(6)
GRID,123,,401.25,150.5,0.,,6
=,*(1),=,*(12.75),==
=(2)
GRID,127,,467.625,150.5,0.,,6
=,*(1),=,*(28.125),==
=(1)
$
GRID,131,,0.,165.165,0.,,
GRID,132,,28.125,165.165,0.,,6
=,*(1),=,*(28.125),==
=(2)
GRID,136,,125.25,165.165,0.,,6
=,*(1),=,*(12.75),==
=(2)
GRID,140,,191.625,165.165,0.,,6
=,*(1),=,*(28.125),==
=(6)
GRID,148,,401.25,165.165,0.,,6
=,*(1),=,*(12.75),==
=(2)
GRID,152,,467.625,165.165,0.,,6
=,*(1),=,*(28.125),==
=(1)
$
GRID,156,,0.,179.83,0.,,
GRID,157,,28.125,179.83,0.,,6
=,*(1),=,*(28.125),==
=(2)
GRID,161,,125.25,179.83,0.,,6
=,*(1),=,*(12.75),==
=(2)
GRID,165,,191.625,179.83,0.,,6
=,*(1),=,*(28.125),==
=(6)
GRID,173,,401.25,179.83,0.,,6
=,*(1),=,*(12.75),==
=(2)
GRID,177,,467.625,179.83,0.,,6
=,*(1),=,*(28.125),==
=(1)
$
GRID,181,,112.5,194.495,0.,,6
=,*(1),=,*(12.75),==
=(3)
GRID,186,,388.5,194.495,0.,,6
=,*(1),=,*(12.75),==
=(3)
$
GRID,191,,0.,209.16,0.,,
GRID,192,,28.125,209.16,0.,,6
=,*(1),=,*(28.125),==
=(2)
GRID,196,,125.25,209.16,0.,,6
=,*(1),=,*(12.75),==
=(2)
GRID,200,,191.625,209.16,0.,,6
=,*(1),=,*(28.125),==
=(1)
GRID,203,,276.0,209.16,0.,,6
GRID,204,,304.125,209.16,0.,,6
=,*(1),=,*(28.125),==
=(2)
GRID,208,,401.25,209.16,0.,,6
=,*(1),=,*(12.75),==
=(2)
GRID,212,,467.625,209.16,0.,,6
=,*(1),=,*(28.125),==
=(1)
$
GRID,217,,28.125,223.825,0.,,
=,*(1),=,*(28.125),==
=(2)
GRID,221,,125.25,223.825,0.,,
=,*(1),=,*(12.75),==
=(2)
GRID,225,,191.625,223.825,0.,,
=,*(1),=,*(28.125),==
=(1)
GRID,228,,276.0,223.825,0.,,
GRID,229,,304.125,223.825,0.,,
=,*(1),=,*(28.125),==
=(2)
GRID,233,,401.25,223.825,0.,,
```

```
=,*(1),=,*(12.75),==
=(2)
GRID,237,,467.625,223.825,0.,,
=,*(1),=,*(28.125),==
=(1)
$
GRID,216,,0.0,223.825,0.,,3
GRID,15,,552.0,0.,0.,,36
=,*(15),=,=,*(21.5),==
=(5)
GRID,130,,552.0,150.5,0.,,36
=,*(25),=,=,*(14.665),==
=(1)
GRID,215,,552.0,209.16,0.,,36
GRID,240,,552.0,223.825,0.,,13
$
$ ********************************************
$ GRID IDENTIFICATION NUMBERS OF WEB'S LOWER HALF
$ ********************************************
$
GRID,316,,0.,-21.5,0.,,
GRID,317,,12.614,-21.5,0.,,6
=,*(1),=,*(12.614),==
=(1)
GRID,320,,238.158,-21.5,0.,,6
=,*(1),=,*(12.614),==
=(1)
GRID,323,,276.0,-21.5,0.,,6
GRID,324,,288.614,-21.5,0.,,6
=,*(1),=,*(12.614),==
=(1)
GRID,327,,514.158,-21.5,0.,,6
=,*(1),=,*(12.614),==
=(1)
$
GRID,331,,0.,-43.0,0.,,
GRID,332,,16.761,-43.0,0.,,6
=,*(1),=,*(16.761),==
=(1)
GRID,335,,225.717,-43.0,0.,,6
=,*(1),=,*(16.761),==
=(5)
GRID,342,,501.717,-43.0,0.,,6
=,*(1),=,*(16.761),==
=(1)
$
GRID,346,,0.,-64.5,0.,,
GRID,347,,20.909,-64.5,0.,,6
=,*(1),=,*(20.909),==
=(1)
GRID,350,,213.273,-64.5,0.,,6
=,*(1),=,*(20.909),==
=(5)
GRID,357,,489.273,-64.5,0.,,6
=,*(1),=,*(20.909),==
=(1)
$
GRID,361,,0.,-86.0,0.,,
GRID,362,,25.057,-86.0,0.,,6
=,*(1),=,*(25.057),==
=(1)
GRID,365,,200.8295,-86.0,0.,,6
=,*(1),=,*(25.057),==
=(5)
GRID,372,,476.829,-86.0,0.,,6
=,*(1),=,*(25.057),==
=(1)
$
GRID,376,,0.,-107.5,0.,,
GRID,377,,29.204,-107.5,0.,,6
=,*(1),=,*(29.204),==
=(1)
GRID,380,,188.384,-107.5,0.,,6
=,*(1),=,*(29.204),==
=(5)
GRID,387,,464.388,-107.5,0.,,6
=,*(1),=,*(29.204),==
=(1)
$
GRID,391,,0.,-129.0,0.,,
GRID,392,,33.352,-129.0,0.,,6
=,*(1),=,*(33.352),==
=(1)
GRID,395,,175.944,-129.0,0.,,6
=,*(1),=,*(33.352),==
=(5)
GRID,402,,451.944,-129.0,0.,,6
=,*(1),=,*(33.352),==
=(1)
$
$
GRID,406,,0.,-150.5,0.,,
GRID,407,,28.125,-150.5,0.,,6
=,*(1),=,*(28.125),==
=(2)
GRID,411,,125.25,-150.5,0.,,6
=,*(1),=,*(12.75),==
=(2)
GRID,415,,191.625,-150.5,0.,,6
=,*(1),=,*(28.125),==
=(6)
GRID,423,,401.25,-150.5,0.,,6
=,*(1),=,*(12.75),==
=(2)
GRID,427,,467.625,-150.5,0.,,6
=,*(1),=,*(28.125),==
=(1)
$
GRID,431,,0.,-165.165,0.,,
GRID,432,,28.125,-165.165,0.,,6
=,*(1),=,*(28.125),==
=(2)
GRID,436,,125.25,-165.165,0.,,6
=,*(1),=,*(12.75),==
=(2)
GRID,440,,191.625,-165.165,0.,,6
=,*(1),=,*(28.125),==
=(6)
GRID,448,,401.25,-165.165,0.,,6
=,*(1),=,*(12.75),==
=(2)
GRID,452,,467.625,-165.165,0.,,6
```

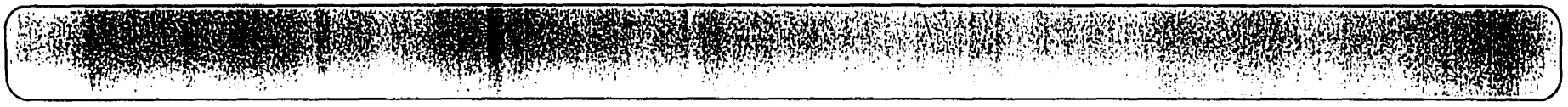

```
=,*(1),=,*(28.125),==
=(1)
$
GRID,456,,0.,-179.83,0.,,
GRID,457,,28.125,-179.83,0.,,6
=,*(1),=,*(28.125),==
=(2)
GRID,461,,125.25,-179.83,0.,,6
=,*(1),=,*(12.75),==
=(2)
GRID,465,,191.625,-179.83,0.,,6
=,*(1),=,*(28.125),==
=(6)
GRID,473,,401.25,-179.83,0.,,6
=,*(1),=,*(12.75),==
=(2)
GRID,477,,467.625,-179.83,0.,,6
=,*(1),=,*(28.125),==
=(1)
$
GRID,481,,112.5,-194.495,0.,,6
=,*(1),=,*(12.75),==
=(3)
GRID,486,,388.5,-194.495,0.,,6
=,*(1),=,*(12.75),==
=(3)
$
GRID,491,,0.,-209.16,0.,,
GRID,492,,28.125,-209.16,0.,,6
=,*(1),=,*(28.125),==
=(2)
GRID,496,,125.25,-209.16,0.,,6
=,*(1),=,*(12.75),==
=(2)
GRID,500,,191.625,-209.16,0.,,6
=,*(1),=,*(28.125),==
=(1)
GRID,503,,276.0,-209.16,0.,,6
GRID,504,,304.125,-209.16,0.,,6
=,*(1),=,*(28.125),==
=(2)
GRID,508,,401.25,-209.16,0.,,6
=,*(1),=,*(12.75),==
=(2)
GRID,512,,467.625,-209.16,0.,,6
=,*(1),=,*(28.125),==
=(1)
$
GRID,517,,28.125,-223.825,0.,,
=,*(1),=,*(28.125),==
=(2)
GRID,521,,125.25,-223.825,0.,,
=,*(1),=,*(12.75),==
=(2)
GRID,525,,191.625,-223.825,0.,,
=,*(1),=,*(28.125),==
=(1)
GRID,528,,276.0,-223.825,0.,,
GRID,529,,304.125,-223.825,0.,,
=,*(1),=,*(28.125),==
=(2)
GRID,533,,401.25,-223.825,0.,,
=,*(1),=,*(12.75),==
=(2)
GRID,537,,467.625,-223.825,0.,,
=,*(1),=,*(28.125),==
=(1)
$
GRID,516,,0.0,-223.825,0.,,3
GRID,330,,552.0,-21.5,0.,,36
=,*(15),=,=,*(-21.5),==
=(4)
GRID,430,,552.0,-150.5,0.,,36
=,*(25),=,=,*(-14.665),==
=(1)
GRID,515,,552.0,-209.16,0.,,36
GRID,540,,552.0,-223.825,0.,,13
$
$ ********************
$ NODES OF TOP FLANGE
$ ********************
$
GRID,241,,0.,223.825,-38.5,,5
=,*(1),=,*(28.125),==
=(3)
GRID,246,,125.25,223.825,-38.5,,5
=,*(1),=,*(12.75),==
=(2)
GRID,250,,191.625,223.825,-38.5,,5
=,*(1),=,*(28.125),==
=(6)
GRID,258,,401.25,223.825,-38.5,,5
=,*(1),=,*(12.75),==
=(2)
GRID,262,,467.625,223.825,-38.5,,5
=,*(1),=,*(28.125),==
=(1)
GRID,265,,552.0,223.825,-38.5,,135
$
GRID,266,,0.,223.825,38.5,,5
=,*(1),=,*(28.125),==
=(3)
GRID,271,,125.25,223.825,38.5,,5
=,*(1),=,*(12.75),==
=(2)
GRID,275,,191.625,223.825,38.5,,5
=,*(1),=,*(28.125),==
=(6)
GRID,283,,401.25,223.825,38.5,,5
=,*(1),=,*(12.75),==
=(2)
GRID,287,,467.625,223.825,38.5,,5
=,*(1),=,*(28.125),==
=(1)
GRID,290,,552.0,223.825,38.5,,135
$
$ ***********************
$ NODES OF BOTTOM FLANGE
$ ***********************
$
GRID,541,,0.,-223.825,-38.5,,5
=,*(1),=,*(28.125),==
```

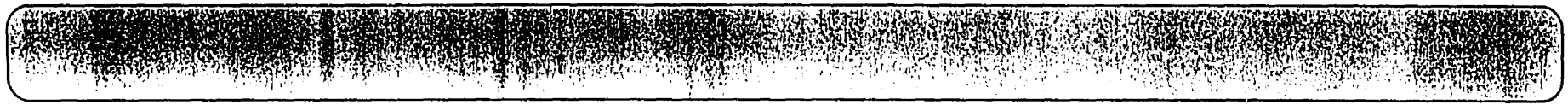

```
=(3)
GRID,546,,125.25,-223.825,-38.5,,5
=,*(1),=,*(12.75),==
=(2)
GRID,550,,191.625,-223.825,-38.5,,5
=,*(1),=,*(28.125),==
=(6)
GRID,558,,401.25,-223.825,-38.5,,5
=,*(1),=,*(12.75),==
=(2)
GRID,562,,467.625,-223.825,-38.5,,5
=,*(1),=,*(28.125),==
=(1)
GRID,565,,552.0,-223.825,-38.5,,135
$
GRID,566,,0.,-223.825,38.5,,5
=,*(1),=,*(28.125),==
=(3)
GRID,571,,125.25,-223.825,38.5,,5
=,*(1),=,*(12.75),==
=(2)
GRID,575,,191.625,-223.825,38.5,,5
=,*(1),=,*(28.125),==
=(6)
GRID,583,,401.25,-223.825,38.5,,5
=,*(1),=,*(12.75),==
=(2)
GRID,587,,467.625,-223.825,38.5,,5
=,*(1),=,*(28.125),==
=(1)
GRID,590,,552.0,-223.825,38.5,,135
$
$
$ *****************
$ SUPPORT STIFFENER
$ *****************
$
GRID,601,,0.0,0.0,-38.5,,4
=,*(1),=,=,*(21.5),==
=(5)
GRID,608,,0.0,150.5,-38.5,,4
=,*(1),=,=,*(14.665),==
=(1)
GRID,611,,0.0,209.16,-38.5,,4
$
GRID,625,,0.0,-21.5,-38.5,,4
=,*(1),=,=,*(-21.5),==
=(4)
GRID,631,,0.0,-150.5,-38.5,,4
=,*(1),=,=,*(-14.665),==
=(1)
GRID,634,,0.0,-209.16,-38.5,,4
$
GRID,613,,0.0,0.0,38.5,,4
=,*(1),=,=,*(21.5),==
=(5)
GRID,620,,0.0,150.5,38.5,,4
=,*(1),=,=,*(14.665),==
=(1)
GRID,623,,0.0,209.16,38.5,,4
$
GRID,636,,0.0,-21.5,38.5,,4
=,*(1),=,=,*(-21.5),==
=(4)
GRID,642,,0.0,-150.5,38.5,,4
=,*(1),=,=,*(-14.665),==
=(1)
GRID,645,,0.0,-209.16,38.5,,4
$
$
$ **********************
$ NODES OF CONCRETE SLAB
$ **********************
$
GRID,701,,0.,,312.825,0.,,
=,*(1),=,*(28.125),==
=(3)
GRID,706,,125.25,312.825,0.,,
=,*(1),=,*(12.75),==
=(2)
GRID,710,,191.625,312.825,0.,,
=,*(1),=,*(28.125),==
=(1)
GRID,713,,276.0,312.825,0.,,
GRID,714,,304.125,312.825,0.,,
=,*(1),=,*(28.125),==
=(2)
GRID,718,,401.25,312.825,0.,,
=,*(1),=,*(12.75),==
=(2)
GRID,722,,467.625,312.825,0.,,
=,*(1),=,*(28.125),==
=(1)
GRID,725,,552.0,312.825,0.,,13
$
$
$ !!!!!!!!!!!!!!!!!!!!!!!!!!!!
$ [2] QUAD4 ELEMENT ALLOCATION
$ !!!!!!!!!!!!!!!!!!!!!!!!!!!!
$
$ ************************
$ UPPER WEB QUAD4 ELEMENTS
$ ************************
$
CQUAD4,1,1,1,2,17,16
=,*(1),=,*(1),*(1),*(1),*(1)
=(1)
CQUAD4,4,1,5,6,21,20
=,*(1),=,*(1),*(1),*(1),*(1)
=(4)
CQUAD4,10,1,12,13,28,27
=,*(1),=,*(1),*(1),*(1),*(1)
=(1)
$
CQUAD4,13,1,16,17,32,31
=,*(1),=,*(1),*(1),*(1),*(1)
=(1)
CQUAD4,16,1,20,21,36,35
=,*(1),=,*(1),*(1),*(1),*(1)
=(4)
CQUAD4,22,1,27,28,43,42
=,*(1),=,*(1),*(1),*(1),*(1)
```

```
=(1)
$
CQUAD4,25,1,31,32,47,46
=,*(1),=,*(1),*(1),*(1),*(1)
=(1)
CQUAD4,28,1,35,36,51,50
=,*(1),=,*(1),*(1),*(1),*(1)
=(4)
CQUAD4,34,1,42,43,58,57
=,*(1),=,*(1),*(1),*(1),*(1)
=(1)
$
CQUAD4,37,1,46,47,62,61
=,*(1),=,*(1),*(1),*(1),*(1)
=(1)
CQUAD4,40,1,50,51,66,65
=,*(1),=,*(1),*(1),*(1),*(1)
=(4)
CQUAD4,46,1,57,58,73,72
=,*(1),=,*(1),*(1),*(1),*(1)
=(1)
$
CQUAD4,49,1,61,62,77,76
=,*(1),=,*(1),*(1),*(1),*(1)
=(1)
CQUAD4,52,1,65,66,81,80
=,*(1),=,*(1),*(1),*(1),*(1)
=(4)
CQUAD4,58,1,72,73,88,87
=,*(1),=,*(1),*(1),*(1),*(1)
=(1)
$
CQUAD4,61,1,76,77,92,91
=,*(1),=,*(1),*(1),*(1),*(1)
=(1)
CQUAD4,64,1,80,81,96,95
=,*(1),=,*(1),*(1),*(1),*(1)
=(4)
CQUAD4,70,1,87,88,103,102
=,*(1),=,*(1),*(1),*(1),*(1)
=(1)
$
CQUAD4,73,1,91,92,107,106
=,*(1),=,*(1),*(1),*(1),*(1)
=(1)
CTRIA3,193,1,109,94,110
CTRIA3,194,1,109,110,135
CQUAD4,77,1,110,111,136,135
=,*(1),=,*(1),*(1),*(1),*(1)
=(2)
CTRIA3,195,1,114,115,139
CTRIA3,196,1,114,95,115
CQUAD4,82,1,95,96,116,115
=,*(1),=,*(1),*(1),*(1),*(1)
=(4)
CTRIA3,197,1,121,101,122
CTRIA3,198,1,121,122,147
CQUAD4,89,1,122,123,148,147
=,*(1),=,*(1),*(1),*(1),*(1)
=(2)
CTRIA3,199,1,126,127,151
CTRIA3,200,1,126,102,127
CQUAD4,94,1,102,103,128,127
=,*(1),=,*(1),*(1),*(1),*(1)
=(1)
$
CQUAD4,97,1,106,107,132,131
=,*(1),=,*(1),*(1),*(1),*(1)
=(1)
CQUAD4,100,1,109,135,160,134
CQUAD4,101,1,135,136,161,160
=,*(1),=,*(1),*(1),*(1),*(1)
=(2)
CQUAD4,105,1,139,115,140,164
CQUAD4,106,1,115,116,141,140
=,*(1),=,*(1),*(1),*(1),*(1)
=(4)
CQUAD4,112,1,121,147,172,146
CQUAD4,113,1,147,148,173,172
=,*(1),=,*(1),*(1),*(1),*(1)
=(2)
CQUAD4,117,1,151,127,152,176
CQUAD4,118,1,127,128,153,152
=,*(1),=,*(1),*(1),*(1),*(1)
=(1)
$
CQUAD4,121,1,131,132,157,156
=,*(1),=,*(1),*(1),*(1),*(1)
=(1)
CQUAD4,124,1,134,160,181,159
CQUAD4,125,1,160,161,182,181
=,*(1),=,*(1),*(1),*(1),*(1)
=(2)
CQUAD4,129,1,164,140,165,185
CQUAD4,130,1,140,141,166,165
=,*(1),=,*(1),*(1),*(1),*(1)
=(4)
CQUAD4,136,1,146,172,186,171
CQUAD4,137,1,172,173,187,186
=,*(1),=,*(1),*(1),*(1),*(1)
=(2)
CQUAD4,141,1,176,152,177,190
CQUAD4,142,1,152,153,178,177
=,*(1),=,*(1),*(1),*(1),*(1)
=(1)
$
CQUAD4,145,1,156,157,192,191
=,*(1),=,*(1),*(1),*(1),*(1)
=(1)
CQUAD4,148,1,159,181,195,194
CQUAD4,149,1,181,182,196,195
=,*(1),=,*(1),*(1),*(1),*(1)
=(2)
CQUAD4,153,1,185,165,200,199
CQUAD4,154,1,165,166,201,200
=,*(1),=,*(1),*(1),*(1),*(1)
=(4)
CQUAD4,160,1,171,186,207,206
CQUAD4,161,1,186,187,208,207
=,*(1),=,*(1),*(1),*(1),*(1)
=(2)
CQUAD4,165,1,190,177,212,211
```

```
CQUAD4,166,1,177,178,213,212
=,*(1),=,*(1),*(1),*(1),*(1)
=(1)
$
CQUAD4,169,1,191,192,217,216
=,*(1),=,*(1),*(1),*(1),*(1)
=(22)
$
$ ************************
$ LOWER WEB QUAD4 ELEMENTS
$ ************************
$
CQUAD4,201,1,316,317,2,1
=,*(1),=,*(1),*(1),*(1),*(1)
=(1)
CQUAD4,204,1,320,321,6,5
=,*(1),=,*(1),*(1),*(1),*(1)
=(4)
CQUAD4,210,1,327,328,13,12
=,*(1),=,*(1),*(1),*(1),*(1)
=(1)
$
CQUAD4,213,1,331,332,317,316
=,*(1),=,*(1),*(1),*(1),*(1)
=(1)
CQUAD4,216,1,335,336,321,320
=,*(1),=,*(1),*(1),*(1),*(1)
=(4)
CQUAD4,222,1,342,343,328,327
=,*(1),=,*(1),*(1),*(1),*(1)
=(1)
$
CQUAD4,225,1,346,347,332,331
=,*(1),=,*(1),*(1),*(1),*(1)
=(1)
CQUAD4,228,1,350,351,336,335
=,*(1),=,*(1),*(1),*(1),*(1)
=(4)
CQUAD4,234,1,357,358,343,342
=,*(1),=,*(1),*(1),*(1),*(1)
=(1)
$
CQUAD4,237,1,361,362,347,346
=,*(1),=,*(1),*(1),*(1),*(1)
=(1)
CQUAD4,240,1,365,366,351,350
=,*(1),=,*(1),*(1),*(1),*(1)
=(4)
CQUAD4,246,1,372,373,358,357
=,*(1),=,*(1),*(1),*(1),*(1)
=(1)
$
CQUAD4,249,1,376,377,362,361
=,*(1),=,*(1),*(1),*(1),*(1)
=(1)
CQUAD4,252,1,380,381,366,365
=,*(1),=,*(1),*(1),*(1),*(1)
=(4)
CQUAD4,258,1,387,388,373,372
=,*(1),=,*(1),*(1),*(1),*(1)
=(1)
$
CQUAD4,261,1,391,392,377,376
=,*(1),=,*(1),*(1),*(1),*(1)
=(1)
CQUAD4,264,1,395,396,381,380
=,*(1),=,*(1),*(1),*(1),*(1)
=(4)
CQUAD4,270,1,402,403,388,387
=,*(1),=,*(1),*(1),*(1),*(1)
=(1)
$
CQUAD4,273,1,406,407,392,391
=,*(1),=,*(1),*(1),*(1),*(1)
=(1)
CTRIA3,393,1,409,410,394
CTRIA3,394,1,409,435,410
CQUAD4,277,1,435,436,411,410
=,*(1),=,*(1),*(1),*(1),*(1)
=(2)
CTRIA3,395,1,439,415,414
CTRIA3,396,1,414,415,395
CQUAD4,282,1,415,416,396,395
=,*(1),=,*(1),*(1),*(1),*(1)
=(4)
CTRIA3,397,1,421,422,401
CTRIA3,398,1,421,447,422
CQUAD4,289,1,447,448,423,422
=,*(1),=,*(1),*(1),*(1),*(1)
=(2)
CTRIA3,399,1,451,427,426
CTRIA3,400,1,426,427,402
CQUAD4,294,1,427,428,403,402
=,*(1),=,*(1),*(1),*(1),*(1)
=(1)
$
CQUAD4,297,1,431,432,407,406
=,*(1),=,*(1),*(1),*(1),*(1)
=(1)
CQUAD4,300,1,434,460,435,409
CQUAD4,301,1,460,461,436,435
=,*(1),=,*(1),*(1),*(1),*(1)
=(2)
CQUAD4,305,1,464,440,415,439
CQUAD4,306,1,440,441,416,415
=,*(1),=,*(1),*(1),*(1),*(1)
=(4)
CQUAD4,312,1,446,472,447,421
CQUAD4,313,1,472,473,448,447
=,*(1),=,*(1),*(1),*(1),*(1)
=(2)
CQUAD4,317,1,476,452,427,451
CQUAD4,318,1,452,453,428,427
= *(1),=,*(1),*(1),*(1),*(1)
=(1)
$
CQUAD4,321,1,456,457,432,431
=,*(1),=,*(1),*(1),*(1),*(1)
=(1)
CQUAD4,324,1,459,481,460,434
CQUAD4,325,1,481,482,461,460
=,*(1),=,*(1),*(1),*(1),*(1)
```

```
=(2)
CQUAD4,329,1,485,465,440,464
CQUAD4,330,1,465,466,441,440
=,*(1),=,*(1),*(1),*(1),*(1)
=(4)
CQUAD4,336,1,471,486,472,446
CQUAD4,337,1,486,487,473,472
=,*(1),=,*(1),*(1),*(1),*(1)
=(2)
CQUAD4,341,1,490,477,452,476
CQUAD4,342,1,477,478,453,452
=,*(1),=,*(1),*(1),*(1),*(1)
=(1)
$
CQUAD4,345,1,491,492,457,456
=,*(1),=,*(1),*(1),*(1),*(1)
=(1)
CQUAD4,348,1,494,495,481,459
CQUAD4,349,1,495,496,482,481
=,*(1),=,*(1),*(1),*(1),*(1)
=(2)
CQUAD4,353,1,499,500,465,485
CQUAD4,354,1,500,501,466,465
=,*(1),=,*(1),*(1),*(1),*(1)
=(4)
CQUAD4,360,1,506,507,486,471
CQUAD4,361,1,507,508,487,486
=,*(1),=,*(1),*(1),*(1),*(1)
=(2)
CQUAD4,365,1,511,512,477,490
CQUAD4,366,1,512,513,478,477
=,*(1),=,*(1),*(1),*(1),*(1)
=(1)
$
CQUAD4,369,1,516,517,492,491
=,*(1),=,*(1),*(1),*(1),*(1)
=(22)
$
$ ***************************
$ UPPER FLANGE QUAD4 ELEMENTS
$ ***************************
$
CQUAD4,401,2,216,217,242,241
=,*(1),=,*(1),*(1),*(1),*(1)
=(22)
$
CQUAD4,425,2,266,267,217,216
=,*(1),=,*(1),*(1),*(1),*(1)
=(22)
$
$ ***************************
$ LOWER FLANGE QUAD4 ELEMENTS
$ ***************************
$
CQUAD4,451,2,516,517,542,541
=,*(1),=,*(1),*(1),*(1),*(1)
=(22)
$
CQUAD4,475,2,566,567,517,516
=,*(1),=,*(1),*(1),*(1),*(1)
=(22)
$
$
$ ******************************
$ SUUPORT STIFFENER QUAD4 ELEMENTS
$ ******************************
$
CQUAD4,501,3,1,601,602,16
=,*(1),=,*(15),*(1),*(1),*(15)
=(5)
CQUAD4,508,3,106,608,609,131
=,*(1),=,*(25),*(1),*(1),*(25)
CQUAD4,510,3,156,610,611,191
$
CQUAD4,511,3,613,1,16,614
=,*(1),=,*(1),*(15),*(15),*(1)
=(5)
CQUAD4,518,3,620,106,131,621
=,*(1),=,*(1),*(25),*(25),*(1)
CQUAD4,520,3,622,156,191,623
$
CQUAD4,521,3,316,625,601,1
CQUAD4,522,3,331,626,625,316
=,*(1),=,*(15),*(1),*(1),*(15)
=(4)
CQUAD4,528,3,431,632,631,406
=,*(1),=,*(25),*(1),*(1),*(25)
CQUAD4,530,3,491,634,633,456
$
CQUAD4,531,3,636,316,1,613
CQUAD4,532,3,637,331,316,636
=,*(1),=,*(1),*(15),*(15),*(1)
=(4)
CQUAD4,538,3,643,431,406,642
=,*(1),=,*(1),*(25),*(25),*(1)
CQUAD4,540,3,645,491,456,644
$
CQUAD4,581,3,191,611,241,216
CQUAD4,582,3,623,191,216,266
CQUAD4,583,3,516,541,634,491
CQUAD4,584,3,566,516,491,645
$
$
$ ******************************
$ SHEAR CONNECTORS "CBEAM" ELEMENTS
$ ******************************
$
CBEAM,701,4,216,701,0.0,0.0,1.0
=,*(1),=,*(1),*(1),==
=(2)
CBEAM,705,5,220,705,0.0,0.0,1.0
=,*(1),=,*(1),*(1),==
=(3)
CBEAM,710,6,225,710,0.0,0.0,1.0
=,*(1),=,*(1),*(1),==
=(5)
CBEAM,717,5,232,717,0.0,0.0,1.0
=,*(1),=,*(1),*(1),==
=(3)
CBEAM,722,4,237,722,0.0,0.0,1.0
=,*(1),=,*(1),*(1),==
=(2)
```

```
$
$ ********************************************
$ "SHEAR SPECIMEN" CONCRETE SLAB "CBEAM" ELEMENTS
$ ********************************************
$
CBEAM,726,7,701,702,0.0,1.0,0.0
=,*(1),=,*(1),*(1),==
=(22)
$
$
$ !!!!!!!!!!!!!!!!!!!!!!!!!!!!!!!!!!!!
$ [3]  MATERIAL & ELEMENT PROPERTIES
$ !!!!!!!!!!!!!!!!!!!!!!!!!!!!!!!!!!!!
$
MAT1,7,200000.,,0.3
MAT1,8,200000.,,0.3
MAT1,9,200000.,,0.3
MAT1,10,200000.,,0.3
MAT1,11,29430.0,,0.2
$
TABLES1,100,,,,,,,,+TAB1
+TAB1,-0.0035,-38.5,-0.00078,-23.0,0.0,0.0,0.000126,3.72,+TAB2
+TAB2,0.0035,3.72,ENDT
MATS1,7,,PLASTIC,0.0,1,1,314.412
MATS1,8,,PLASTIC,0.0,1,1,317.86
MATS1,9,,PLASTIC,0.0,1,1,317.86
MATS1,10,,PLASTIC,0.0,1,1,344.75
MATS1,11,100,NLELAST
$
PSHELL,1,7,4.69,7
PSHELL,2,8,5.35,8
PSHELL,3,9,9.525,9
$
PBEAM,4,10,362.836,10476.35,10476.35,,20952.71,,+PB1
+PB1,,,,,,,,,+PB2
+PB2,NO,1.0,362.836,10476.35,10476.35,,20952.71,,+PB3
+PB3,,,,,,,,,
$
PBEAM,5,10,218.506,3799.425,3799.425,,7598.851,,+PB4
+PB4,,,,,,,,,+PB5
+PB5,NO,1.0,218.506,3799.425,3799.425,,7598.851,,+PB6
+PB6,,,,,,,,,
$
PBEAM,6,10,387.888,11972.97,11972.97,,23945.95,,+PB7
+PB7,,,,,,,,,+PB8
+PB8,NO,1.0,387.888,11972.97,11972.97,,23945.95,,+PB9
+PB9,,,,,,,,,
$
PBEAM,7,11,44516.04,21.54+6,1.266+9,,79.08+6,,+PB10
+PB10,38.1,-292.1,38.1,292.1,-38.1,292.1,-38.1,-292.1,+PB11
+PB11,YES,1.0,44516.04,21.54+6,1.266+9,,79.08+6,,+PB12
+PB12,38.1,-292.1,38.1,292.1,-38.1,292.1,-38.1,-292.1
$
$
$
$ !!!!!!!!!!!!!!!!!
$ [4] APPLIED LOADS
$ !!!!!!!!!!!!!!!!!
$
FORCE,10,240,,20000.0,0.0,-1.0,0.0
FORCE,10,540,,20000.0,0.0,-1.0,0.0
$
FORCE,20,240,,32500.0,0.0,-1.0,0.0
FORCE,20,540,,32500.0,0.0,-1.0,0.0
$
FORCE,30,240,,45000.0,0.0,-1.0,0.0
FORCE,30,540,,45000.0,0.0,-1.0,0.0
$
FORCE,40,240,,65000.0,0.0,-1.0,0.0
FORCE,40,540,,65000.0,0.0,-1.0,0.0
$
$
ENDDATA
```

SAMPLE "RESTART" NASTRAN INPUT FILE

```
$ !!!!!!!!!!!!!!!!!!!!!!!!!!!!!!!!!!!!!!!!!!!!!!!!!!!!
$ A RESTART FILE FOR MOD6-58.IN, ECC = 0" = 0mm
$ !!!!!!!!!!!!!!!!!!!!!!!!!!!!!!!!!!!!!!!!!!!!!!!!!!!!
$
RESTART VERSION=1 KEEP
ASSIGN MASTER='mod6-58.MASTER'
$
ID MOD6-58r, Nlbuckling analysis of a composite castellated beam.
SOL 106
TIME=900
INCLUDE 'nlbshape.dat'
CEND
$
TITLE = TRIAL#4: Mid-depth case; <3"slab! ho=11.85"! phi=59.94! 2"weld>
$
SET 2 = ALL
ECHO = NONE
  DISPLACEMENT = 2
  METHOD = 100
PARAM,BUCKLE,1
PARAM,SUBID,5
PARAM,LOOPID,14
$
SUBCASE 1
  LOAD = 10
  NLPARM = 10
SUBCASE 2
  LOAD = 20
  NLPARM = 20
SUBCASE 3
  LOAD = 30
  NLPARM = 30
SUBCASE 4
  LOAD = 40
  NLPARM = 40
SUBCASE 5
  LOAD = 50
  NLPARM = 50
$
BEGIN BULK
EIGB,100,SINV,-5.0,5.0,,3,3,,+EIGB
+EIGB,MAX
NLPARM,50,2,,AUTO,1,,,YES
$
FORCE,50,240,,43750.0,0.0,-1.0,0.0
FORCE,50,540,,43750.0,0.0,-1.0,0.0
$
$
ENDDATA
```

FILE "nlbshape.dat" USED TO OBTAIN NL-MODE SHAPES

```
compile nlstatic souin=mscsou nolist noref $
alter 393 $ V68.2, after SDR2 for OPHIG
message //'NEXT DISPLACMENT VECTOR IS CRITICAL BUCKLING MODE SHAPE' $
OFP OPHIG,,,,// $ mode shape
IF ( POST=0 ) THEN $
DBC   OPHIG,,,,,,,,,,,,,,,,,,,,//
       'OUG'//////////////////////
       -1/DBCPATH/S,N,CP/APP1/ICYCLIC/GEOMU/LOADU/POSTU/
       DBCDIAG/DBCPROG/DBCOVWRT/DESITER $
ENDIF $ (post = 0)
alter 401 $ critical displacement vector
IF ( POST=0 ) THEN $
DBC   OCRUG,,,,,,,,,,,,,,,,,,,,//
       'OUG'//////////////////////
       -1/DBCPATH/S,N,CP/APP1/ICYCLIC/GEOMU/LOADU/POSTU/
       DBCDIAG/DBCPROG/DBCOVWRT/DESITER $
ENDIF $ (post = 0)
```

IMAGE EVALUATION
TEST TARGET (QA-3)

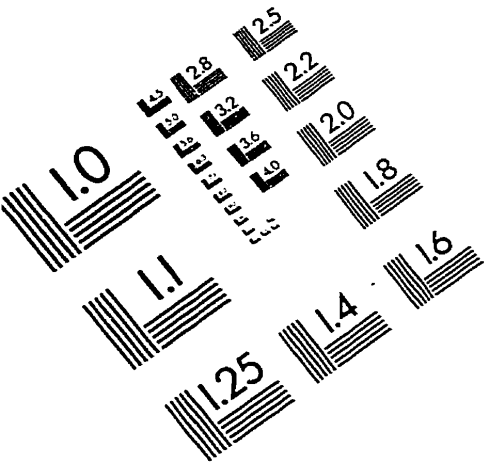

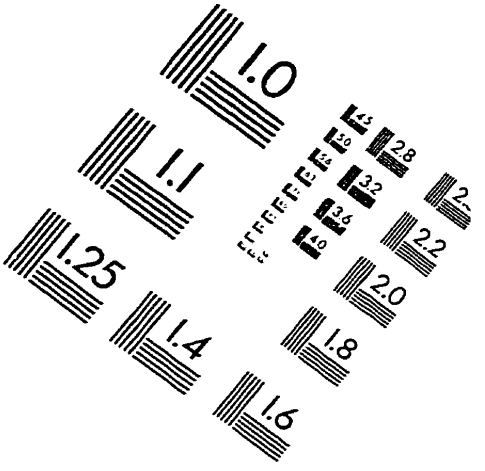

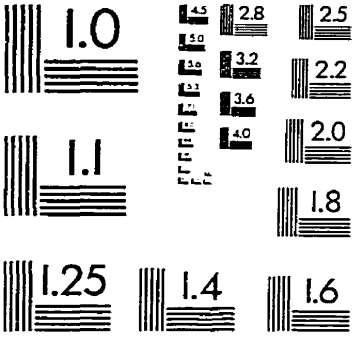

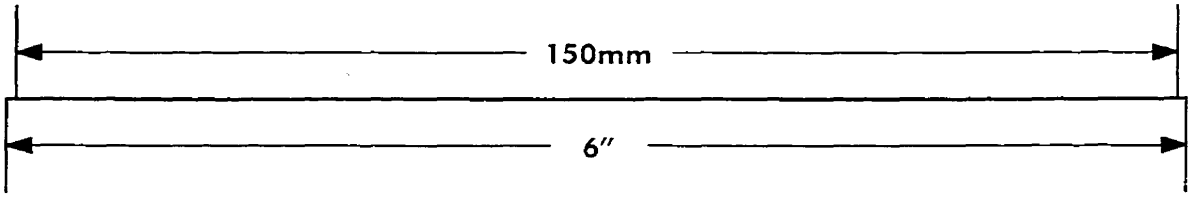

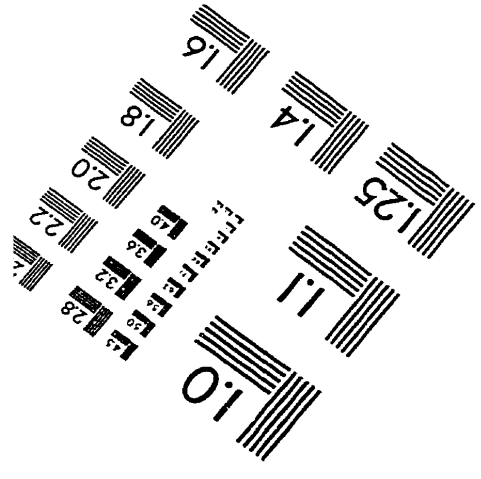

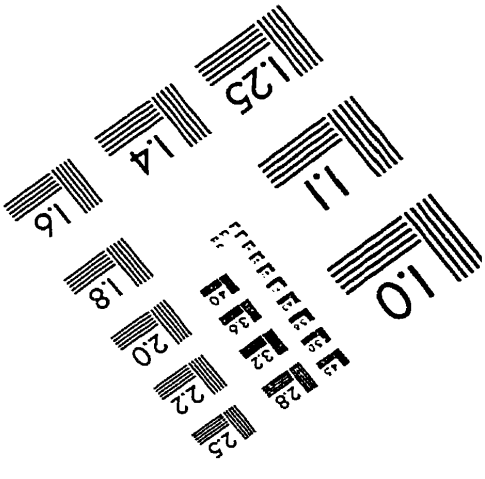

APPLIED IMAGE, Inc
1653 East Main Street
Rochester, NY 14609 USA
Phone: 716/482-0300
Fax: 716/288-5989